Supplementary materials:

Revealing the neurobiology underlying interpersonal neural synchronization with multimodal data fusion

Leon D. Lotter, Simon H. Kohl, Christian Gerloff, Laura Bell, Alexandra Niephaus, Jana A. Kruppa, Juergen Dukart, Martin Schulte-Rüther, Vanessa Reindl, Kerstin Konrad

Published in *Neuroscience & Biobehavioral Reviews*
(https://doi.org/10.1016/j.neubiorev.2023.105042)

Table of Contents

1 Supplementary Materials and Methods

1.1 Literature search and data extraction

1.1.1 Search string

```
(([hyperscanning] OR
  [neural entrainment] OR
  (([brain-to-brain] OR
    [interbrain] OR
    [inter-brain] OR q
    [interpersonal]) AND
   ([synchrony] OR
    [synchronization] OR
    [coupling] OR
    [connectivity] OR
    [networks] OR
    [alignment] OR
    [coherence]))) AND
([fNIRS] OR
 [NIRS] OR
 [near-infrared spectroscopy] OR
 [fMRI] OR
 [MRI] OR
 [magnetic resonance imaging]))
```

1.1.2 Study inclusion criteria

- **Article type**: original research, peer-reviewed or preprint, English language (exclude: conference paper, review, meta-analysis, opinion)
- **Subjects**: human, healthy, between 18 and 65 years
- **Imaging Technology**: fNIRS or fMRI
- **Methodological study design**: "hyperscanning" or "pseudohyperscanning"
- **Task**: uni- or bidirectional interaction between ≥ two subjects
- **Analysis**: temporal synchrony between data derived from hemodynamic signals of ≥ two subjects
    - **fMRI**: analysis of data on whole-brain level (exclude: "region of interest" approaches)
    - **fNIRS**: analysis of channel-wise signals (exclude: data analysis after averaging data from multiple channels to form a "region of interest")
- **Data availability**:
    - **fMRI**: reporting of coordinates in Montreal Neurological Institute (MNI) or Talairach space, or availability of coordinates or 3D volumes on request
    - **fNIRS**: reporting of coordinates in MNI or Talairach space, or availability of coordinates or fNIRS probe setups on request, or reporting of ≥ one coordinate in

international 10-10 system, alignment to a reference plane, and usage of a square probe setup, thus allowing for reconstruction of the probe positioning

1.1.3 Extracted study information

- **General**: authors, publication year, title, journal, identifier
- **Sample:** number of subjects, number of dyads, male/female ratio, relationship between interacting subjects, mean age, age standard deviation, age range
- **Method:** imaging technology, hyperscanning or pseudohyperscanning, general analysis technique, applied contrasts
    - **fMRI:** repetition time, time lag, analysis frequency band, analysis level (voxel-wise, independent component analysis, seed-to-voxel, whole-brain parcellation), analysis software
    - **fNIRS:** device, wavelength of emitted light, sampling rate, analyzed data (HbO, HbR), analysis frequency band, time lag, optode array format and positioning
- **Task and setting:** general domain, exact applied task, setting
    - **fMRI:** (live) audio/video contact
    - **fNIRS:** positioning of subjects to each other (side-by-side, face-to-face, separated)
- **Coordinate data:** coordinates in MNI or Talairach space, author contact information if no coordinates were available
    - **fNIRS:** source of coordinates (virtual registration, digitization, MRI-registration)

1.1.4 Sample data extraction

Sample data were extracted as reported in included studies. If a study reported exclusion of subjects, e.g., due to low data quality, sample sizes after exclusion of these subjects were retained. When, e.g., in case of pseudo-hyperscanning fMRI and some fNIRS studies, demographic data was provided for the study sample and a small group of "special" participants who were scanned repeatedly, sample sizes were determined by the overall sum of participants, while the number of dyads equaled the number of formed dyads, and age mean and standard deviation were calculated as weighted averages. For example, if a study included $n = 20$ students (mean age 20 years) and $n = 2$ teachers (mean age 24 years), forming $n = 20$ dyads with teachers being scanned repeatedly, we set the sample size to 22, the number of dyads to 20, and the mean age to 20.37 years.

When a study split its sample in multiple groups with independent subjects and independently analyzed data, these groups were included as separate experiments. When sample information (i.e., male/female ratio, age) were reported only for the whole sample but not for subgroups, this information was applied to all subgroups at the risk of small inaccuracies (which only apply to the results Tables S1 and S2 but have no influence on our meta-analytic results).

When samples between different studies overlapped, i.e., data derived from the same subjects was analyzed and published multiple times, these data, and reported brain coordinates, were concatenated into one experiment. If it was most likely that (according to the descriptions of sample characteristics, tasks, and the publishing authors), a sample was analyzed twice but this was not mentioned in the papers and the authors did not answer requests, we chose a conservative approach

and concatenated respective data into one experiment. When concatenating data, the lowest reported sample size of all individual studies was used for the resulting "experiment" to be included in meta-analyses.

1.1.5 fMRI coordinate data extraction

Coordinates provided in MNI space were not modified. Coordinates in Talairach space were converted to MNI using the Lancaster transform (*1*).

When authors sent thresholded volumetric imaging data, we extracted a maximum of three peak coordinates from each cluster (minimum distance of 10 mm, minimum size of 10 voxels).

When authors sent independent component analysis results in the form of volumetric data depicting independent components, we Z-normalized these maps while excluding zero-voxels, applied a cluster threshold of $Z > 2.5$ and retained only clusters exceeding a volume of 0.1% of all non-zero in-brain voxels. From all studies applying independent component analysis, for each reported or estimated cluster, a maximum number of three peak coordinates with a minimum distance of 10 mm was retained for meta-analysis.

When data was analyzed using a whole-brain parcellation, for each parcel showing INS, the center of mass was used as focus coordinates.

When authors analyzed INS not only for homologous brain areas (voxels, parcels, independent components) but in a pairwise fashion for the whole brain, foci representing all connected regions were retained for meta-analysis (e.g., when significant INS was found between the right temporoparietal junction of subject 1 and the right insula of subject 2, we would include foci representing both regions).

1.1.6 fNIRS coordinate data extraction and reconstruction

For studies that did not report coordinates, we obtained MNI coordinates according to the following workflow:

When studies reported to have used the virtual registration method (*2*) and used a common static rectangular optode placeholder, we used coordinates provided by Tsuzuki et al. (http://brain-lab.jp/wp/?page_id=58). If studies did not report to have used the virtual registration method but their description of optode placements matched one of the probe setups for which virtual registration results were available, we used these for the analyses [e.g., Cui et al., 2012 (*3*) matched Fpz_low3_HorSag_3x5].

In some cases, a probe set configuration reported by study A was used in study B as well and study B was published by authors from the same research group or University. When coordinates for study B were available, we used these for study A as well [e.g., for Liu et al, 2019 (*4*), we used the temporoparietal coordinates from Lu et al, 2020b (*5*)].

When this was not possible, we reconstructed the probe sets based on the spatial information provided by the studies using AtlasViewer (https://openfnirs.org/software/homer) and registered it to a scaled version of the Colin27 MNI atlas. Since head size information were not provided by the studies in question, we could not register the Colin27 atlas in AtlasViewer to study-specific head sizes but had to rely on a standard head size for all reconstructions. In order to get an appropriate approximation of the average head shape, we calculated the average head sizes for white and Asian

women and men (560.01 mm) based on data provided by Ball (*6*) (https://repository.tudelft.nl/islandora/object/uuid:2d038418-8923-4605-92e8-ca3df57ea731) and Harrison & Robinette (*7*) (https://apps.dtic.mil/sti/pdfs/ADA406674.pdf). To be suited for reconstruction, studies had to report at least two anatomical landmarks of the EEG 10-10 or 10-5 system. We rated the "reconstructability" of studies as *high* if EEG channel positions for every single optode were reported, as *medium* if at least two EEG channel positions for each optode array were given, or as l*ow* if one EEG channel position and some additional spatial information about the alignment of the probe set, e.g., "15° angle between probe patches and transverse plane" was reported. When only one landmark but no additional information or no information at all was reported, these studies were excluded.

When studies analyzed and reported fNIRS data in voxel space and reported significant voxel-level MNI coordinates, we obtained coordinates according to the workflow lined out above and retained, for each reported significant voxel, coordinates of the three fNIRS channels most closely located to this voxel.

1.2 Calculation of the fail-safe-N

The robustness against publication bias of each cluster was estimated as the fail-safe-N (*8*). For each cluster, noise experiments with sample sizes and foci numbers drawn from the actual included fMRI experiments were generated. Foci coordinates for these noise studies were randomly drawn from all gray matter voxels excluding those in the brain quadrant where the respective cluster's center of mass was located. Based on preset minimum and maximum numbers of added noise experiments (the number of contributing experiments and the number of noise studies needed to reach a minimum contribution of 10% of studies) (*8*), we iteratively searched for the minimum number of noise experiments needed to render the cluster insignificant while applying standard voxel-level and cluster-level thresholds ($p < .001$ and $p < .05$). The resulting number mirrors the hypothetical minimum of negative studies that could have "remained in the file drawer" necessary for the respective cluster to fail significance thresholds.

1.3 Modelling of spatial uncertainty in fNIRS meta-analyses

To incorporate spatial uncertainty of fNIRS data in fNIRS meta-analyses, we iteratively recalculated both the parcel-wise fNIRS meta-analysis and the combined ALE after randomization of fNIRS coordinates within a 10 mm radius and a strongly constrained cortical MNI-152 template (1,000 iterations). The radius choice was based on previous data showing a localization error of 18 mm in preregistered model-based fNIRS-fMRI registration (*9*, *10*).

To evaluate the fNIRS-only meta-analytic results, we calculated, for each parcel, the percentage of sub-threshold *p* values ($p < .05$) relative to the total number of iterations as well as the median *p* value resulting from all iterations.

The combined ALE was repeated with randomized coordinates in the same fashion as the main analysis. However, we adopted the cluster mass threshold estimated from the maximum cluster size distribution of the original fNIRS-fMRI ALE instead of recalculating individual thresholds for each fNIRS coordinate randomization iteration to reduce the required computational power.

We then evaluated the results by calculating the proportion of thresholded ALE maps for which nonzero ALE values were present within the clusters derived from the main combined fMRI-fNIRS ALE.

1.4 Resting-state fMRI data processing

To estimate the functional connectivity pattern present within the task-based coactivation network, $N = 120$ unrelated subjects from the Human Connectome Project S900 release (*11*) were randomly selected from age and gender groups (20 females and 20 males from each age group: 22–25, 26–30, and 31–35 years). We used the S900 extensively preprocessed volumetric data (ICA-FIX denoised) thoroughly described in the reference manual (*12*). Further processing in CONN (https://web.conn-toolbox.org/) included: resampling of the data to a 3 mm isotropic MNI-152 template, concatenation of the first two resting-state sessions (resulting in 30 min), linear detrending and bandpass filtering (0.01–0.08 Hz), averaging of voxel-wise timeseries across MACM clusters, and calculation of semipartial correlations between clusters (*13*). After exclusion of subjects exceeding framewise displacement cutoffs of 2 mm translation or 2 degree rotation ($n = 5$), we calculated two-sided one-sample t-tests against zero on the r-to-Z transformed semipartial correlation coefficients representing each (directed) functional connection. To identify the strongest functional connections, the resulting p value matrix was thresholded at FWE-corrected $p < .05$ (Bonferroni) and only positive connections were interpreted to exclude potential spurious negative connections introduced through noise regression (*14*).

1.5 Relative and absolute distributions within major resting-state networks

To characterize the ALE clusters and the associated MACM networks in respect to their spatial overlap with established brain-wide resting-state networks (*15–17*), we adopted a frequently used method characterizing the absolute and relative distributions of our target volumes across these networks (*18*). The *relative distribution* refers to the proportion of activated voxels within a reference network compared to all activated voxels, while the *absolute distribution* is calculated as the proportion of activated voxels compared to all voxels within a reference network. To estimate significance of these spatial associations, we then permuted the input coordinates (1,000 repetitions; fMRI INS coordinates and rTPJ-associated BrainMap coordinates, respectively) within a grey-matter mask (MNI-152, thresholded at > .2), performed ALE analyses on these coordinates, and iteratively reassessed the resting-state network overlaps to generate null distributions of the overlap metrics. From these null distributions, we calculated empirical p values denoting the probability of a false positive finding under the null hypothesis of random spatial localizations of INS/MACM coordinates. The p values were FDR-corrected for each metric across the combined rTPJ and MACM results. To reduce computational cost, we did not run the full cluster mass permutation procedure as in the main ALE/MACM analyses but extracted the cluster mass thresholds from the primary analyses and used these to perform cluster-level inference on the null data after applying a voxel-level threshold of $p < .001$.

1.6 Processing of Allen Brain Atlas mRNA expression data

Regional microarray expression data were obtained from 6 post-mortem brains (1 female, age range 24.0–57.0 years, mean age 42.50 ± 13.38 years) provided by the Allen Human Brain Atlas (https://human.brain-map.org) (*19*). Data were processed with the abagen toolbox (version 0.1.3; https://github.com/rmarkello/abagen) (*20*) using a volumetric atlas in MNI space covering 116 cortical and subcortical brain regions (*21*, *22*).

First, microarray probes were reannotated using data provided by Arnatkevičiūtė et al. (*23*); probes not matched to a valid Entrez ID were discarded. Next, probes were filtered based on their expression intensity relative to background noise (*24*), such that probes with intensity less than the background in $\geq 50\%$ of samples across donors were discarded, yielding 31,569 probes. When multiple probes indexed the expression of the same gene, we selected and used the probe with the most consistent pattern of regional variation across donors [i.e., differential stability (*25*)], calculated with:

$$\Delta_S(p) = \frac{1}{\binom{N}{2}} \sum_{i=1}^{N-1} \sum_{j=i+1}^{N} \rho\left[B_i(p), B_j(p)\right]$$

where p is Spearman's rank correlation of the expression of a single probe, p, across regions in two donors B_i and B_j, and N is the total number of donors. Here, regions correspond to the structural designations provided in the ontology from the Allen Human Brain Atlas. The MNI coordinates of tissue samples were updated to those generated via non-linear registration using the Advanced Normalization Tools (https://github.com/chrisfilo/alleninf). Samples were assigned to brain regions in the provided atlas if their MNI coordinates were within 2mm of a given parcel. All tissue samples not assigned to a brain region in the provided atlas were discarded. Inter-subject variation was addressed by normalizing tissue sample expression values across genes using a robust sigmoid function (*26*):

$$x_{norm} = \frac{1}{1 + exp - \left(\frac{(x - \langle x \rangle)}{IQR_x}\right)}$$

where $\langle x \rangle$ is the median and IQR_x is the normalized interquartile range of the expression of a single tissue sample across genes. Normalized expression values were then rescaled to the unit interval:

$$x_{scaled} = \frac{x_{norm} - \min(x_{norm})}{\max(x_{norm}) - \min(x_{norm})}$$

Gene expression values were then normalized across tissue samples using an identical procedure. Samples assigned to the same brain region were averaged separately for each donor and then across donors, yielding a regional expression matrix with 116 rows, corresponding to brain regions, and 15,633 columns, corresponding to the retained genes.

1.7 Validation analyses for in-vivo INS-$GABA_A$ associations

To validate the spatial association found between INS and the $GABA_A$ receptor distribution, the following list of GABA-related genes was collected (*27*, *28*) and data were extracted from the

Allen Brain atlas: GABRA1, GABRA2, GABRA3, GABRA4, GABRA5, GABRB1, GABRB2, GABRB3, GABRG1, GABRG2, GABRG3, GABRD, GABRE, GAD1, GAD2, PVALB, SST, VIP, CCK, NPY, CALB1, CALB2, NOS1, RELN, ADRB2, LHX6, TAC1, TAC3, TAC4, SLC6A1, SLC6A13, SLC6A12, SLC32A1, GABBR1, GABBR2.

Following genes were not available after preprocessing of Allen Brain Atlas data: GABRA6, GABRP, GABRQ, GABRR1, GABRR2, GABRR3, LAMB5, SLC6A11.

The expression data from all genes were pairwise correlated using Spearman correlations and the correlation matrix was clustered using the default unsupervised hierarchical clustering method implemented in scipy (*29*), based on Euclidean distances and estimating cluster proximity using the nearest point algorithm. Normalized expression values of all genes within a cluster were Z-standardized, averaged and correlated with the INS ALE-Z-map using JuSpyce (*30*) as described in the main methods section (partial Spearman correlations, adjusted for local gray matter volume). Resulting *p* values were FDR-corrected.

1.8 Dominance analysis on nuclear imaging and neuronal cell type data

Dominance analysis is designed to determine the relative contribution of each predictor in a multivariate regression model to the overall explained variance as an intuitive measure of predictor importance (*31*). It does so by calculating all subset models of a multivariate linear model, i.e., re-calculating the regression analysis with all possible combinations of predictors. We implemented the method in JuSpyce to estimate three different dominance statistics of which we focused on two. *Total dominance* is the average contribution of a predictor to the total R^2 across all subset models and can be interpreted as the amount of explained variance of a predictor relative to the total explained variance. For comparison, we further evaluated *individual dominance*, which is the R^2 resulting from the univariate regression of a single predictor on the target variable and thus quantifies the amount of information explained by a predictor alone. As the main goal of this analysis was to quantify the amount of INS variance explained by PET and cell type maps, we submitted only those maps to dominance analysis that showed significant positive relationships to INS (FDR-corrected) in the previous analyses. PET data was atlas-wise parcellated, Z-standardized, and averaged across atlases using the same tracer. Neuronal cell type maps were generated by Z-standardizing each parcel-wise gene expression vector and calculating the average gene expression per cell type category. Parcel-wise gray matter volume was regressed out of the INS map and each predictor map before performing the regression analysis to align with the main correlation analyses.

1.9 Clustering and visualization of INS-associated GeneOntology categories

Results from GeneOntology (GO) gene-category enrichment analyses as obtained from ABAnnotate (*32*) were further clustered based on semantic similarity using GO-Figure! which was described in detail elsewhere (*33*, *34*). Briefly, the dimensionality of the list of significantly associated GO terms is reduced by calculating pairwise semantic similarity scores based on (i) the distance of two GO terms within the directed acyclic organization of GO categories and (ii) the frequency of each GO term in a large database of genes (equaling “specificity” of each GO term).

Based on an arbitrary similarity threshold, GO terms are then grouped into clusters, a representative term is selected, and a multidimensional scaling algorithm is applied to generate a two-dimensional visualization. Here, we chose a liberal threshold of $\geq .2$ to capture the overall biological functions of the identified GO clusters at the cost of specificity.

2 Supplementary Results

2.1 FMRI meta-analysis sensitivity analyses

2.1.1 Influence of individual experiments

To estimate the influence of individual experiments on observed interpersonal neural synchrony (INS) clusters, we applied a jacknife approach and recalculated ALE analyses while iteratively excluding one experiment at a time.

Using these data, we estimated that 12 of 22 experiments contributed to the right temporoparietal junction (rTPJ) cluster, with a maximum contribution of 16% using the conservative threshold ($p < .001$). In contrast, the right superior temporal and right insula clusters were driven by a lower number of studies with corresponding stronger contributions (Table S1). Accordingly, the spatial conjunction of all jackknife-derived thresholded maps proofed only the right temporoparietal junction (rTPJ) cluster as stable against the influence of individual experiments (Figure 2A).

2.1.2 Risk of publication bias

Coordinate-based meta-analytic techniques, such as ALE, only allow for limited possibilities for structured bias assessment. However, to assess the robustness of ALE results against publication bias, calculation of the cluster-wise *fail-safe-N* was proposed (*8*). Adopting this method, we tested how many noise-experiments generated with characteristics similar to the original INS data we could add to the INS ALE analysis before the originally observed clusters were no longer significant.

Based on the inclusion of a minimum of 12 (the number of contributing experiments) and a maximum of 98 ($\frac{12}{98+22} = 10\%$) of noise-experiments, we observed a fail-safe-N of 66 for the rTPJ cluster indicating that even if 66 "negative" experiments were not available for this analysis due to publication bias, we would still have observed spatial convergence of INS in the rTPJ. By contrast, the cluster in the right superior temporal gyrus did not survive the inclusion of the defined minimum of 12 additional noise-experiments.

2.2 FNIRS meta-analysis sensitivity analyses

2.2.1 Alternative "fNIRS-Indices"

In addition to the "INS-to-all-channel-ratio" weighted by subject number, we also evaluated the ratio weighted by the number of experiments as well as the raw count of "INS-channels" as parcel-wise indices. We, however, emphasize that only the first index which is reported in the main paper incorporates all available information (presence of "INS-channels" in relation to the times a region was sampled and number of subjects)

Based on exact p values estimated from permutation of parcel-channel assignments, we observed significant results for left inferior-anterior prefrontal regions across all evaluated measures. Additionally, while evaluation of the channel ratio weighted by subjects indicated right temporal brain regions, results based on the INS channel count pointed to left temporal and parietal regions and based on the channel-ratio weighted by the number of experiments we found a significant right frontomedial parcel (Figure S5). Again, no p value survived FDR correction.

2.2.2 Modelling of spatial uncertainty

To account for spatial uncertainty of fNIRS data in all fNIRS meta-analyses, we iteratively repeated the parcel-wise fNIRS meta-analysis as well as the ALE analysis with spatially randomized fNIRS coordinates (1 cm radius, 1,000 iterations) and assessed the percentages of iterations in which significant results at the original brain locations were observed.

In the fNIRS-only meta-analysis, we generally observed a high sensitivity of cluster significance towards randomization of parcel-coordinates. Especially the relatively small rTPJ parcel was highly sensitive, showing sub-threshold p values in only 7.9 % of iterations ($median\ p = .28$) in the main evaluated fNIRS index. The highest consistency was found for the right inferior temporal parcel showing persistence in 48 % of iterations ($median\ p = .052$). The overall results for all fNIRS indices are displayed in Table S6 and Figure S5. Concerning the combined fMRI-fNIRS ALE, coordinate randomization least affected the rTPJ and the left and right superior frontal clusters which emerged in 100 % of iterations, while the right middle frontal cluster was found in 89.1 % of iterations.

2.2.3 Restricted set of fNIRS experiments

To confirm our fNIRS-results, we restricted the included experiments to a more conservative selection including only experiments explicitly contrasting interaction with control, rest, or randomization conditions and recalculated all analyses.

We observed a generally comparable pattern but in the parcellation-based fNIRS-only meta-analysis only prefrontal parcels showed significance for the "INS channel ratios" weighted by number of subjects or experiments while the fNIRS evaluation based on the raw INS channel count remained stable (p uncorrected; Figure S5). In the combined fMRI-fNIRS ALE, we mainly observed a reduction of cluster sizes (Tables S1 and S2).

2.3 MACM sensitivity analyses

2.3.1 Controlling for baseline activation probability

Specific coactivation likelihood estimation (SCALE) is an alternative meta-analytic connectivity modeling (MACM) algorithm controlling for the baseline probability of observing coactivation independent of the chosen seed (*35*). We calculated a SCALE analysis using all studies in the BrainMap database as baseline (N = 3,098), to estimate the brain regions most uniquely coactivating with the rTPJ.

Here, we observed the left TPJ region, and to a lesser extent right insula, as specific functional connections of the rTPJ, further indicating the TPJs as hub regions of the observed INS-related network (Figure S3B).

2.3.2 Spatial alignment between INS-ALE and MACM activation patterns

To estimate whether the MACM network mirrors a brain-wide activation pattern that was already present in the original meta-analytic INS map beyond the rTPJ activation, we correlated the parcellated whole-brain maps derived from both analyses.

We observed a spatial alignment pattern driven by bilateral TPJs, insulae as well as dorsolateral prefrontal cortices, possibly indicating a role of these regions in INS but a lack of power to detect these as areas of spatial convergence in the main meta-analysis (Figure S3C).

2.4 Spatial relationships to established resting-state networks

We characterized the rTPJ cluster and the MACM network in respect to their spatial overlap with established brain-wide resting-state networks (*15*). We adopted a frequently used method characterizing the *absolute* and *relative distributions* of our target volumes across these networks (see method). We then permuted the input coordinates within all gray matter voxels (1,000 iterations), tested the resulting maps for meta-analytic convergence, and calculated absolute and relative distributions for each null map. From these null distributions, empirical p values were estimated.

The result is shown in Figure 2E. Looking at the absolute distributions, the rTPJ cluster was significantly associated with the default mode network ($p = .001, q = .002$), the dorsal attention ($p = .001, q = .002$), and the ventral attention network ($p = .026, q = .040$). The MACM network showed a widespread pattern (default mode, dorsal attention, ventral attention, frontoparietal, and somatomotor network: $p = .001, q = .002$). Concerning the relative distributions, the rTPJ cluster did not show significant associations while, in confirmation of the relationship between INS and attention networks, associations significant at an uncorrected alpha-level were observed between the MACM network and the ventral ($p = .004, q = .056$) and dorsal ($p = .047, q = .243$) attention networks.

2.5 Neurotransmitter-associations sensitivity analyses

2.5.1 $GABA_A$-related mRNA expression

To validate the strong association found to the $GABA_A$ receptor, and further clarify which subtype of $GABA_A$ receptors may drive the association, we collected a list of GABA-related genes (*27*, *28*), clustered these according to their spatial co-expression profiles (Figure S7A), and assessed spatial correlation patterns between INS and cluster-wise mRNA expression data.

Two GABA gene clusters were significantly associated with INS ($Z = .43, p = .007, q = .014$ and $Z = .45, p = .005, q = .014$). In line with prior data on the molecular target of the applied $GABA_A$ tracer (*27*), one of these clusters comprised the α1-$GABA_A$ receptor subunit (GABRA1) and parvalbumin (PVALB), of which the latter is considered a marker of fast-spiking parvalbumin-expressing interneurons, the largest group of cortical inhibitory neurons (*36*) (Figure S7B, clusters 2 and 3; Table S8).

3 Supplementary References

1. J. L. Lancaster, D. Tordesillas-Gutiérrez, M. Martinez, F. Salinas, A. Evans, K. Zilles, J. C. Mazziotta, P. T. Fox, Bias between MNI and Talairach coordinates analyzed using the ICBM-152 brain template. *Hum. Brain Mapp.* **28**, 1194–1205 (2007).
2. D. Tsuzuki, V. Jurcak, A. K. Singh, M. Okamoto, E. Watanabe, I. Dan, Virtual spatial registration of stand-alone fNIRS data to MNI space. *NeuroImage*. **34**, 1506–1518 (2007).
3. X. Cui, D. M. Bryant, A. L. Reiss, NIRS-based hyperscanning reveals increased interpersonal coherence in superior frontal cortex during cooperation. *Neuroimage*. **59**, 2430–2437 (2012).
4. J. Liu, R. Zhang, B. Geng, T. Zhang, D. Yuan, S. Otani, X. Li, Interplay between prior knowledge and communication mode on teaching effectiveness: Interpersonal neural synchronization as a neural marker. *Neuroimage*. **193**, 93–102 (2019).
5. K. Lu, T. Yu, N. Hao, Creating while taking turns, the choice to unlocking group creative potential. *NeuroImage*. **219**, 117025 (2020).
6. R. M. Ball, thesis (2011).
7. C. R. Harrison, K. M. Robinette, "CAESAR: Summary statistics for the adult population (ages 18-65) of the United States of America" (AIR FORCE RESEARCH LAB WRIGHT-PATTERSON AFB OH HUMAN EFFECTIVENESS DIRECTORATE, 2002).
8. F. Acar, R. Seurinck, S. Eickhoff, B. Moerkerke, Assessing robustness against potential publication bias in Activation Likelihood Estimation (ALE) meta-analyses for fMRI. *PLOS ONE*. **13**, e0208177 (2018).
9. R. J. Cooper, M. Caffini, J. Dubb, Q. Fang, A. Custo, D. Tsuzuki, B. Fischl, W. Wells, I. Dan, D. A. Boas, Validating atlas-guided DOT: A comparison of diffuse optical tomography informed by atlas and subject-specific anatomies. *NeuroImage*. **62**, 1999–2006 (2012).
10. D. Tsuzuki, I. Dan, Spatial registration for functional near-infrared spectroscopy: From channel position on the scalp to cortical location in individual and group analyses. *NeuroImage*. **85**, 92–103 (2014).
11. D. C. Van Essen, S. M. Smith, D. M. Barch, T. E. J. Behrens, E. Yacoub, K. Ugurbil, The WU-Minn Human Connectome Project: An overview. *NeuroImage*. **80**, 62–79 (2013).
12. WU-Minn Consortium Human Connectome Project, WU-Minn HCP 900 Subjects Data Release Reference Manual (2015), (available at https://www.humanconnectome.org/study/hcp-young-adult/document/900-subjects-data-release).
13. S. Whitfield-Gabrieli, A. Nieto-Castanon, Conn: a functional connectivity toolbox for correlated and anticorrelated brain networks. *Brain connectivity*. **2**, 125–141 (2012).
14. K. Murphy, R. M. Birn, D. A. Handwerker, T. B. Jones, P. A. Bandettini, The impact of global signal regression on resting state correlations: Are anti-correlated networks introduced? *NeuroImage*. **44**, 893–905 (2009).
15. B. T. T. Yeo, F. M. Krienen, J. Sepulcre, M. R. Sabuncu, D. Lashkari, M. Hollinshead, J. L. Roffman, J. W. Smoller, L. Zöllei, J. R. Polimeni, B. Fischl, H. Liu, R. L. Buckner, The organization of the human cerebral cortex estimated by intrinsic functional connectivity. *Journal of Neurophysiology*. **106**, 1125–1165 (2011).
16. E. Y. Choi, B. T. T. Yeo, R. L. Buckner, The organization of the human striatum estimated by intrinsic functional connectivity. *J Neurophysiol*. **108**, 2242–2263 (2012).
17. B. T. T. Yeo, Thalamic resting-state networks. *Twitter* (2020), (available at https://twitter.com/bttyeo/status/1248992127985434624).
18. T. Chen, B. Becker, J. Camilleri, L. Wang, S. Yu, S. B. Eickhoff, C. Feng, A domain-general brain network underlying emotional and cognitive interference processing: evidence from coordinate-based and functional connectivity meta-analyses. *Brain Struct Funct*. **223**, 3813–3840 (2018).
19. M. J. Hawrylycz, E. S. Lein, A. L. Guillozet-Bongaarts, E. H. Shen, L. Ng, J. A. Miller, L. N. van de Lagemaat, K. A. Smith, A. Ebbert, Z. L. Riley, C. Abajian, C. F. Beckmann, A. Bernard, D. Bertagnolli, A. F. Boe, P. M. Cartagena, M. M. Chakravarty, M. Chapin, J. Chong, R. A. Dalley, B. D. Daly, C. Dang, S. Datta, N. Dee, T. A. Dolbeare, V. Faber, D. Feng, D. R. Fowler, J. Goldy, B. W. Gregor, Z. Haradon, D. R. Haynor, J. G. Hohmann, S. Horvath, R. E. Howard, A. Jeromin, J. M. Jochim, M. Kinnunen, C. Lau, E. T. Lazarz, C. Lee, T. A. Lemon, L. Li, Y. Li, J. A. Morris, C. C. Overly, P. D. Parker, S. E. Parry, M. Reding, J. J. Royall, J. Schulkin, P. A. Sequeira, C. R. Slaughterbeck, S. C. Smith, A. J. Sodt, S. M. Sunkin, B. E. Swanson, M. P. Vawter, D. Williams, P. Wohnoutka, H. R. Zielke, D. H. Geschwind, P. R. Hof, S. M. Smith, C. Koch, S. G. N. Grant, A. R. Jones, An anatomically comprehensive atlas of the adult human brain transcriptome. *Nature*. **489**, 391–399 (2012).
20. R. D. Markello, A. Arnatkeviciute, J.-B. Poline, B. D. Fulcher, A. Fornito, B. Misic, Standardizing workflows in imaging transcriptomics with the abagen toolbox. *eLife*. **10**, e72129 (2021).
21. A. Schaefer, R. Kong, E. M. Gordon, T. O. Laumann, X.-N. Zuo, A. J. Holmes, S. B. Eickhoff, B. T. T. Yeo, Local-Global Parcellation of the Human Cerebral Cortex from Intrinsic Functional Connectivity MRI. *Cereb Cortex*. **28**, 3095–3114 (2018).
22. Y. Tian, D. S. Margulies, M. Breakspear, A. Zalesky, Topographic organization of the human subcortex unveiled with functional connectivity gradients. *Nat Neurosci*. **23**, 1421–1432 (2020).
23. A. Arnatkevičiūtė, B. D. Fulcher, A. Fornito, A practical guide to linking brain-wide gene expression and neuroimaging data. *NeuroImage*. **189**, 353–367 (2019).
24. J. Quackenbush, Microarray data normalization and transformation. *Nat Genet*. **32 Suppl**, 496–501 (2002).
25. M. Hawrylycz, J. A. Miller, V. Menon, D. Feng, T. Dolbeare, A. L. Guillozet-Bongaarts, A. G. Jegga, B. J. Aronow, C.-K. Lee, A. Bernard, M. F. Glasser, D. L. Dierker, J. Menche, A. Szafer, F. Collman, P. Grange, K. A. Berman, S. Mihalas, Z. Yao, L. Stewart, A.-L. Barabási, J. Schulkin, J. Phillips, L. Ng, C. Dang, D. R. Haynor, A. Jones, D. C. Van Essen, C. Koch, E. Lein, Canonical genetic signatures of the adult human brain. *Nat Neurosci*. **18**, 1832–1844 (2015).
26. B. D. Fulcher, M. A. Little, N. S. Jones, Highly comparative time-series analysis: the empirical structure of time series and their methods. *Journal of The Royal Society Interface*. **10**, 20130048 (2013).
27. P. B. Lukow, D. Martins, M. Veronese, A. C. Vernon, P. McGuire, F. E. Turkheimer, G. Modinos, Cellular and molecular signatures of in vivo GABAergic neurotransmission in the human brain (2021), , doi:10.1101/2021.06.17.448812.
28. L. Martini, R. Bardini, S. D. Carlo, Meta-Analysis of cortical inhibitory interneurons markers landscape and their performances in scRNA-seq studies (2021), , doi:10.1101/2021.11.03.467049.
29. P. Virtanen, R. Gommers, T. E. Oliphant, M. Haberland, T. Reddy, D. Cournapeau, E. Burovski, P. Peterson, W. Weckesser, J. Bright, S. J. van der Walt, M. Brett, J. Wilson, K. J. Millman, N. Mayorov, A. R. J. Nelson, E. Jones, R. Kern, E. Larson, C. J. Carey, İ. Polat, Y. Feng, E. W. Moore, J. VanderPlas, D. Laxalde, J. Perktold, R. Cimrman, I. Henriksen, E. A. Quintero, C. R. Harris, A. M. Archibald, A. H. Ribeiro, F. Pedregosa, P. van Mulbregt, SciPy 1.0: fundamental algorithms for scientific computing in Python. *Nat Methods*. **17**, 261–272 (2020).
30. L. D. Lotter, J. Dukart, JuSpyce - a toolbox for flexible assessment of spatial associations between brain images (2022), , doi:10.5281/zenodo.6884932.

31. R. Azen, D. V. Budescu, The dominance analysis approach for comparing predictors in multiple regression. *Psychol Methods*. **8**, 129–148 (2003).
32. L. D. Lotter, J. Dukart, B. D. Fulcher, ABAnnotate: A toolbox for ensemble-based multimodal gene-category enrichment analysis of human neuroimaging data (2022), , doi:10.5281/zenodo.6463329.
33. M. J. M. F. Reijnders, R. M. Waterhouse, Summary Visualizations of Gene Ontology Terms With GO-Figure! *Frontiers in Bioinformatics*. **1** (2021) (available at https://www.frontiersin.org/article/10.3389/fbinf.2021.638255).
34. C. Pesquita, "Semantic Similarity in the Gene Ontology" in *The Gene Ontology Handbook*, C. Dessimoz, N. Škunca, Eds. (Springer, New York, NY, 2017; https://doi.org/10.1007/978-1-4939-3743-1_12), *Methods in Molecular Biology*, pp. 161–173.
35. R. Langner, C. Rottschy, A. R. Laird, P. T. Fox, S. B. Eickhoff, Meta-analytic connectivity modeling revisited: Controlling for activation base rates. *NeuroImage*. **99**, 559–570 (2014).
36. R. Tremblay, S. Lee, B. Rudy, GABAergic Interneurons in the Neocortex: From Cellular Properties to Circuits. *Neuron*. **91**, 260–292 (2016).
37. E. Bilek, M. Ruf, A. Schäfer, C. Akdeniz, V. D. Calhoun, C. Schmahl, C. Demanuele, H. Tost, P. Kirsch, A. Meyer-Lindenberg, Information flow between interacting human brains: Identification, validation, and relationship to social expertise. *Proc Natl Acad Sci USA*. **112**, 5207–5212 (2015).
38. I. Gordon, S. Wallot, Y. Berson, Group-level physiological synchrony and individual-level anxiety predict positive affective behaviors during a group decision-making task. *Psychophysiology*. **58**, e13857 (2021).
39. T. Koike, H. C. Tanabe, S. Okazaki, E. Nakagawa, A. T. Sasaki, K. Shimada, S. K. Sugawara, H. K. Takahashi, K. Yoshihara, J. Bosch-Bayard, N. Sadato, Neural substrates of shared attention as social memory: A hyperscanning functional magnetic resonance imaging study. *Neuroimage*. **125**, 401–412 (2016).
40. T. Koike, M. Sumiya, E. Nakagawa, S. Okazaki, N. Sadato, What Makes Eye Contact Special? Neural Substrates of On-Line Mutual Eye-Gaze: A Hyperscanning fMRI Study. *eNeuro*. **6** (2019), doi:10.1523/ENEURO.0284-18.2019.
41. T. Koike, H. C. Tanabe, S. Adachi-Abe, S. Okazaki, E. Nakagawa, A. T. Sasaki, K. Shimada, S. K. Sugawara, H. K. Takahashi, K. Yoshihara, N. Sadato, Role of the right anterior insular cortex in joint attention-related identification with a partner. *Soc Cogn Affect Neurosci*. **14**, 1131–1145 (2019).
42. K. Miyata, T. Koike, E. Nakagawa, T. Harada, M. Sumiya, T. Yamamoto, N. Sadato, Neural substrates for sharing intention in action during face-to-face imitation. *NeuroImage*. **233**, 117916 (2021).
43. D. N. Saito, H. C. Tanabe, K. Izuma, M. J. Hayashi, Y. Morito, H. Komeda, H. Uchiyama, H. Kosaka, H. Okazawa, Y. Fujibayashi, N. Sadato, "Stay Tuned": Inter-Individual Neural Synchronization During Mutual Gaze and Joint Attention. *Front. Integr. Neurosci.* **4** (2010), doi:10.3389/fnint.2010.00127.
44. M. Salazar, D. J. Shaw, M. Gajdoš, R. Mareček, K. Czekóová, M. Mikl, M. Brázdil, You took the words right out of my mouth: Dual-fMRI reveals intra- and inter-personal neural processes supporting verbal interaction. *NeuroImage*. **228**, 117697 (2021).
45. D. J. Shaw, K. Czekóová, R. Staněk, R. Mareček, T. Urbánek, J. Špalek, L. Kopečková, J. Řezáč, M. Brázdil, A dual-fMRI investigation of the iterated Ultimatum Game reveals that reciprocal behaviour is associated with neural alignment. *Scientific Reports*. **8**, 10896 (2018).
46. D. J. Shaw, K. Czekóová, B. Špiláková, M. Salazar, P. Řezáč, V. Kurečková, P. Zámečník, M. Brázdil, A neuroscientific evaluation of driver rehabilitation: Functional neuroimaging demonstrates the effectiveness of empathy induction in altering brain responses during social information processing. *PLoS One*. **15**, e0232222 (2020).
47. K. Spiegelhalder, S. Ohlendorf, W. Regen, B. Feige, L. Tebartz van Elst, C. Weiller, J. Hennig, M. Berger, O. Tüscher, Interindividual synchronization of brain activity during live verbal communication. *Behavioural Brain Research*. **258**, 75–79 (2014).
48. B. Špiláková, D. J. Shaw, K. Czekóová, R. Mareček, M. Brázdil, Getting into sync: Data-driven analyses reveal patterns of neural coupling that distinguish among different social exchanges. *Human Brain Mapping*. **41**, 1072–1083 (2020).
49. L.-S. Wang, J.-T. Cheng, I.-J. Hsu, S. Liou, C.-C. Kung, D.-Y. Chen, M.-H. Weng, Distinct cerebral coherence in task-based fMRI hyperscanning: cooperation versus competition (2022), , doi:10.1093/cercor/bhac075.
50. H. Xie, I. I. Karipidis, A. Howell, M. Schreier, K. E. Sheau, M. K. Manchanda, R. Ayub, G. H. Glover, M. Jung, A. L. Reiss, M. Saggar, Finding the neural correlates of collaboration using a three-person fMRI hyperscanning paradigm. *PNAS*. **117**, 23066–23072 (2020).
51. A. Yoshioka, H. C. Tanabe, M. Sumiya, E. Nakagawa, S. Okazaki, T. Koike, N. Sadato, Neural substrates of shared visual experiences: a hyperscanning fMRI study. *Social Cognitive and Affective Neuroscience*. **16**, 1264–1275 (2021).
52. S. Anders, J. Heinzle, N. Weiskopf, T. Ethofer, J.-D. Haynes, Flow of affective information between communicating brains. *NeuroImage*. **54**, 439–446 (2011).
53. S. Dikker, L. J. Silbert, U. Hasson, J. D. Zevin, On the Same Wavelength: Predictable Language Enhances Speaker–Listener Brain-to-Brain Synchrony in Posterior Superior Temporal Gyrus. *J. Neurosci.* **34**, 6267–6272 (2014).
54. K. Kostorz, V. L. Flanagin, S. Glasauer, Synchronization between instructor and observer when learning a complex bimanual skill. *NeuroImage*. **216**, 116659 (2020).
55. L. Liu, X. Ding, H. Li, Q. Zhou, D. Gao, C. Lu, G. Ding, Reduced listener–speaker neural coupling underlies speech understanding difficulty in older adults. *Brain Struct Funct*. **226**, 1571–1584 (2021).
56. L. Liu, H. Li, Z. Ren, Q. Zhou, Y. Zhang, C. Lu, J. Qiu, H. Chen, G. Ding, The "Two-Brain" Approach Reveals the Active Role of Task-Deactivated Default Mode Network in Speech Comprehension. *Cerebral Cortex* (2022), doi:10.1093/cercor/bhab521.
57. L. J. Silbert, C. J. Honey, E. Simony, D. Poeppel, U. Hasson, Coupled neural systems underlie the production and comprehension of naturalistic narrative speech. *PNAS*. **111**, E4687–E4696 (2014).
58. D. Smirnov, H. Saarimäki, E. Glerean, R. Hari, M. Sams, L. Nummenmaa, Emotions amplify speaker–listener neural alignment. *Human Brain Mapping*. **40**, 4777–4788 (2019).
59. G. J. Stephens, L. J. Silbert, U. Hasson, Speaker-listener neural coupling underlies successful communication. *Proceedings of the National Academy of Sciences*. **107**, 14425–14430 (2010).
60. M. Balconi, G. Fronda, M. E. Vanutelli, Donate or receive? Social hyperscanning application with fNIRS. *Curr Psychol*. **38**, 991–1002 (2019).
61. M. Balconi, L. Pezard, J.-L. Nandrino, M. E. Vanutelli, Two is better than one: The effects of strategic cooperation on intra- and inter-brain connectivity by fNIRS. *PLOS ONE*. **12**, e0187652 (2017).
62. M. Balconi, M. E. Vanutelli, L. Gatti, Functional brain connectivity when cooperation fails. *Brain Cogn*. **123**, 65–73 (2018).
63. R. Cañigueral, X. Zhang, J. A. Noah, I. Tachtsidis, A. F. de C. Hamilton, J. Hirsch, Facial and neural mechanisms during interactive disclosure of biographical information. *NeuroImage*. **226**, 117572 (2021).
64. M. Chen, T. Zhang, R. Zhang, N. Wang, Q. Yin, Y. Li, J. Liu, T. Liu, X. Li, Neural alignment during face-to-face spontaneous deception: Does gender make a difference? *Human Brain Mapping*. **41**, 4964–4981 (2020).
65. X. Cheng, X. Li, Y. Hu, Synchronous brain activity during cooperative exchange depends on gender of partner: A fNIRS-based hyperscanning study. *Hum Brain Mapp*. **36**, 2039–2048 (2015).

66. X. Cheng, Y. Pan, Y. Hu, Y. Hu, Coordination Elicits Synchronous Brain Activity Between Co-actors: Frequency Ratio Matters. *Frontiers in Neuroscience*. **13** (2019) (available at https://www.frontiersin.org/article/10.3389/fnins.2019.01071).
67. X. Cheng, Y. Zhu, Y. Hu, X. Zhou, Y. Pan, Y. Hu, Integration of social status and trust through interpersonal brain synchronization. *NeuroImage*. **246**, 118777 (2022).
68. H. Duan, T. Yang, X. Wang, Y. Kan, H. Zhao, Y. Li, W. Hu, Is the creativity of lovers better? A behavioral and functional near-infrared spectroscopy hyperscanning study. *Current Psychology*. **41**, 41–54 (2022).
69. X. Feng, B. Sun, C. Chen, W. Li, Y. Wang, W. Zhang, W. Xiao, Y. Shao, Self–other overlap and interpersonal neural synchronization serially mediate the effect of behavioral synchronization on prosociality. *Social Cognitive and Affective Neuroscience*. **15**, 203–214 (2020).
70. G. Fronda, M. Balconi, The effect of interbrain synchronization in gesture observation: A fNIRS study. *Brain and Behavior*. **10**, e01663 (2020).
71. Y. Hu, Y. Hu, X. Li, Y. Pan, X. Cheng, Brain-to-brain synchronization across two persons predicts mutual prosociality. *Social Cognitive and Affective Neuroscience*. **12**, 1835–1844 (2017).
72. T. Koide, S. Shimada, Cheering Enhances Inter-Brain Synchronization Between Sensorimotor Areas of Player and Observer. *Japanese Psychological Research*. **60**, 265–275 (2018).
73. L. Li, H. Wang, H. Luo, X. Zhang, R. Zhang, X. Li, Interpersonal Neural Synchronization During Cooperative Behavior of Basketball Players: A fNIRS-Based Hyperscanning Study. *Frontiers in Human Neuroscience*. **14** (2020) (available at https://www.frontiersin.org/article/10.3389/fnhum.2020.00169).
74. Y. Li, M. Chen, R. Zhang, X. Li, Experiencing happiness together facilitates dyadic coordination through the enhanced interpersonal neural synchronization. *Social Cognitive and Affective Neuroscience*, nsab114 (2021).
75. Y. Li, R. Chen, O. Turel, T. Feng, C.-Z. Zhu, Q. He, Dyad sex composition effect on inter-brain synchronization in face-to-face cooperation. *Brain Imaging and Behavior*. **15**, 1667–1675 (2021).
76. J. Liu, R. Zhang, B. Geng, T. Zhang, D. Yuan, S. Otani, X. Li, Interplay between prior knowledge and communication mode on teaching effectiveness: Interpersonal neural synchronization as a neural marker. *Neuroimage*. **193**, 93–102 (2019).
77. N. Liu, C. Mok, E. E. Witt, A. H. Pradhan, J. E. Chen, A. L. Reiss, NIRS-Based Hyperscanning Reveals Inter-brain Neural Synchronization during Cooperative Jenga Game with Face-to-Face Communication. *Front. Hum. Neurosci.* **10** (2016), doi:10.3389/fnhum.2016.00082.
78. T. Liu, G. Saito, C. Lin, H. Saito, Inter-brain network underlying turn-based cooperation and competition: A hyperscanning study using near-infrared spectroscopy. *Scientific Reports*. **7**, 8684 (2017).
79. W. Liu, H. P. Branigan, L. Zheng, Y. Long, X. Bai, K. Li, H. Zhao, S. Zhou, M. J. Pickering, C. Lu, Shared neural representations of syntax during online dyadic communication. *Neuroimage*. **198**, 63–72 (2019).
80. Y. Long, C. Chen, K. Wu, S. Zhou, F. Zhou, L. Zheng, H. Zhao, Y. Zhai, C. Lu, Interpersonal Conflict Increases Interpersonal Neural Synchronization in Romantic Couples. *Cerebral Cortex*, bhab413 (2021).
81. Y. Long, L. Zheng, H. Zhao, S. Zhou, Y. Zhai, C. Lu, Interpersonal Neural Synchronization during Interpersonal Touch Underlies Affiliative Pair Bonding between Romantic Couples. *Cerebral Cortex*. **31**, 1647–1659 (2021).
82. K. Lu, N. Hao, When do we fall in neural synchrony with others? *Social Cognitive and Affective Neuroscience*. **14**, 253–261 (2019).
83. K. Lu, X. Qiao, N. Hao, Praising or keeping silent on partner's ideas: Leading brainstorming in particular ways. *Neuropsychologia*. **124**, 19–30 (2019).
84. K. Lu, J. Teng, N. Hao, Gender of partner affects the interaction pattern during group creative idea generation. *Exp Brain Res*. **238**, 1157–1168 (2020).
85. K. Lu, H. Xue, T. Nozawa, N. Hao, Cooperation Makes a Group be More Creative. *Cerebral Cortex*. **29**, 3457–3470 (2019).
86. T. Nozawa, K. Sakaki, S. Ikeda, H. Jeong, S. Yamazaki, K. H. dos S. Kawata, N. Y. dos S. Kawata, Y. Sasaki, K. Kulason, K. Hirano, Y. Miyake, R. Kawashima, Prior physical synchrony enhances rapport and inter-brain synchronization during subsequent educational communication. *Sci Rep*. **9**, 12747 (2019).
87. T. Nozawa, Y. Sasaki, K. Sakaki, R. Yokoyama, R. Kawashima, Interpersonal frontopolar neural synchronization in group communication: An exploration toward fNIRS hyperscanning of natural interactions. *Neuroimage*. **133**, 484–497 (2016).
88. Y. Pan, X. Cheng, Z. Zhang, X. Li, Y. Hu, Cooperation in lovers: An fNIRS-based hyperscanning study. *Hum Brain Mapp*. **38**, 831–841 (2017).
89. Y. Pan, S. Dikker, P. Goldstein, Y. Zhu, C. Yang, Y. Hu, Instructor-learner brain coupling discriminates between instructional approaches and predicts learning. *NeuroImage*. **211**, 116657 (2020).
90. Y. Pan, C. Guyon, G. Borragán, Y. Hu, P. Peigneux, Interpersonal brain synchronization with instructor compensates for learner's sleep deprivation in interactive learning. *Biochemical Pharmacology*. **191**, 114111 (2021).
91. Y. Pan, G. Novembre, B. Song, X. Li, Y. Hu, Interpersonal synchronization of inferior frontal cortices tracks social interactive learning of a song. *NeuroImage*. **183**, 280–290 (2018).
92. P. Pinti, A. Devoto, I. Greenhalgh, I. Tachtsidis, P. W. Burgess, A. F. de C Hamilton, The role of anterior prefrontal cortex (area 10) in face-to-face deception measured with fNIRS. *Social Cognitive and Affective Neuroscience*. **16**, 129–142 (2021).
93. L. E. Quiñones-Camacho, F. A. Fishburn, K. Belardi, D. L. Williams, T. J. Huppert, S. B. Perlman, Dysfunction in interpersonal neural synchronization as a mechanism for social impairment in autism spectrum disorder. *Autism Research*. **14**, 1585–1596 (2021).
94. B. Sun, W. Xiao, X. Feng, Y. Shao, W. Zhang, W. Li, Behavioral and brain synchronization differences between expert and novice teachers when collaborating with students. *Brain and Cognition*. **139**, 105513 (2020).
95. B. Sun, W. Xiao, S. Lin, Y. Shao, W. Li, W. Zhang, Cooperation with partners of differing social experience: An fNIRS-based hyperscanning study. *Brain and Cognition*. **154**, 105803 (2021).
96. H. Tang, X. Mai, S. Wang, C. Zhu, F. Krueger, C. Liu, Interpersonal brain synchronization in the right temporo-parietal junction during face-to-face economic exchange. *Social Cognitive and Affective Neuroscience*. **11**, 23–32 (2016).
97. C. Wang, T. Zhang, Z. Shan, J. Liu, D. Yuan, X. Li, Dynamic interpersonal neural synchronization underlying pain-induced cooperation in females. *Hum Brain Mapp*. **40**, 3222–3232 (2019).
98. H. Xue, K. Lu, N. Hao, Cooperation makes two less-creative individuals turn into a highly-creative pair. *Neuroimage*. **172**, 527–537 (2018).
99. J. Yang, H. Zhang, J. Ni, C. K. W. De Dreu, Y. Ma, Within-group synchronization in the prefrontal cortex associates with intergroup conflict. *Nat Neurosci*. **23**, 754–760 (2020).
100. M. Zhang, H. Jia, G. Wang, Interbrain Synchrony of Team Collaborative Decision-Making: An fNIRS Hyperscanning Study. *Frontiers in Human Neuroscience*. **15** (2021) (available at https://www.frontiersin.org/article/10.3389/fnhum.2021.702959).
101. M. Zhang, H. Jia, M. Zheng, Interbrain Synchrony in the Expectation of Cooperation Behavior: A Hyperscanning Study Using Functional Near-Infrared Spectroscopy. *Frontiers in Psychology*. **11** (2020) (available at https://www.frontiersin.org/article/10.3389/fpsyg.2020.542093).

102. M. Zhang, H. Jia, M. Zheng, T. Liu, Group decision-making behavior in social dilemmas: Inter-brain synchrony and the predictive role of personality traits. *Personality and Individual Differences*. **168**, 110315 (2021).
103. M. Zhang, T. Liu, M. Pelowski, D. Yu, Gender difference in spontaneous deception: A hyperscanning study using functional near-infrared spectroscopy. *Scientific Reports*. **7**, 7508 (2017).
104. M. Zhang, T. Liu, M. Pelowski, H. Jia, D. Yu, Social risky decision-making reveals gender differences in the TPJ: A hyperscanning study using functional near-infrared spectroscopy. *Brain Cogn*. **119**, 54–63 (2017).
105. R. Zhang, X. Zhou, D. Feng, D. Yuan, S. Li, C. Lu, X. Li, Effects of acute psychosocial stress on interpersonal cooperation and competition in young women. *Brain and Cognition*. **151**, 105738 (2021).
106. Y. Zhang, T. Meng, Y. Yang, Y. Hu, Experience-Dependent Counselor-Client Brain Synchronization during Psychological Counseling. *eNeuro*. **7** (2020), doi:10.1523/ENEURO.0236-20.2020.
107. H. Zhao, Y. Li, Y. Wang, X. Wang, Y. Kan, T. Yang, W. Hu, H. Duan, Acute stress makes women's group decisions more rational: A functional near-infrared spectroscopy (fNIRS)–based hyperscanning study. *Journal of Neuroscience, Psychology, and Economics*. **14**, 20–35 (2021).
108. Y. Zhao, R.-N. Dai, X. Xiao, Z. Zhang, L. Duan, Z. Li, C.-Z. Zhu, Independent component analysis-based source-level hyperlink analysis for two-person neuroscience studies. *JBO*. **22**, 027004 (2017).
109. L. Zheng, C. Chen, W. Liu, Y. Long, H. Zhao, X. Bai, Z. Zhang, Z. Han, L. Liu, T. Guo, B. Chen, G. Ding, C. Lu, Enhancement of teaching outcome through neural prediction of the students' knowledge state. *Hum Brain Mapp*. **39**, 3046–3057 (2018).
110. L. Zheng, W. Liu, Y. Long, Y. Zhai, H. Zhao, X. Bai, S. Zhou, K. Li, H. Zhang, L. Liu, T. Guo, G. Ding, C. Lu, Affiliative bonding between teachers and students through interpersonal synchronisation in brain activity. *Social Cognitive and Affective Neuroscience*. **15**, 97–109 (2020).
111. Y. Zhu, V. Leong, Y. Hou, D. Zhang, Y. Pan, Y. Hu, Instructor–learner neural synchronization during elaborated feedback predicts learning transfer. *Journal of Educational Psychology* (2021), doi:10.1037/edu0000707.
112. Y. Hou, B. Song, Y. Hu, Y. Pan, Y. Hu, The averaged inter-brain coherence between the audience and a violinist predicts the popularity of violin performance. *NeuroImage*. **211**, 116655 (2020).
113. Z. Li, J. Li, B. Hong, G. Nolte, A. K. Engel, D. Zhang, Speaker–Listener Neural Coupling Reveals an Adaptive Mechanism for Speech Comprehension in a Noisy Environment. *Cerebral Cortex*. **31**, 4719–4729 (2021).
114. Y. Liu, E. A. Piazza, E. Simony, P. A. Shewokis, B. Onaral, U. Hasson, H. Ayaz, Measuring speaker–listener neural coupling with functional near infrared spectroscopy. *Sci Rep*. **7**, 43293 (2017).
115. C. M. Aasted, M. A. Yücel, R. J. Cooper, J. Dubb, D. Tsuzuki, L. Becerra, M. P. Petkov, D. Borsook, I. Dan, D. A. Boas, Anatomical guidance for functional near-infrared spectroscopy: AtlasViewer tutorial. *NPh*. **2**, 020801 (2015).
116. M. P. Notter, D. Gale, P. Herholz, R. Markello, M.-L. Notter-Bielser, K. Whitaker, AtlasReader: A Python package to generate coordinate tables, region labels, and informative figures from statistical MRI images. *Journal of Open Source Software*. **4**, 1257 (2019).
117. E. T. Rolls, C.-C. Huang, C.-P. Lin, J. Feng, M. Joliot, Automated anatomical labelling atlas 3. *NeuroImage*. **206**, 116189 (2020).
118. M. Savli, A. Bauer, M. Mitterhauser, Y.-S. Ding, A. Hahn, T. Kroll, A. Neumeister, D. Haeusler, J. Ungersboeck, S. Henry, S. A. Isfahani, F. Rattay, W. Wadsak, S. Kasper, R. Lanzenberger, Normative database of the serotonergic system in healthy subjects using multi-tracer PET. *Neuroimage*. **63**, 447–459 (2012).
119. J.-D. Gallezot, N. Nabulsi, A. Neumeister, B. Planeta-Wilson, W. A. Williams, T. Singhal, S. Kim, R. P. Maguire, T. McCarthy, J. J. Frost, Y. Huang, Y.-S. Ding, R. E. Carson, Kinetic modeling of the serotonin 5-HT(1B) receptor radioligand [(11)C]P943 in humans. *J Cereb Blood Flow Metab*. **30**, 196–210 (2010).
120. V. Beliveau, M. Ganz, L. Feng, B. Ozenne, L. Højgaard, P. M. Fisher, C. Svarer, D. N. Greve, G. M. Knudsen, A High-Resolution In Vivo Atlas of the Human Brain's Serotonin System. *J Neurosci*. **37**, 120–128 (2017).
121. R. Radhakrishnan, N. Nabulsi, E. Gaiser, J.-D. Gallezot, S. Henry, B. Planeta, S. Lin, J. Ropchan, W. Williams, E. Morris, D. C. D'Souza, Y. Huang, R. E. Carson, D. Matuskey, Age-Related Change in 5-HT6 Receptor Availability in Healthy Male Volunteers Measured with 11C-GSK215083 PET. *J Nucl Med*. **59**, 1445–1450 (2018).
122. F. J. G. Gómez, I. Huertas, J. A. L. Ramírez, D. G. Solís, Elaboración de una plantilla de SPM para la normalización de imágenes de PET con 18F-DOPA. *Imagen Diagnóstica*. **9**, 23–25 (2018).
123. S. Kaller, M. Rullmann, M. Patt, G.-A. Becker, J. Luthardt, J. Girbardt, P. M. Meyer, P. Werner, H. Barthel, A. Bresch, T. H. Fritz, S. Hesse, O. Sabri, Test-retest measurements of dopamine D1-type receptors using simultaneous PET/MRI imaging. *Eur J Nucl Med Mol Imaging*. **44**, 1025–1032 (2017).
124. C. M. Sandiego, J.-D. Gallezot, K. Lim, J. Ropchan, S. Lin, H. Gao, E. D. Morris, K. P. Cosgrove, Reference region modeling approaches for amphetamine challenge studies with [11C]FLB 457 and PET. *J Cereb Blood Flow Metab*. **35**, 623–629 (2015).
125. C. T. Smith, J. L. Crawford, L. C. Dang, K. L. Seaman, M. D. San Juan, A. Vijay, D. T. Katz, D. Matuskey, R. L. Cowan, E. D. Morris, D. H. Zald, G. R. Samanez-Larkin, Partial-volume correction increases estimated dopamine D2-like receptor binding potential and reduces adult age differences. *J Cereb Blood Flow Metab*. **39**, 822–833 (2019).
126. J. Dukart, Š. Holiga, C. Chatham, P. Hawkins, A. Forsyth, R. McMillan, J. Myers, A. R. Lingford-Hughes, D. J. Nutt, E. Merlo-Pich, C. Risterucci, L. Boak, D. Umbricht, S. Schobel, T. Liu, M. A. Mehta, F. O. Zelaya, S. C. Williams, G. Brown, M. Paulus, G. D. Honey, S. Muthukumaraswamy, J. Hipp, A. Bertolino, F. Sambataro, Cerebral blood flow predicts differential neurotransmitter activity. *Sci Rep*. **8**, 4074 (2018).
127. F. J. García-Gómez, D. García-Solís, F. J. Luis-Simón, V. A. Marín-Oyaga, F. Carrillo, P. Mir, R. J. Vázquez-Albertino, [Elaboration of the SPM template for the standardization of SPECT images with 123I-Ioflupane]. *Rev Esp Med Nucl Imagen Mol*. **32**, 350–356 (2013).
128. S. Hesse, G.-A. Becker, M. Rullmann, A. Bresch, J. Luthardt, M. K. Hankir, F. Zientek, G. Reißig, M. Patt, K. Arelin, D. Lobsien, U. Müller, S. Baldofski, P. M. Meyer, M. Blüher, M. Fasshauer, W. K. Fenske, M. Stumvoll, A. Hilbert, Y.-S. Ding, O. Sabri, Central noradrenaline transporter availability in highly obese, non-depressed individuals. *Eur J Nucl Med Mol Imaging*. **44**, 1056–1064 (2017).
129. Y.-S. Ding, T. Singhal, B. Planeta-Wilson, J.-D. Gallezot, N. Nabulsi, D. Labaree, J. Ropchan, S. Henry, W. Williams, R. E. Carson, A. Neumeister, R. T. Malison, PET imaging of the effects of age and cocaine on the norepinephrine transporter in the human brain using (S,S)-[(11)C]O-methylreboxetine and HRRT. *Synapse*. **64**, 30–38 (2010).
130. M. Nørgaard, V. Beliveau, M. Ganz, C. Svarer, L. H. Pinborg, S. H. Keller, P. S. Jensen, D. N. Greve, G. M. Knudsen, A high-resolution in vivo atlas of the human brain's benzodiazepine binding site of GABAA receptors. *Neuroimage*. **232**, 117878 (2021).
131. J. M. DuBois, O. G. Rousset, J. Rowley, M. Porras-Betancourt, A. J. Reader, A. Labbe, G. Massarweh, J.-P. Soucy, P. Rosa-Neto, E. Kobayashi, Characterization of age/sex and the regional distribution of mGluR5 availability in the healthy human brain measured by high-resolution [(11)C]ABP688 PET. *Eur J Nucl Med Mol Imaging*. **43**, 152–162 (2016).
132. J. Y. Hansen, G. Shafiei, R. D. Markello, K. Smart, S. M. L. Cox, M. Nørgaard, V. Beliveau, Y. Wu, J.-D. Gallezot, É. Aumont, S. Servaes, S. G. Scala, J. M. DuBois, G. Wainstein, G. Bezgin, T. Funck, T. W. Schmitz, R. N. Spreng, M. Galovic, M. J. Koepp, J. S. Duncan, J. P.

Coles, T. D. Fryer, F. I. Aigbirhio, C. J. McGinnity, A. Hammers, J.-P. Soucy, S. Baillet, S. Guimond, J. Hietala, M.-A. Bedard, M. Leyton, E. Kobayashi, P. Rosa-Neto, M. Ganz, G. M. Knudsen, N. Palomero-Gallagher, J. M. Shine, R. E. Carson, L. Tuominen, A. Dagher, B. Misic, Mapping neurotransmitter systems to the structural and functional organization of the human neocortex. *Nat Neurosci*, 1–13 (2022).

133. K. Smart, S. M. L. Cox, S. G. Scala, M. Tippler, N. Jaworska, M. Boivin, J. R. Séguin, C. Benkelfat, M. Leyton, Sex differences in [11C]ABP688 binding: a positron emission tomography study of mGlu5 receptors. *Eur J Nucl Med Mol Imaging*. **46**, 1179–1183 (2019).
134. M. Galovic, A. Al-Diwani, U. Vivekananda, F. Torrealdea, K. Erlandsson, T. D. Fryer, Y. T. Hong, B. A. Thomas, C. J. McGinnity, E. Edmond, K. Sander, E. Årstad, I. Jelcic, F. I. Aigbirhio, A. M. Groves, K. Thielemans, B. Hutton, A. Hammers, J. S. Duncan, J. P. Coles, A. Barnes, C. J. Stagg, M. C. Walker, S. R. Irani, M. J. Koepp, for the N. Investigators, In vivo NMDA receptor function in people with NMDA receptor antibody encephalitis (2021), , doi:1v.
135. A. T. Hillmer, I. Esterlis, J. D. Gallezot, F. Bois, M. Q. Zheng, N. Nabulsi, S. F. Lin, R. L. Papke, Y. Huang, O. Sabri, R. E. Carson, K. P. Cosgrove, Imaging of cerebral α4β2* nicotinic acetylcholine receptors with (-)-[(18)F]Flubatine PET: Implementation of bolus plus constant infusion and sensitivity to acetylcholine in human brain. *Neuroimage*. **141**, 71–80 (2016).
136. M. Naganawa, N. Nabulsi, S. Henry, D. Matuskey, S.-F. Lin, L. Slieker, A. J. Schwarz, N. Kant, C. Jesudason, K. Ruley, A. Navarro, H. Gao, J. Ropchan, D. Labaree, R. E. Carson, Y. Huang, First-in-Human Assessment of 11C-LSN3172176, an M1 Muscarinic Acetylcholine Receptor PET Radiotracer. *Journal of Nuclear Medicine*. **62**, 553–560 (2021).
137. M. Aghourian, C. Legault-Denis, J.-P. Soucy, P. Rosa-Neto, S. Gauthier, A. Kostikov, P. Gravel, M.-A. Bédard, Quantification of brain cholinergic denervation in Alzheimer's disease using PET imaging with [18F]-FEOBV. *Mol Psychiatry*. **22**, 1531–1538 (2017).
138. M.-A. Bedard, M. Aghourian, C. Legault-Denis, R. B. Postuma, J.-P. Soucy, J.-F. Gagnon, A. Pelletier, J. Montplaisir, Brain cholinergic alterations in idiopathic REM sleep behaviour disorder: a PET imaging study with 18F-FEOBV. *Sleep Med*. **58**, 35–41 (2019).
139. T. Kantonen, T. Karjalainen, J. Isojärvi, P. Nuutila, J. Tuisku, J. Rinne, J. Hietala, V. Kaasinen, K. Kalliokoski, H. Scheinin, J. Hirvonen, A. Vehtari, L. Nummenmaa, Interindividual variability and lateralization of μ-opioid receptors in the human brain. *NeuroImage*. **217**, 116922 (2020).
140. J.-D. Gallezot, B. Planeta, N. Nabulsi, D. Palumbo, X. Li, J. Liu, C. Rowinski, K. Chidsey, D. Labaree, J. Ropchan, S.-F. Lin, A. Sawant-Basak, T. J. McCarthy, A. W. Schmidt, Y. Huang, R. E. Carson, Determination of receptor occupancy in the presence of mass dose: [11C]GSK189254 PET imaging of histamine H3 receptor occupancy by PF-03654746. *J Cereb Blood Flow Metab*. **37**, 1095–1107 (2017).
141. M. D. Normandin, M.-Q. Zheng, K.-S. Lin, N. S. Mason, S.-F. Lin, J. Ropchan, D. Labaree, S. Henry, W. A. Williams, R. E. Carson, A. Neumeister, Y. Huang, Imaging the cannabinoid CB1 receptor in humans with [11C]OMAR: assessment of kinetic analysis methods, test-retest reproducibility, and gender differences. *J Cereb Blood Flow Metab*. **35**, 1313–1322 (2015).
142. S. J. Finnema, N. B. Nabulsi, T. Eid, K. Detyniecki, S.-F. Lin, M.-K. Chen, R. Dhaher, D. Matuskey, E. Baum, D. Holden, D. D. Spencer, J. Mercier, J. Hannestad, Y. Huang, R. E. Carson, Imaging synaptic density in the living human brain. *Sci Transl Med*. **8**, 348ra96 (2016).
143. E. H. Shen, C. C. Overly, A. R. Jones, The Allen Human Brain Atlas: Comprehensive gene expression mapping of the human brain. *Trends in Neurosciences*. **35**, 711–714 (2012).
144. J. Dukart, S. Holiga, M. Rullmann, R. Lanzenberger, P. C. T. Hawkins, M. A. Mehta, S. Hesse, H. Barthel, O. Sabri, R. Jech, S. B. Eickhoff, JuSpace: A tool for spatial correlation analyses of magnetic resonance imaging data with nuclear imaging derived neurotransmitter maps. *Human Brain Mapping*. **42**, 555–566 (2021).
145. R. D. Markello, J. Y. Hansen, Z.-Q. Liu, V. Bazinet, G. Shafiei, L. E. Suárez, N. Blostein, J. Seidlitz, S. Baillet, T. D. Satterthwaite, M. M. Chakravarty, A. Raznahan, B. Misic, neuromaps: structural and functional interpretation of brain maps. *Nat Methods*, 1–8 (2022).
146. D. Wang, S. Liu, J. Warrell, H. Won, X. Shi, F. C. P. Navarro, D. Clarke, M. Gu, P. Emani, Y. T. Yang, M. Xu, M. J. Gandal, S. Lou, J. Zhang, J. J. Park, C. Yan, S. K. Rhie, K. Manakongtreecheep, H. Zhou, A. Nathan, M. Peters, E. Mattei, D. Fitzgerald, T. Brunetti, J. Moore, Y. Jiang, K. Girdhar, G. E. Hoffman, S. Kalayci, Z. H. Gümüş, G. E. Crawford, PsychENCODE Consortium, P. Roussos, S. Akbarian, A. E. Jaffe, K. P. White, Z. Weng, N. Sestan, D. H. Geschwind, J. A. Knowles, M. B. Gerstein, Comprehensive functional genomic resource and integrative model for the human brain. *Science*. **362**, eaat8464 (2018).
147. B. B. Lake, R. Ai, G. E. Kaeser, N. S. Salathia, Y. C. Yung, R. Liu, A. Wildberg, D. Gao, H.-L. Fung, S. Chen, R. Vijayaraghavan, J. Wong, A. Chen, X. Sheng, F. Kaper, R. Shen, M. Ronaghi, J.-B. Fan, W. Wang, J. Chun, K. Zhang, Neuronal subtypes and diversity revealed by single-nucleus RNA sequencing of the human brain. *Science*. **352**, 1586–1590 (2016).
148. D. Polioudakis, L. de la Torre-Ubieta, J. Langerman, A. G. Elkins, X. Shi, J. L. Stein, C. K. Vuong, S. Nichterwitz, M. Gevorgian, C. K. Opland, D. Lu, W. Connell, E. K. Ruzzo, J. K. Lowe, T. Hadzic, F. I. Hinz, S. Sabri, W. E. Lowry, M. B. Gerstein, K. Plath, D. H. Geschwind, A Single-Cell Transcriptomic Atlas of Human Neocortical Development during Mid-gestation. *Neuron*. **103**, 785-801.e8 (2019).
149. J. A. Miller, S.-L. Ding, S. M. Sunkin, K. A. Smith, L. Ng, A. Szafer, A. Ebbert, Z. L. Riley, K. Aiona, J. M. Arnold, C. Bennet, D. Bertagnolli, K. Brouner, S. Butler, S. Caldejon, A. Carey, C. Cuhaciyan, R. A. Dalley, N. Dee, T. A. Dolbeare, B. A. C. Facer, D. Feng, T. P. Fliss, G. Gee, J. Goldy, L. Gourley, B. W. Gregor, G. Gu, R. E. Howard, J. M. Jochim, C. L. Kuan, C. Lau, C.-K. Lee, F. Lee, T. A. Lemon, P. Lesnar, B. McMurray, N. Mastan, N. F. Mosqueda, T. Naluai-Cecchini, N.-K. Ngo, J. Nyhus, A. Oldre, E. Olson, J. Parente, P. D. Parker, S. E. Parry, A. S. Player, M. Pletikos, M. Reding, J. J. Royall, K. Roll, D. Sandman, M. Sarreal, S. Shapouri, N. V. Shapovalova, E. H. Shen, N. Sjoquist, C. R. Slaughterbeck, M. Smith, A. J. Sodt, D. Williams, L. Zöllei, B. Fischl, M. B. Gerstein, D. H. Geschwind, I. A. Glass, M. J. Hawrylycz, R. F. Hevner, H. Huang, A. R. Jones, J. A. Knowles, P. Levitt, J. W. Phillips, N. Sestan, P. Wohnoutka, C. Dang, A. Bernard, J. G. Hohmann, E. S. Lein, Transcriptional Landscape of the Prenatal Human Brain. *Nature*. **508**, 199–206 (2014).
150. J. Piñero, J. M. Ramírez-Anguita, J. Saüch-Pitarch, F. Ronzano, E. Centeno, F. Sanz, L. I. Furlong, The DisGeNET knowledge platform for disease genomics: 2019 update. *Nucleic Acids Research*. **48**, D845–D855 (2020).
151. M. Ashburner, C. A. Ball, J. A. Blake, D. Botstein, H. Butler, J. M. Cherry, A. P. Davis, K. Dolinski, S. S. Dwight, J. T. Eppig, M. A. Harris, D. P. Hill, L. Issel-Tarver, A. Kasarskis, S. Lewis, J. C. Matese, J. E. Richardson, M. Ringwald, G. M. Rubin, G. Sherlock, Gene Ontology: tool for the unification of biology. *Nat Genet*. **25**, 25–29 (2000).
152. The Gene Ontology Consortium, S. Carbon, E. Douglass, B. M. Good, D. R. Unni, N. L. Harris, C. J. Mungall, S. Basu, R. L. Chisholm, R. J. Dodson, E. Hartline, P. Fey, P. D. Thomas, L.-P. Albou, D. Ebert, M. J. Kesling, H. Mi, A. Muruganujan, X. Huang, T. Mushayahama, S. A. LaBonte, D. A. Siegele, G. Antonazzo, H. Attrill, N. H. Brown, P. Garapati, S. J. Marygold, V. Trovisco, G. dos Santos, K. Falls, C. Tabone, P. Zhou, J. L. Goodman, V. B. Strelets, J. Thurmond, P. Garmiri, R. Ishtiaq, M. Rodríguez-López, M. L. Acencio, M. Kuiper, A. Lægreid, C. Logie, R. C. Lovering, B. Kramarz, S. C. C. Saverimuttu, S. M. Pinheiro, H. Gunn, R. Su, K. E. Thurlow, M. Chibucos, M. Giglio, S. Nadendla, J. Munro, R. Jackson, M. J. Duesbury, N. Del-Toro, B. H. M. Meldal, K. Paneerselvam, L. Perfetto, P. Porras, S. Orchard, A. Shrivastava, H.-Y. Chang, R. D. Finn, A. L. Mitchell, N. D. Rawlings, L. Richardson, A. Sangrador-Vegas, J. A. Blake, K. R. Christie, M. E. Dolan, H. J. Drabkin, D. P. Hill, L. Ni, D. M. Sitnikov, M. A. Harris, S. G. Oliver, K. Rutherford, V. Wood, J. Hayles, J. Bähler, E. R. Bolton, J. L. De Pons, M. R. Dwinell, G. T. Hayman, M. L. Kaldunski, A. E. Kwitek, S. J. F. Laulederkind, C. Plasterer,

M. A. Tutaj, M. Vedi, S.-J. Wang, P. D'Eustachio, L. Matthews, J. P. Balhoff, S. A. Aleksander, M. J. Alexander, J. M. Cherry, S. R. Engel, F. Gondwe, K. Karra, S. R. Miyasato, R. S. Nash, M. Simison, M. S. Skrzypek, S. Weng, E. D. Wong, M. Feuermann, P. Gaudet, A. Morgat, E. Bakker, T. Z. Berardini, L. Reiser, S. Subramaniam, E. Huala, C. N. Arighi, A. Auchincloss, K. Axelsen, G. Argoud-Puy, A. Bateman, M.-C. Blatter, E. Boutet, E. Bowler, L. Breuza, A. Bridge, R. Britto, H. Bye-A-Jee, C. C. Casas, E. Coudert, P. Denny, A. Estreicher, M. L. Famiglietti, G. Georghiou, A. Gos, N. Gruaz-Gumowski, E. Hatton-Ellis, C. Hulo, A. Ignatchenko, F. Jungo, K. Laiho, P. Le Mercier, D. Lieberherr, A. Lock, Y. Lussi, A. MacDougall, M. Magrane, M. J. Martin, P. Masson, D. A. Natale, N. Hyka-Nouspikel, S. Orchard, I. Pedruzzi, L. Pourcel, S. Poux, S. Pundir, C. Rivoire, E. Speretta, S. Sundaram, N. Tyagi, K. Warner, R. Zaru, C. H. Wu, A. D. Diehl, J. N. Chan, C. Grove, R. Y. N. Lee, H.-M. Muller, D. Raciti, K. Van Auken, P. W. Sternberg, M. Berriman, M. Paulini, K. Howe, S. Gao, A. Wright, L. Stein, D. G. Howe, S. Toro, M. Westerfield, P. Jaiswal, L. Cooper, J. Elser, The Gene Ontology resource: enriching a GOld mine. *Nucleic Acids Research*. **49**, D325–D334 (2021).

153. B. D. Fulcher, A. Arnatkeviciute, A. Fornito, Overcoming false-positive gene-category enrichment in the analysis of spatially resolved transcriptomic brain atlas data. *Nat Commun*. **12**, 2669 (2021).
154. M. J. M. F. Reijnders, R. M. Waterhouse, Summary Visualizations of Gene Ontology Terms With GO-Figure! *Frontiers in Bioinformatics*. **1** (2021), doi:10.3389/fbinf.2021.638255.
155. S. Darmanis, S. A. Sloan, Y. Zhang, M. Enge, C. Caneda, L. M. Shuer, M. G. Hayden Gephart, B. A. Barres, S. R. Quake, A survey of human brain transcriptome diversity at the single cell level. *Proc Natl Acad Sci USA*. **112**, 7285–7290 (2015).
156. S. Grote, K. Prüfer, J. Kelso, M. Dannemann, ABAEnrichment: an R package to test for gene set expression enrichment in the adult and developing human brain. *Bioinformatics*. **32**, 3201–3203 (2016).
157. X. Jiao, B. T. Sherman, D. W. Huang, R. Stephens, M. W. Baseler, H. C. Lane, R. A. Lempicki, DAVID-WS: a stateful web service to facilitate gene/protein list analysis. *Bioinformatics*. **28**, 1805–1806 (2012).
158. T. Salo, K. L. Bottenhorn, T. E. Nichols, M. C. Riedel, M. T. Sutherland, T. Yarkoni, A. R. Laird, NiMARE: a neuroimaging meta-analysis research environment. *F1000Research*. **7** (2018), doi:10.7490/f1000research.1115905.1.
159. C. Feng, S. B. Eickhoff, T. Li, L. Wang, B. Becker, J. A. Camilleri, S. Hétu, Y. Luo, Common brain networks underlying human social interactions: evidence from large-scale neuroimaging meta-analysis. *Neuroscience & Biobehavioral Reviews* (2021), doi:10.1016/j.neubiorev.2021.03.025.
160. M. Schurz, J. Radua, M. G. Tholen, L. Maliske, D. S. Margulies, R. B. Mars, J. Sallet, P. Kanske, Toward a hierarchical model of social cognition: A neuroimaging meta-analysis and integrative review of empathy and theory of mind. *Psychol Bull*. **147**, 293–327 (2021).
161. L. Ficco, L. Mancuso, J. Manuello, A. Teneggi, D. Liloia, S. Duca, T. Costa, G. Z. Kovacs, F. Cauda, Disentangling predictive processing in the brain: a meta-analytic study in favour of a predictive network. *Sci Rep*. **11**, 16258 (2021).
162. D. Bzdok, R. Langner, L. Schilbach, O. Jakobs, C. Roski, S. Caspers, A. R. Laird, P. T. Fox, K. Zilles, S. B. Eickhoff, Characterization of the temporo-parietal junction by combining data-driven parcellation, complementary connectivity analyses, and functional decoding. *NeuroImage*. **81**, 381–392 (2013).

4 Supplementary Tables

Publication	DOI	Experiment ID	Type	Area	Task	A/V	Contrast	Subjects	Dyads	Female	Age		Space	Method	TR	Lag	Band	Foci	ALE cluster contributions								
																			fMRI (p < .001)		fMRI (p < .01)			fMRI+fNIRS (p < .001)			
								[N]	*[N]*	*proportion*	*mean [y]*	*SD [y]*						*[N]*	*rTPJ [%]*	*rSTG [%]*	*rTPJ [%]*	*rSTG [%]*	*rIns [%]*	*rTPJ [%]*	*lSFG [%]*	*rSFG [%]*	*rMFG [%]*
Anders et al., 2011	10.1016/j.neuroimage.2010.07.004	Anders 2011	pseudo	emotion	express emotions/ emphasize	V	prediction of perciever's from sender's voxel-wise activity	12	6	0.50	23.00	n.a.	MNI	Seed	2000	0	n.a.	7	**0.00**	**0.00**	**0.00**	**0.00**	**0.00**	**0.00**	**0.00**	**0.00**	**0.05**
Bilek et al., 2015	10.1073/pnas.1421831112	Bilek 2015 1	hyper	joint attention	show target via button press	V	(dyad-INS during interaction > no interaction) > random-INS	26	13	0.62	24.50	4.60	MNI	wb-ICA	1550	0-1.55	n.a.	2	**5.63**	**0.00**	**4.08**	**0.00**	**0.00**	**4.67**	**0.00**	**0.07**	**0.00**
		Bilek 2015 2	hyper	joint attention	show target via button press	V	(dyad-INS during interaction > no interaction) > random-INS	50	25	1.00	23.40	3.30	MNI	wb-ICA	1550	0-1.55	n.a.	1	**9.28**	**0.00**	**5.66**	**0.00**	**0.00**	**7.03**	**0.00**	**0.00**	**0.00**
Dikker et al., 2014	10.1523/JNEUROSCI.3796-13.2014	Dikker 2014	pseudo	communication	isten to image description	A	speaker/listener-INS > 0	10	9	0.80	25.05	5.00	MNI	ts-VW	1500	0	n.a.	1	**0.00**	**0.00**	**0.00**	**0.00**	**0.00**	**0.00**	**0.00**	**0.00**	**0.00**
Koike et al., 2016/ 2019b	10.1016/j.neuroimage.2015.09.076	Koike 2016 1 3 + 2019b	hyper	joint attention	look at target cued by partner's gaze	V	dyad-INS during JA > random-INS	64	32	0.59	22.40	5.08	MNI	wb-VW	2500	0	.01-.08	20	**12.70**	**0.00**	**13.22**	**0.03**	**11.35**	**11.51**	**0.00**	**0.00**	**0.00**
	10.1093/scan/nsz087	Koike 2016 2	hyper	joint attention	look at partner & think about feelings	V	dyad-INS during mutual gaze without JA task > random-INS	30	15	0.47	20.60	2.92	MNI	wb-VW	2500	0	.01-.08	1	**2.49**	**0.00**	**3.44**	**0.00**	**0.00**	**1.55**	**0.00**	**0.00**	**0.00**
Koike et al., 2019a	10.1523/ENEURO.0284-18.2019	Koike 2019a	hyper	joint attention	look at partner & think about feelings	V	dyad-INS during mutual gaze with live video > delayed video	28	14	0.36	21.80	2.17	MNI	wb-VW	1000	0	>.008	6	**0.00**	**0.00**	**0.00**	**0.00**	**0.00**	**0.00**	**0.00**	**0.00**	**0.00**
Kostorz et al., 2020	10.1016/j.neuroimage.2020.116659	Kostorz 2020	pseudo	learning	watch origami folding & memorize	V	intructor-observer-INS > 0	29	28	0.52	27.20	n.a.	MNI	wb-VW	590	0	>.001	27	**8.92**	**0.00**	**10.73**	**0.00**	**0.00**	**7.94**	**0.00**	**0.00**	**0.00**
Liu et al., 2021a/ 2021b	10.1007/s00429-021-02271-2 10.1101/2021.03.02.433669	Liu 2021a + 2021b	pseudo	communication	listen to auto-biographic story	A	speaker/listener-INS > 0	33	32	0.52	23.00	n.a.	MNI	wb-Atlas	2000	0	>.008	15	**0.00**	**20.70**	**0.05**	**25.06**	**0.00**	**0.00**	**0.00**	**0.00**	**0.00**
Miyata et al., 2021	10.1016/j.neuroimage.2021.117916	Miyata 2021	hyper	joint action	show or imitate facial expression	V	dyad-INS during imitation > random-INS	32	16	0.69	22.42	n.a.	MNI	wb-VW	3500	0	>.008	6	**0.05**	**0.00**	**1.72**	**0.00**	**0.00**	**0.02**	**0.00**	**0.00**	**0.00**
Saito et al., 2010	10.3389/fnint.2010.00127	Saito 2010	hyper	joint attention	look at target cued by partner's gaze	V	dyad-INS during JA > random-INS	38	19	0.00	24.50	4.10	MNI	wb-VW	3000	0	>.008	3	**0.00**	**0.00**	**0.00**	**0.00**	**19.60**	**0.00**	**0.00**	**0.00**	**0.00**
Salazar et al., 2021	10.1016/j.neuroimage.2020.117697	Salazar 2021	hyper	joint action	try to say the same word	A	dyad-INS during JAct > random-INS	44	22	0.45	26.80	3.80	MNI	ts-ICA	2000	0	>.008	6	**0.00**	**0.00**	**0.00**	**0.00**	**0.00**	**0.00**	**0.00**	**0.00**	**0.00**
Shaw et al., 2018	10.1038/s41598-018-29233-9	Shaw 2018	hyper	decision making	iterated ultimatum game	no	dyad-INS during ultimatum game > control	38	19	0.00	24.60	3.70	MNI	wb-VW	2000	0	σ = 60	12	**0.00**	**0.00**	**0.00**	**0.00**	**8.66**	**0.00**	**1.01**	**0.00**	**0.19**
Shaw et al., 2020	10.1371/journal.pone.0232222	Shaw 2020	hyper	coop/comp	interactive pattern game	no	dyad-INS during coop/comp > random-INS	54	27	0.00	34.90	10.08	MNI	ts-ICA	2300	0	σ = 50	19	**7.79**	**20.46**	**5.06**	**9.92**	**0.00**	**6.95**	**0.00**	**0.00**	**0.00**
Silbert et al., 2014	10.1073/pnas.1323812111	Silbert 2014	pseudo	communication	listen to auto-biographic story	A	speaker/listener-INS > random correlation	14	11	n.a.	30.50	n.a.	TAL	wb-VW	1500	0	"high-pass"	22	**10.53**	**0.33**	**9.80**	**8.26**	**13.48**	**7.69**	**0.00**	**0.00**	**0.00**
Smirnov et al., 2019	10.1002/hbm.24736	Smirnov 2019	pseudo	communication	listen to auto-biographic story	A	speaker/listener-INS > random correlation	18	16	1.00	25.00	n.a.	MNI	wb-VW	1700	0	.04-.07	34	**0.01**	**4.24**	**0.15**	**11.65**	**0.00**	**0.02**	**0.01**	**0.00**	**0.00**
Spiegelhalder et al., 2014	10.1016/j.bbr.2013.10.015	Spiegelhalder 2014	hyper	communication	listen to auto-biographic story	A	dyad-INS during speak/listen > control	22	11	1.00	27.20	2.90	MNI	Seed	2660	0	>.008	9	**8.48**	**0.65**	**5.39**	**1.43**	**0.00**	**6.52**	**0.00**	**0.00**	**0.00**
Špiláková et al., 2020	10.1002/hbm.24861	Spilakova 2020	hyper	coop/comp	interactive pattern game	no	dyad-INS during coop/comp > random-INS	38	19	0.42	22.44	1.90	MNI	ts-ICA	2000	0	σ = 50	18	**15.99**	**21.90**	**10.09**	**10.87**	**0.00**	**12.69**	**0.00**	**6.12**	**15.00**
Stephens et al., 2010	10.1073/pnas.1008662107	Stephens 2010	pseudo	communication	listen to story	A	speaker-listener-INS > listener-listener-INS	14	22	n.a.	25.50	n.a.	TAL	wb-VW	1500	0-4	"high-pass"	20	**8.43**	**0.01**	**6.39**	**8.05**	**12.15**	**6.43**	**0.00**	**0.01**	**0.00**
Wang et al., 2022	10.1101/2021.07.21.452832	Wang 2021	hyper	coop/comp	"treasure chest" game	no	dyad-INS during coop/comp > 0	66	33	n.a.	23.40	2.90	TAL	Seed	2000	0	"high-pass"	9	**0.38**	**16.28**	**2.01**	**12.98**	**0.00**	**0.49**	**3.33**	**0.00**	**0.00**
Xie et al., 2020	10.1073/pnas.1917407117	Xie 2020	hyper (3)	coop/comp	draw picture & guess drawing	no	dyad-INS during collaborative drawing > random-INS	36	12	0.44	27.44	4.98	MNI	wb-Atlas	2000	0	.008-.09	42	**5.00**	**0.01**	**9.39**	**0.09**	**0.00**	**4.58**	**0.00**	**0.00**	**0.00**
Yoshioka et al., 2021	10.1093/scan/nsab082	Yoshioka 2021	hyper	joint attention	direct attention to place or object	A/V	dyad-INS (task-dependent and independent) > random-INS	44	22	0.55	21.27	2.38	MNI	wb-VW	2500	0	>.008	17	**3.48**	**14.84**	**12.21**	**11.24**	**34.40**	**1.85**	**0.00**	**3.63**	**0.00**
Summary (weighted)								***740***	***423***	***0.42***	***24.79***	***3.28***						***297***	***99.15***	***99.44***	***99.40***	***99.58***	***99.64***	***79.94***	***4.35***	***9.83***	***15.23***

Table S1: fMRI experiments included for meta-analysis

See the separate supplementary file for the original table in Excel format. Data from 14 hyperscanning fMRI publications (*37–51*) and 8 pseudohyperscanning fMRI publications (*52–59*) were included in the analyses. *Publications* refers to the single publications (n = 22 publications with n = 26 experiments) that were included in the meta-analyses. *Experiment ID* refers to the aggregated experiments when considering reanalyses of existing data (n = 22 experiments). Note that the experiment "Wang 2021" corresponding to Wang et al. (2022) (*49*) was included at the publication's preprint stage and updated later. The results did not differ between pre- and postprint

versions. *A/V* indicates whether participants in the experiments had contact per audio and/or video during fMRI scanning (live transmission in the case of hyperscanning experiments). *Method* refers to the general type of analysis method: Seed: seed-to-voxel (whole-brain), foci within the "target-brain" were included. Wb-ICA: ICA on whole-brain level, foci were peak coordiantes of reported independent components. ts-ICA: only independent components sensitive to the applied task were analyzed. wb-VW: voxel-wise analysis on whole-brain level. ts-VW: voxel-wise analysis on voxels sensitive to the applied task. wb-Atlas: a whole-brain atlas was applied, foci correspond to center-of-masses of reported parcels. *Lag* refers to whether time-series of interacting subjects were analyzed with time lag. If possible, we restricted the included foci to those from "zero lag" analyses. *Band* indicates whether a band pass or high pass filter was applied. *Contributions* refers to the relative contribution of each study to each cluster in the main fMRI ALE using the conservative voxel-level threshold ($p < .001$) or the lenient threshold ($p < .01$), and the combined fMRI and fNIRS ALE using the conservative thresholding. The ALE method incorporates nonlinear procedures causing the percentages to not add up to 100%.
Abbreviations: ALE = activation likelihood estimation, hyper(3) = hyperscanning (in one case between 3 subjects), pseudo = pseudo-hyperscanning, A = audio, V = video, INS = interpersonal neural synchronization, JA = join attention, JAct = joint action, y = years, MNI = montral neurological institute space, TAL = talairach space, wb = whole-brain, ts = task-specific, ICA = independent component analysis, VW = voxel-wise, TR = repitition time, rTPJ = right temporoparietal junction, rSTG = right superior temporal gyrus, rIns = right insula, r/lSFG = right/left superior frontal gyrus, lMFG = left medial frontal gyrus.

Publication	DOI	Experiment ID	Type	Area	Task	Setting	Contrast	Subjects	Dyads	Female	Age		Device	Length	Rate	Hb	Band	Coverage	Array	Source	Channels		Contributions (fMRI+fNIRS (p < .001))			
								[N]	[N]	proportion	mean [y]	SD [y]		[nm]	[Hz]						all [N]	INS [N]	rTPJ [%]	lSFG [%]	rSFG [%]	rMFG [%]
Balconi et al., 2017	10.1371/journal.pone.0187652	Balconi 2017	hyper	cooperation	synchronize sustained attention, pos feedback	side-by-side	ISC post positive feedback > ISC pre positive feedback	26	13	0.50	24.08	1.78	NIRScout	760, 850	6.25	HbO	.01-.03	frontRL	2x 2x2	AV(3)	8	2	**0.00**	**0.00**	**0.00**	**0.00**
Balconi et al., 2018	10.1016/j.bandc.2018.02.009	Balconi 2018	hyper	cooperation	synchronize sustained attention, neg feedback	side-by-side, screen	ISC pre negative feedback/control > ISC post negatoe feedback	26	13	n.a.	25.89	1.21	NIRScout	760, 850	6.25	HbO	.01-.03	frontRL	2x 2x2	AV(3)	8	2	**0.00**	**0.00**	**0.00**	**0.00**
Balconi et al., 2019	10.1007/s12144-019-00247-4	Balconi 2019	hyper	cooperation	synchronize selective attention after gift exchange	side-by-side, screen	ISC after material gift </> ISC after experiential gift	32	16	1.00	22.59	1.83	NIRScout	760, 850	6.25	HbO	.01-.03	frontRL	2x 2x2	AV(3)	8	4	**0.00**	**0.00**	**0.02**	**0.63**
Cañigueral et al., 2021	10.1016/j.neuroimage.2020.117572	Canigueral 2021	hyper	communication	answering statement about oneself, shared vs. not shared	face-to-face, screen	prediction of partner's ISC from rTPJ during shared > private conditions	30	15	0.73	28.20	7.33	LABNIRS	780, 805, 830	27	HbR	whole	frontlempparRL	custom	Dig(voxel)	58	3	**0.00**	**0.00**	**0.00**	**0.00**
Chen et al., 2020	10.1002/hbm.25173	Chen 2020 1	hyper	deception	spontaneous sender–receiver deception task, female dyads	face-to-face, screen	female dyad ISC during deception > rest	44	22	1.00	21.30	2.50	ETG-7100	n.a.	10	HbO	.02-.07	frontRL, tempR	4x4, 4x4	VR, AV(1)	48	1	**0.00**	**0.00**	**0.27**	**0.00**
		Chen 2020 2	hyper	deception	spontaneous sender–receiver deception task, male dyads	face-to-face, screen	male dyad ISC during deception > rest	38	19	0.00	21.30	2.50	ETG-7100	n.a.	10	HbO	.02-.07	frontRL, tempR	4x4, 4x4	VR, AV(1)	48	3	**0.00**	**0.00**	**0.00**	**0.00**
Cheng et al., 2015	10.1002/hbm.22754	Cheng 2015	hyper	coop/comp	synchronize button press	side-by-side	ISC synchronize > press faster/rest in all participants	90	45	0.51	21.96	2.15	ETG-4000	n.a.	10	HbO	.08-.31	frontRL	3x5	VR	22	2	**0.00**	**6.09**	**7.97**	**0.00**
Cheng et al., 2019	10.3389/fnins.2019.01071	Cheng 2019	hyper	cooperation	joint drawing task (joint controlling of brush)	face-to-face, wall	ISC during interpersonal coordination > rest	62	31	0.76	21.39	2.36	ETG-7100	n.a.	10	HBO	.08-.31	frontRL	2x5	VR	13	7	**0.00**	**15.23**	**0.01**	**0.00**
Cheng et al., 2021	10.1016/j.neuroimage.2021.118777	Cheng 2021	hyper	cooperation	repeated trust game with subject's "social status" pre-determined	face-to-face, wall	ISC during trust interaction > rest	198	99	1.00	21.05	2.47	ETG-7100	n.a.	10	HbO	.01-.05	frontRL, tempparR	3x5, 4x4	VR, Wang 2019	46	1	**0.00**	**0.00**	**0.00**	**0.00**
Cui et al., 2012	10.1016/j.neuroimage.2011.09.003	Cui 2012	hyper	coop/comp	synchronize button press	side-by-side	ISC synchronize > press faster/rest	22	11	0.55	26.00	6.00	ETG-4000	n.a.	10	HbO	.08-.3	frontRL	3x5	VR	22	1	**0.00**	**0.00**	**7.97**	**0.00**
Duan et al., 2020	10.1007/s12144-020-01093-5	Duan 2020 1	hyper	cooperation	realistic presented problem, lovers dyads	face-to-face, screen	ISC during problem solving in lovers > rest	40	20	0.50	20.30	0.84	LABNIRS	n.a.	10	HbO	.08-.31	frontRL, tempR	3x3, 3x2	Wang 2019	19	2	**0.00**	**7.54**	**0.00**	**0.00**
		Duan 2020 2	hyper	cooperation	realistic presented problem, strangers dyads	face-to-face, screen	ISC during problem solving in strangers > rest	44	22	0.50	20.30	0.84	LABNIRS	n.a.	10	HbO	.08-.31	frontRL, tempR	3x3, 3x2	Wang 2019	19	0	**n.a.**	**n.a.**	**n.a.**	**n.a.**
Feng et al., 2020	10.1093/scan/nsaa017	Feng 2020	hyper	cooperation	simultaneous button pressing after cue	face-to-face, screen	ISC during simultaneous button press > rest	60	30	n.a.	20.60	1.51	ETG-4000	695, 830	10	HbO	.08-.3	frontRL	3x5	VR	22	1	**0.00**	**0.00**	**0.03**	**0.00**
Fronda & Balconi, 2020	10.1002/brb3.1663	Fronda & Balconi 2020	hyper	communication	Repeat cued social vs. affective vs. informative gestures	side-by-side	ISC during affective > social/informative gestures	34	17	0.82	26.89	0.03	NIRScout	760, 850	6.25	HbO	.01-.03	frontRL	2x 2x2	AV(3)	8	1	**0.00**	**0.00**	**0.00**	**0.00**
Hou et al., 2020	10.1016/j.neuroimage.2020.116655	Hou 2020	pseudo	music	watching/listening video of violinist	video	watching/listening to violinist > rest	17	16	0.94	20.35	1.92	ETG-7100	695, 830	10	HbO	.3-.7	frontlempparL, frontlempparR	3x5, 3x5	VR	44	4	**0.00**	**0.00**	**0.00**	**0.00**
Hu et al. , 2017	10.1093/scan/nsx118	Hu 2017	hyper	cooperation	synchronize button press	face-to-face, wall	ISC synchronize > rest	70	35	1.00	n.a.	n.a.	ETG-7100	n.a.	10	HbO	.02-.08	frontRL	3x5	VR	22	1	**0.00**	**0.01**	**0.00**	**0.00**
Koide & Shimada, 2018	10.1111/jpr.12202	Koide & Shimada 2018	hyper	communication	cheering during rock-paper-scissors	side by side	ISC player-observer while playing > control	64	32	0.00	21.30	1.60	ONM-3000	n.a.	10	HbO	n.a.	frontparL	4x4	AV(1)	24	2	**0.00**	**0.00**	**0.00**	**0.00**
Li et al., 2020	10.3389/fnhum.2020.00169	Li 2020 1	hyper	cooperation	joint drawing task	face-to-face, screen	ISC during cooperation > rest	24	12	0.00	19.95	1.43	ETG-7100	695, 830	10	HbO	.08-.17	frontRL	3x5	VR	22	0	**n.a.**	**n.a.**	**n.a.**	**n.a.**
		Li 2020 2	hyper	cooperation	joint drawing task	face-to-face, screen	ISC during cooperation > rest	24	12	0.00	19.70	1.87	ETG-7100	695, 830	10	HbO	.08-.17	frontRL	3x5	VR	22	0	**n.a.**	**n.a.**	**n.a.**	**n.a.**
Li Ya. et al., 2021	10.1093/scan/nsab114	Li Ya 2021	hyper	coop/comp	watch emotional or neutral movie; joint button press task	face-to-face, wall	ISC during cooperation after emotional movie > random-ISC	62	31	0.61	21.96	2.64	LABNIRS	780, 805, 830	24	HBO	.08-.31	frontRL	3x5	n.a.	22	1	**0.00**	**0.00**	**0.00**	**0.00**
Li Yu. et al., 2021	10.1007/s11682-020-00361-z	Li Yu 2021	hyper	coop/comp	jenga game, cooperation vs. competition vs. independent	face-to-face	ISC during cooperation > independence	26	13	0.00	21.14	2.01	FOIRE-3000/16	780, 805, 830	4	HbO	.04-.08	frontRL	3x5	Dig	22	1	**0.00**	**0.02**	**0.00**	**0.00**
Li Z. et al., 2021	10.1093/cercor/bhab118	Li Z 2021	pseudo	communication	listen to narrative stories, different noise levels	audio	speaker-listener ISC modulated by noise level	22	16	0.50	n.a.	n.a.	NirScan	785, 808, 850	12	HbO	.01-.03	frontRL, tempparL, tempparR	custom, 2x4, 2x4	n.a.	36	20	**2.60**	**5.78**	**9.53**	**0.00**
Liu N. et al., 2016	10.3389/fnhum.2016.00082	Liu N 2016	hyper	coop/comp	jenga game, cooperation vs. competition vs. independent	face-to-face	ISC during coop/comp > rest	18	9	0.50	21.10	1.70	ETG-4000	n.a.	10	HbO	.04-.08	frontRL, tempparR	3x3, 3x3	VR(voxel)	19	3	**0.00**	**0.06**	**3.65**	**0.00**
Liu T. et al., 2017	10.1038/s41598-017-09226-w	Liu T 2017	hyper	coop/comp	pattern building game	side-by-side	ISC during coop/comp > random ISC	44	22	0.00	19.00	1.40	LABNIRS	n.a.	37	HbO	n.a.	frontparL, frontparR	4x4, 4x4	AV(1)	48	6	**0.00**	**0.00**	**0.01**	**17.28**
Liu Y. et al, 2017	10.1038/srep43293	Liu Y 2017	pseudo	communication	listen to real-life story, english (native) or turkish	audio	speaker-listener ISC > 0	18	15	0.44	n.a.	n.a.	fNIR-1100, ETG-4000	n.a.	2	HbO	.01-.05	frontRL, parL, parR	custom, 3x3, 3x3	VR	40	15	**6.27**	**0.00**	**0.00**	**0.00**
Liu J. et al., 2019	10.1016/j.neuroimage.2019.03.004	Liu J 2019	hyper	learning	teaching face-to-face or pc-mediated	face-to-face vs. back-to-back	ISC during face-to-face teaching > rest	84	42	0.76	21.00	2.30	ETG-7100	n.a.	10	HbO	.02-1	frontRL, tempparR	3x5, 4x4	VR, Lu 2020b	46	3	**0.00**	**0.00**	**0.00**	**0.00**
Liu W. et al., 2019	10.1016/j.neuroimage.2019.05.035	Liu W 2019	hyper	communication	complete sentence via picture, partner rates correspondence	face-to-face vs. back-to-back	ISC during same > different syntactic structures, eye-contact > no eye contact	180	90	0.56	20.00	1.60	ETG-4000	695, 830	10	HbO	.02-.05	frontparR, frontparL	2x4, 2x4	AV(1)	20	2	**0.00**	**8.03**	**0.00**	**0.00**
Long et al., 2021a/ 2021b	10.1093/cercor/bhab413 10.1093/cercor/bhaa316	Long 2021a + Long 2021b	hyper	communication/ touch	communicate freely or hold each other's hands	face-to-face	ISC interaction of communication mode x topic/ during touch > verbal communication/ in couples > friends	88	44	0.50	21.27	2.04	LABNIRS	780, 805, 830	55.6	HbO	.04-.08	frontparL, frontparL	2x5, 2x5	MRI(1)	26	3	**0.00**	**0.00**	**0.00**	**0.00**
Lu et al., 2019a	10.1016/j.neuropsychologia.2019.01.004	Lu 2019a 1	hyper	communication	"brainstorming" - neg/pos/no feedback	face-to-face, in triangle	ISC during pos feedback after brainstorming > rest	40	20	n.a.	20.72	2.47	ETG-7100	696, 830	10	HbO	.018-.048	frontRL	3x5	Lu 2020b	22	12	**0.00**	**5.24**	**11.32**	**15.63**
		Lu 2019a 2	hyper	communication	"brainstorming" - neg/pos/no feedback	face-to-face, in triangle	ISC during neg feedback after brainstorming > rest	38	19	n.a.	20.72	2.47	ETG-7100	696, 830	10	HbO	.018-.048	frontRL	3x5	Lu 2020b	22	7	**0.00**	**0.00**	**6.04**	**15.63**
Lu et al., 2019a 3/ Lu & Hao, 2019	10.1016/j.neuropsychologia.2019.01.004 10.1093/scan/nsz012	Lu 2019a 3 + Lu & Hao 2019	hyper	communication	"brainstorming" - neg/pos/no feedback	face-to-face, in triangle	ISC during/ after brainstorming > rest	38	19	n.a.	20.72	2.47	ETG-7100	696, 830	10	HbO	.018-.048	frontRL	3x5	Lu 2020b	44	2	**0.00**	**0.00**	**6.07**	**0.05**
Lu et al., 2019b	10.1093/cercor/bhy215	Lu 2019b 1	hyper	communication	"brainstorming": find alternative uses for everyday objects (AUT)	face-to-face	ISC during cooperative AUT > rest	50	25	n.a.	21.00	1.52	ETG-7100	695, 830	10	HbO	.042-.045	frontRL, tempparR	3x5, 4x4	Lu 2020b	46	4	**0.00**	**0.00**	**6.07**	**0.05**
		Lu 2019b 2	hyper	communication	"brainstorming": find typical uses for everyday objects (OTC)	face-to-face	ISC during cooperative OCT > rest	52	26	n.a.	21.00	1.52	ETG-7100	695, 830	10	HbO	.042-.045	frontRL, tempparR	3x5, 4x4	Lu 2020b	46	0	**n.a.**	**n.a.**	**n.a.**	**n.a.**
Lu et al., 2020a	10.1007/s00221-020-05799-7	Lu 2020a	hyper	communication	"brainstorming": AUT vs. OCT	face-to-face	ISC during brainstorming > male & mixed dyads	132	66	0.56	21.23	2.91	ETG-7100	695, 830	10	HbO	.08-.14	frontRL, tempparR	3x5, 4x4	Lu 2020b	46	1	**0.00**	**0.00**	**0.00**	**0.00**
Lu et al., 2020b	10.1016/j.neuroimage.2020.117025	Lu 2020b	hyper	communication	generating creative uses for everyday objects	face-to-face, wall	ISC during turn taking > normal/virtual communication	54	27	0.81	20.52	2.22	ETG-7100	695, 830	10	HbO	.34-.48	frontRL, tempparR	3x5, 4x4	NA	46	1	**0.00**	**0.00**	**0.00**	**0.00**
Nozawa et al., 2016	10.1016/j.neuroimage.2016.03.059	Nozawa 2016	hyper	cooperation	word-chain game	face-to-face, around table	(dyad-ISC during word-chain game > control) > random-ISC	48	12	0.42	21.90	NA	self-build	810	10	HbT	.01-1	front	1x3	AV(3)	1	1	**0.00**	**0.01**	**0.00**	**0.00**
Nozawa et al., 2019	10.1038/s41598-019-49257-z	Nozawa 2019	hyper	learning	1. moving arm in sync/indep.; 2. teaching/learning unknown words	face-to-face	ISC during teaching/learning after synchronized > independent movement	64	32	0.28	21.50	1.50	HOT-1000	810	NA	HbT	NA-.2	frontR, frontL	1x3, 1x3	AV(3)	2	1	**0.00**	**4.41**	**0.00**	**0.00**
Pan et al., 2017	10.1002/hbm.23421	Pan 2017 1	hyper	cooperation	synchronize button press; "lovers"	side-by-side, wall	dyad-ISC during joint button press > rest	34	17	0.50	21.07	1.85	ETG-4000	695, 830	10	HbO	.08-.31	frontparR	3x5	VR	22	1	**0.00**	**0.00**	**0.00**	**0.00**
		Pan 2017 2	hyper	cooperation	synchronize button press; "friends"	side-by-side, wall	dyad-ISC during joint button press > rest	32	16	0.50	21.07	1.85	ETG-4000	695, 830	10	HbO	.08-.31	frontparR	3x5	VR	22	0	**n.a.**	**n.a.**	**n.a.**	**n.a.**
		Pan 2017 3	hyper	cooperation	synchronize button press; "strangers"	side-by-side, wall	dyad-ISC during joint button press > rest	32	16	0.50	21.07	1.85	ETG-4000	695, 830	10	HbO	.08-.31	frontparR	3x5	VR	22	0	**n.a.**	**n.a.**	**n.a.**	**n.a.**
Pan et al., 2018	10.1016/j.neuroimage.2018.08.005	Pan 2018 1	hyper	learning	learn to sing a song - "learn phrase by phrase"	face-to-face	dyad-ISC during interactive learning > rest	13	12	1.00	20.69	2.15	ETG-7100	695, 830	10	HbO	.07-.15	frontparR, frontparL	3x5, 3x5	VR	44	4	**0.08**	**0.00**	**0.00**	**0.00**
		Pan 2018 2	hyper	learning	learn to sing a song - "whole song at once"	face-to-face	dyad-ISC during interactive learning > rest	13	12	1.00	20.69	2.15	ETG-7100	695, 830	10	HbO	.07-.15	frontparR, frontparL	3x5, 3x5	VR	44	4	**0.08**	**0.00**	**0.00**	**0.00**
Pan et al., 2020	10.1016/j.neuroimage.2020.116657	Pan 2020	hyper	learning	dynamic conceptual learning	face-to-face	interactive learning > rest	48	24	1.00	21.46	2.75	ETG-7100	695, 830	10	HbO	-17-.27, .45-.57	frontRL, tempparL	3x5, 4x4	VR	46	22	**0.00**	**15.23**	**0.04**	**17.28**
Pan et al., 2021	10.1016/j.bcp.2020.114111	Pan 2021	hyper	learning	teaching of numerical reasoning	side-by-side	ISC during teaching > rest	18	16	1.00	22.72	1.99	BrainSight	685, 830	10	HbO	.16-.19	frontlempparR, frontlempparL	custom	Dig	26	13	**3.93**	**0.00**	**0.00**	**0.00**
Pinti et al., 2021	10.1093/scan/nsaa086	Pinti 2021	hyper	deception	card game, telling truth/lying, followed by guessing	face-to-face	predict guesser's from informer's activity	46	23	n.a.	26.40	10.10	LIGHTNIRS	780, 805, 830	13.33	HbT	.01-.4	frontRL	2x8	Dig(1)	22	2	**0.00**	**4.28**	**1.17**	**0.00**
Quiñones-Camacho et al., 2021	10.1002/aur.2513	Quinones-Camacho 2021	hyper	communication	free conversation with prompted topics, moderated by experimenter	face-to-face	HC-dyad-ISC during communication > random-ISC	26	23	n.a.	NA	NA	NIRScout	760, 850	15.63	HbO	NA	tempR, frontR, frontR, frontR	custom	AV(3)	8	4	**0.00**	**0.00**	**0.00**	**0.00**
Sun et al., 2020	10.1016/j.bandc.2019.105513	Sun 2020 1	hyper	cooperation	cooperative solving of math equations, novice-student	face-to-face, wall	ISC during cooperation > rest	32	16	0.31	22.98	3.18	ETG-4000	NA	10	HbO	.04-.16	frontRL	3x5	VR	22	0	**n.a.**	**n.a.**	**n.a.**	**n.a.**
		Sun 2020 2	hyper	cooperation	cooperative solving of math equations, expert-student	face-to-face, wall	ISC during cooperation > rest	36	18	0.28	29.08	2.99	ETG-4000	NA	10	HbO	.04-.16	frontRL	3x5	VR	22	1	**0.00**	**0.05**	**0.00**	**0.00**
Sun et al., 2021	10.1016/j.bandc.2021.105803	Sun 2021	hyper	cooperation	drawing task, control pointer alone or jointly	face-to-face, wall	ISC interaction of student-student vs teacher-student x task condition	86	43	0.81	25.71	3.18	ETG-4000	NA	10	HbO	.02-.08	frontRL	3x5	VR	22	1	**0.00**	**0.06**	**0.00**	**0.00**
Tang et al., 2016	10.1093/scan/nsv092	Tang 2016 1	hyper	decision making	modified ultimatum game - "face to face"	face-to-face, screen	dyad ISC during ultimatum game > rest	102	51	0.57	22.68	2.07	ETG-4000	NA	10	HbO	.02-.08	frontR, tempparR	3x3, 2x3	AV(1)	19	2	**4.42**	**0.00**	**0.00**	**0.00**
		Tang 2016 2	hyper	decision making	modified ultimatum game - "face blocked"	face-to-face, screen	dyad ISC during ultimatum game > rest	92	46	0.50	22.20	2.18	ETG-4000	NA	10	HbO	.02-.08	frontR, tempparR	3x3, 2x3	AV(1)	19	1	**1.55**	**0.00**	**0.00**	**0.00**
Wang et al., 2019	10.1002/hbm.24592	Wang 2019	hyper	coop/comp	synchronize button press (physical pain feedback)	face-to-face, screen	ISC during cooperation with pain feedback > rest	32	16	1.00	20.90	2.10	ETG-7100	NA	10	HbO	.08-.16	frontRL, tempparR	3x5, 4x4	VR	46	8	**0.00**	**0.00**	**3.65**	**17.28**
Xue et al., 2018	10.1016/j.neuroimage.2018.02.007	Xue 2018 1	hyper	cooperation	brainstorming on problem; high-low dyads	face-to-face, in circle	ISC in high-low creativity dyads during brainstorming > rest	20	10	n.a.	21.00	1.40	ETG-7100	695, 830	10	HbO	.02-.08	frontRL, tempparR	3x5, 4x4	VR, Wang 2019	46	1	**0.00**	**7.54**	**0.00**	**0.00**
		Xue 2018 2	hyper	cooperation	brainstorming on problem; high-high dyads	face-to-face, in circle	ISC in high-high creativity dyads during brainstorming > rest	20	10	0.00	21.00	1.40	ETG-7100	695, 830	10	HbO	.02-.08	frontRL, tempparR	3x5, 4x4	VR, Wang 2019	46	0	**n.a.**	**n.a.**	**n.a.**	**n.a.**
		Xue 2018 3	hyper	cooperation	brainstorming on problem; low-low dyads	face-to-face, in circle	ISC in low-low creativity dyads during brainstorming > rest	20	10	0.00	21.00	1.40	ETG-7100	695, 830	10	HbO	.02-.08	frontRL, tempparR	3x5, 4x4	VR, Wang 2019	46	4	**0.00**	**7.54**	**7.97**	**0.00**
Yang et al., 2020	10.1038/s41593-020-0630-x	Yang 2020	hyper(6)	cooperation	incentive comp. game, "attack" vs. "defend", "bonding vs no-bonding"	face-to-face, in circle	within-group ISC interaction of bonding/no-bonding x attack/defend	516	86	0.56	22.01	1.29	LABNIRS	780, 805, 830	47.62	HbO	.026-.167	frontR, tempR	2x3, 3x2	MRI(6)	14	4	**0.01**	**0.00**	**1.07**	**0.02**
Zhang M. et al., 2017a/ 2017b	10.1038/s41598-017-06764-1 10.1016/j.bandc.2017.08.008	Zhang M 2017a + 2017b	hyper	deception, decision making	poker-like card game	face-to-face	ISC during "deception" > "honesty", "risk-seeking" > "risk-averting"	36	18	0.50	22.30	2.40	LABNIRS	780, 805, 830	57	HbO	.05-.2	frontRL, tempL	3x3, 2x3	Dig	27	6	**0.00**	**0.00**	**5.68**	**0.00**
Zhang M. et al., 2020/ 2021a	10.3389/fpsyg.2020.542093 10.3389/fnhum.2021.702959	Zhang M 2020 + 2021a	hyper	cooperation	prisoner's dilemma with high/low incentive reward	side-by-side, screen	ISC during cooperation > rest, high > low reward	62	31	0.52	22.30	2.40	LABNIRS	NA	42	HbO	.01-.2	frontR, frontRL, frontL	2x2, 2x3, 2x2	Dig	30	4	**0.00**	**0.00**	**5.69**	**0.00**
Zhang M. et al., 2021b	10.1016/j.paid.2020.110315	Zhang M 2021b	hyper	decision making	prisoner's dilemma, dyads act as group & play against experimenter	side-by-side, in front of exper.	ISC during group > individual decision making	54	27	0.48	20.70	3.10	LABNIRS	NA	NA	HbO	.01-.2	frontR, frontRL, frontL	2x2, 2x3, 2x2	Dig	15	1	**0.00**	**0.00**	**0.00**	**0.00**
Zhang R. et al., 2021	10.1016/j.bandc.2021.105738	Zhang R 2021 1	hyper	coop/comp	responding simultaneously to visual cue with vs. without stress	face-to-face, screen	ISC during cooperation with stress > random ISC	38	19	1.00	20.90	2.30	ETG-7100	695, 830	10	HbO	.08-.17	frontRL, tempparR	3x5, 4x4	Wang 2019	46	4	**0.00**	**0.01**	**0.01**	**0.00**
		Zhang R 2021 2	hyper	coop/comp	respondingsimultaneously to visual cue with vs. without stress	face-to-face, screen	ISC during cooperation without stress > random ISC	42	21	1.00	20.90	2.30	ETG-7100	695, 830	10	HbO	.08-.17	frontRL, tempparR	3x5, 4x4	Wang 2019	46	1	**0.00**	**0.00**	**0.00**	**0.00**
Zhang Y. et al., 2020	10.1523/ENEURO.0236-20.2020	Zhang Y 2020 1	hyper	communication	psychological counseling, expert counselor (manual)	face-to-face	ISC during psychological counseling by expert > rest	17	14	1.00	23.50	NA	ETG-7100	695, 830	10	HbO	.024-.045	tempparR	4x4	Wang 2019	24	6	**0.06**	**0.00**	**0.00**	**0.00**
		Zhang Y 2020 2	hyper	communication	psychological counseling, novice counselor (manual)	face-to-face	ISC during psychological counseling by novice > rest	21	16	1.00	21.98	NA	ETG-7100	695, 830	10	HbO	.024-.045	tempparR	4x4	Wang 2019	24	1	**0.00**	**0.00**	**0.00**	**0.00**
Zhao et al., 2017	10.1117/1.JBO.22.2.027004	Zhao 2017	hyper	joint action	joint tapping task	back-to-back	ISC during joint tapping > 0	48	24	0.50	22.77	2.19	ETG-4000	NA	NA	HbO	NA	frontRL	2x4	AV(1)	10	2	**0.00**	**0.00**	**0.22**	**0.00**
Zhao et al., 2021	10.1037/npe0000138	Zhao 2021 1	hyper	decision making	Iowa gambling task after Trier social stress test	side-by-side, single screen	ISC during decision making after stress > rest	42	21	1.00	21.35	2.40	LABNIRS	780, 805, 830	10	HbO	.031-.125	frontRL, tempparL	3x3, 2x3	Dig	19	2	**0.00**	**0.00**	**0.00**	**0.00**
		Zhao 2021 2	hyper	decision making	Iowa gambling task after control task	side-by-side, single screen	ISC during decision making without stress > rest	42	21	1.00	21.35	2.40	LABNIRS	780, 805, 830	10	HbO	.031-.125	frontRL, tempparL	3x3, 2x3	Dig	19	1	**0.00**	**0.00**	**4.84**	**0.00**
Zheng et al., 2018/ 2021 1	10.1002/hbm.24059 10.1037/edu0000707	Zheng 2018 + 2020 1	hyper	learning	teaching numerical reasoning, interact vs. no interact vs. recorded	side-by-side, screen	ISC during live > prerecorded video teaching, post > pre interaction	64	60	0.50	23.13	2.31	ETG-4000	686, 830	10	HbO	.06-.07	tempparR, frontparL	2x4, 2x4	MRI(1)	40	3	**0.02**	**0.00**	**0.00**	**0.00**
Zhu et al., 2021	10.1037/edu0000707	Zhu 2021 1	hyper	learning	teaching/learning definitions, elaborated feedback from instructor	face-to-face	(dyad-ISC during elaborated feedback > rest) > random-ISC	36	24	1.00	20.34	2.11	ETG-7100	695, 830	10	HbO	.017-.025	frontRL, tempparL	3x5, 4x4	VR	46	5	**0.00**	**7.55**	**0.00**	**0.00**
		Zhu 2021 2	hyper	learning	teaching/learning definitions, simple feedback from instructor	face-to-face	(dyad-ISC during simple feedback > rest) > random-ISC	36	24	1.00	20.28	2.16	ETG-7100	695, 830	10	HbO	.01-.7	frontRL, tempparL	3x5, 4x4	VR	46	0	**n.a.**	**n.a.**	**n.a.**	**n.a.**
Summary (weighted)								***3721***	***1793***	***0.54***	***20.53***	***2.05***									***1987***	***228***	***19.04***	***94.70***	***89.29***	***83.85***

Table S2: fNIRS experiments included for meta-analysis

See the separate supplementary file for the original table in Excel format. Data from 54 hyperscanning fNIRS publications (*3*, *5*, *60–111*) and 3 pseudohyperscanning fNIRS publications (*112–114*) were included in the analyses. *Publications* refers to the single publications (n = 57) that were included in meta-analyses. *Experiment ID* refers to the aggregated experiments when considering separately analyzed subgroups and reanalyses of existing data (n = 69 experiments). *Setting* indicates how participants were seated during the experiment. When subjects were seated side-by-side or face-to-face, they nevertheless often were separated by a portable wall or similar. *Length* refers to the wave-length of the light emitted by the fNIRS device. *Band* indicates how band pass filtering was applied. *Coverage* refers to the general placement of fNIRS probe arrays on the head. Multiple entries indicate multiple separated probe arrays. *Array* refers to the desing of the probe array, "custom" indicates a non-square format. *Sources* lists the source of fNIRS coordinates: AV: AtlasViewer (*115*), Dig: 3D digitizer, VR: virtual registration (*2*), MRI: anatomical MRI-based registration, or from another publication. For "Dig" and "MRI", numbers in brackets following the abbreviations indicate the number of subjects in the sample from which coordinates were estimated. For "AV", numbers in brackets show reconstruction quality coded as: 3 = all optodes have assigned 10-10 positions, 2 = at least two 10-10 positions for each optode array, 1 = one 10-10 positions and information about the array alignment. *Contributions* refers to the relative contribution of each study to each cluster in the ALE analysis on the combined fMRI and fNIRS data. Of note, the ALE method incorporates nonlinear procedures causing the percentages to not add up to 100%.
Abbreviations: ALE = activation likelihood estimation, hyper = hyperscanning, pseudo = pseudo-hyperscanning, INS = interpersonal neural synchronization, y = years, rTPJ = right temporoparietal junction, r/lSFG = right/left superior frontal gyrus, lMFG = left medial frontal gyrus.

Target system	Target function	Atlases				
		Name	**Tracer**	**Subjects (N)**	**Mean age (y)**	**Source**
Serotonin	serotonin receptor 1a	5HT1a	(11C)WAY100635	35	26.3	Savli et al., 2012 (*118*)
	serotonin receptor 1b	5HT1b	(11C)P943	65, 23	33.7, 28.7	Gallezot et al., 2010; Savli et al., 2012 (*118*, *119*)
	serotonin receptor 2a	5HT2a	(11C)Cimbi-36	29	22.6	Beliveau et al., 2017 (*120*)
	serotonin receptor 4	5HT4	(11C)SB207145	59	25.9	Beliveau et al., 2017 (*120*)
	serotonin receptor 6	5HT6	(11C)GSK215083	30	36.6	Radhakrishnan et al., 2018 (*121*)
	serotonin transporter	5HTT	(11C)DASB	100, 18	25.1, 30.5	Beliveau et al., 2017; Savli et al., 2012 (*118*, *120*)
Dopamine	dopamine synthesis	FDOPA	(18F)fluorodopa	12	n.a.	García-Gómez et al., 2018 (*122*)
	dopamine receptor 1	D1	(11C)SCH23390	13	33	Kaller et al., 2017 (*123*)
	dopamine receptor 2	D2	(11C)FLB-457	37, 55	48.4, 32.5	Sandiego et al., 2015; Smith et al., 2019 (*124*, *125*)
	dopamine transporter	DAT	(123I)FP-CIT	174, 30	61, *n.a.*	Dukart et al., 2018; García-Gómez et al., 2013 (*126*, *127*)
Noradrenaline	noradrenaline transporter	NET	(11C)O-MRB	77, 10	33.4, 33.3	Hesse et al., 2017; Ding et al., 2010 (*128*, *129*)
GABA	GABA receptor A	GABAa	(11C)flumazenil	6, 16	*n.a.*, 26.6	Dukart et al., 2018; Nørgaard et al., 2021 (*126*, *130*)
Glutamate	metabotropic receptor 5	mGluR5	(11C)ABP688	73, 22, 28	19.9, 67.9, 33.1	DuBois et al., 2016; Hansen et al., 2022; Smart et al., 2019 (*131–133*)
	NMDA receptor	NMDA	(18F)GE-179	29	41	Galovic et al., 2021 (*134*)
Acetylcholine	α4β2 nicotinic receptor	a4b2	(F18)flubatine	30	33.5	Hillmer et al., 2016 (*135*)
	muscarinic receptor 1	M1	(11C)LSN3172176	24	40.5	Naganawa et al., 2021 (*136*)
	vesicular Ach transporter	VachT	(18F)FEOBV	4, 18, 5	37, 66.8, 68.3	Aghourian et al., 2017; Bedard et al., 2019; Hansen et al., 2022 (*132*, *137*, *138*)
Endorphins	μ receptor	MU	(11C)carfentanil	204, 39	32.3, *n.a.*	Hansen et al., 2022; Kantonen et al., 2020 (*132*, *139*)
Histamine	histamine receptor 3	H3	(11C)GSK189254	8	31.7	Gallezot et al., 2017 (*140*)
Cannabinoid	cannabinoid receptor 1	CB1	(11C)OMAR	77	30	Normandin et al., 2015 (*141*)
Synaptic density	vesicle glycoprotein 2A	SV2a	(11C)UCB-J	10	36	Finnema et al., 2016 (*142*)
Oxytocin	oxytocin	OXT	mRNA expression	up to 6	24 – 57	Shen et al., 2012; Markello et al., 2021 (*143*, *20*)
	oxytocin receptor	OXTR				
	oxytocin release	CD38				

Table S3: Sources of neurotransmitter maps

All nuclear imaging invivo neurotransmitter atlases are drawn from JuSpace or neuromaps (*144*, *145*), mRNA expression atlases are derived from the Allen brain atlas (*143*) using the abagen toolbox with default settings (*20*). Sources listed in the table are the original sources of the atlases. For spatial correlation analyses, the atlases were parcellated, Z-standardized, and the weighted mean was calculated if multiple atlases using the same tracer were available.

Abbreviations: y = years.

Analysis	Dataset	Sources	N (categories)		N (genes)
			all	included	
Neuronal cell types	*PsychENCODE* cell markers (transcripts per kilobase counts)	Wang et al., 2018; Darmanis et al., 2015; Lake et al., 2016 (*146*, *147*, *155*)	24	24	2 – 83
Developmental regional enrichment	*BrainSpan* expression data (expression > 0.9^{th} quantile, annotated to ≤ 20% of categories)	Miller et al., 2014; Grote et al., 2016 (*149*, *156*)	80	80	5 – 224
Psychiatric disorders	*DisGeNET* disease markers (manually curated dataset)	Piñero et al., 2020; Jiao et al., 2012 (*150*, *157*)	332	150	5 – 697
Biological functions	*Gene Ontology* biological processes (annotations propagated through the hierarchy, retrieved March 2022)	Ashburner et al., 2000; The Gene Ontology Consortium et al., 2021; Jiao et al., 2012 (*151*, *152*, *157*)	15,039	6,947	5 – 200

Table S4: Gene category enrichment datasets

All datasets, except for *BrainSpan* data, were available as genetic "markers". Gene-wise expression values in the *BrainSpan* dataset were thresholded according to the above settings to identify markers for each of 80 categories. *DisGeNET* and *BrainSpan* categories were thresholded to contain at least 5 genes, *Gene Ontology* categories were thresholded to contain between 5 and 200 genes (*153*).
URLs: *PsychENCODE*: http://resource.psychencode.org/, *BrainSpan*: https://www.brainspan.org/, *ABAEnrichment*: https://bioconductor.org/packages/ABAEnrichment/, *DisGeNET*: https://www.disgenet.org/, *Gene Ontology*: http://geneontology.org/, *DAVID*: https://david.ncifcrf.gov/.

Analysis	Cluster	X	Y	Z	Estimate	Volume	AAL regions
ALE (p < .001)	rTPJ	62	-48	16	0.019	2856	58.26% Temporal_Mid_R; 36.41% Temporal_Sup_R
	rSTG	50	-20	-6	0.017	752	82.98% Temporal_Sup_R; 15.96% Temporal_Mid_R
ALE (p < .01)	rTPJ	62	-48	16	0.041	7856	47.45% Temporal_Mid_R; 25.25% Temporal_Sup_R; 12.02% SupraMarginal_R; 8.66% Temporal_Inf_R
	rSTG	50	-20	-6	0.025	3368	88.84% Temporal_Sup_R; 8.55% Temporal_Mid_R
	rIns	38	20	-2	0.021	3296	52.43% Insula_R; 18.69% Frontal_Inf_Orb_2_R; 13.11% Frontal_Inf_Tri_R; 10.19% Frontal_Inf_Oper_R; 5.58% no_label
ALE (no pseudo)	rTPJ	62	-48	16	0.016	2152	63.94% Temporal_Mid_R; 32.71% Temporal_Sup_R
ALE & fNIRS (all fNIRS)	rTPJ	62	-48	16	0.019	3440	63.95% Temporal_Mid_R; 34.42% Temporal_Sup_R
	lSFG	-26	66	8	0.021	2248	64.41% Frontal_Sup_2_L; 20.28% no_label; 10.32% Frontal_Sup_Medial_L
	rSFG	28	54	32	0.020	2040	47.84% Frontal_Sup_2_R; 23.92% Frontal_Sup_Medial_R; 23.14% Frontal_Mid_2_R; 5.10% no_label
	rMFG	36	38	42	0.021	784	100.00% Frontal_Mid_2_R
ALE & fNIRS (restricted fNIRS)	rTPJ	60	-48	16	0.022	3368	63.42% Temporal_Mid_R; 34.92% Temporal_Sup_R
	lSFG	-26	66	8	0.021	2064	64.34% Frontal_Sup_2_L; 19.38% no_label; 10.85% Frontal_Sup_Medial_L
	rMFG/ rSFG	28	54	32	0.021	824	51.46% Frontal_Mid_2_R; 42.72% Frontal_Sup_2_R; 5.83% no_label
	rMFG	36	38	42	0.021	792	100.00% Frontal_Mid_2_R
MACM	rTPJ	60	-48	16	0.085	28576	39.39% Temporal_Mid_R; 18.20% Temporal_Sup_R; 11.62% SupraMarginal_R; 9.55% Temporal_Inf_R; 7.84% Fusiform_R; 6.63% Occipital_Inf_R
	lTPJ	-58	-42	22	0.066	26280	35.43% Temporal_Mid_L; 17.08% SupraMarginal_L; 15.68% Temporal_Sup_L; 8.80% Fusiform_L; 5.02% Temporal_Inf_L
	lPFCIns	-32	20	2	0.068	22456	24.90% Frontal_Inf_Tri_L; 21.66% Insula_L; 18.28% Precentral_L; 15.57% Frontal_Inf_Oper_L; 12.22% Frontal_Inf_Orb_2_L
	rPFCIns	36	20	-2	0.069	19760	22.43% Frontal_Inf_Oper_R; 19.64% Insula_R; 19.51% Precentral_R; 18.70% Frontal_Inf_Tri_R; 6.80% Frontal_Inf_Orb_2_R; 5.71% no_label
	SMA	-4	12	48	0.070	11416	32.94% Supp_Motor_Area_L; 24.04% Supp_Motor_Area_R; 20.88% Cingulate_Mid_R; 9.39% Cingulate_Mid_L; 8.20% Frontal_Sup_Medial_L
	lTh	-10	-18	4	0.066	5672	54.72% Thalamus_L; 16.50% no_label; 14.10% Hippocampus_L; 10.86% Amygdala_L
	lIPL	-34	-50	46	0.061	5448	64.32% Parietal_Inf_L; 27.02% Parietal_Sup_L; 5.87% Precuneus_L
	rTh	10	-16	6	0.061	4664	49.40% Thalamus_R; 24.19% no_label; 17.67% Pallidum_R; 6.69% Caudate_R
	rIPL	32	-58	48	0.061	2872	37.33% Parietal_Inf_R; 31.20% Angular_R; 30.08% Parietal_Sup_R
	lPrec	-2	-56	34	0.063	1520	50.53% Precuneus_L; 31.58% Cingulate_Post_L; 15.26% Precuneus_R

Table S5: Information on clusters resulting from ALE and MACM analyses

Data derived from ALE maps after application of a cluster-level threshold at familywise error-corrected $p < .05$. AtlasReader (*116*) was used to estimate peak MNI coordinates (*X, Y, Z*), the average ALE value (*Estimate*), the cluster volume in mm (*Volume*), and coverage of anatomical regions relative to the cluster according the the AAL atlas (*117*). Abbreviations: ALE = activation likelihood estimation, pseudo = pseudo-hyperscanning, fNIRS = functional near-infrared spectroscopy, MACM = meta-analytic connectivity modelling, AAL = automated anatomic labelling atlas, r/lTPJ = right/left temporoparietal junction, rSTG = right superior temporal gyrus, rIns = right insula, r/lPFCIns = right/left prefrontal cortex-insula, SMA = supplementary motor area, r/lTh = left thalamus, r/lIPL = left inferior parietal lobule, lPrec = left precuneus.

All included fNIRS experiments

Parcel	N (ch)						N (exp)		N (sub)		Ratio * N (sub-all)				Ratio * N (exp-all)				AAL region
	all	*sync*	*ratio*	*p*	*p (M)*	*p (%)*	*all*	*sync*	*all*	*sync*	*value*	*p*	*p (M)*	*p (%)*	*value*	*p*	*p (M)*	*p (%)*	
RH_Vis_3	19	4	0.21	0.169	0.320	0.024	18	4	1339	592	281.89	0.014	0.052	0.481	3.79	0.075	0.236	0.056	52.97% Temporal_Inf_R
LH_Default_PFC_2	56	11	0.20	0.057	0.092	0.295	44	7	2205	268	433.13	0.018	0.116	0.181	8.64	0.007	0.091	0.303	37.52% Frontal_Inf_Tri_L
LH_DorsAttn_Post_6	5	3	0.60	0.013	0.058	0.480	4	3	154	118	92.40	0.047	0.149	0.114	2.40	0.012	0.102	0.288	57.52% Parietal_Sup_L
RH_SalVentAttn_TempOccPar_1	35	5	0.14	0.437	0.556	<0.001	31	4	2145	176	306.43	0.048	0.280	0.079	4.43	0.188	0.484	0.001	53.36% Temporal_Sup_R
RH_Default_PFCdPFCm_1	38	6	0.16	0.264	0.477	0.011	38	6	1844	280	291.16	0.076	0.317	0.027	6.00	0.044	0.293	0.066	29.90% Frontal_Med_Orb_R
LH_SalVentAttn_FrOperIns_2	4	1	0.25	0.396	0.999	0.004	3	1	242	18	60.50	0.111	0.999	0.107	0.75	0.395	0.999	0.004	64.87% Insula_L
RH_Default_PFCdPFCm_2	114	17	0.15	0.151	0.295	0.006	46	13	2818	1002	420.23	0.124	0.339	0.002	6.86	0.278	0.555	<0.001	41.38% Frontal_Sup_Medial_R
LH_Default_Temp_2	6	1	0.17	0.544	0.768	<0.001	6	1	444	48	74.00	0.142	0.612	<0.001	1.00	0.457	0.733	<0.001	88.43% Temporal_Mid_L
RH_Cont_PFCl_3	87	12	0.14	0.319	0.349	0.034	47	11	2756	912	380.14	0.146	0.215	0.066	6.48	0.259	0.388	0.020	65.37% Frontal_Mid_2_R
LH_Default_PFC_4	113	21	0.19	0.015	0.029	0.691	43	12	2098	506	389.89	0.205	0.228	0.007	7.99	0.102	0.132	0.086	55.26% Frontal_Sup_2_L
RH_Cont_PFCl_2	61	7	0.11	0.599	0.652	<0.001	42	5	2545	206	292.05	0.222	0.377	0.014	4.82	0.413	0.557	0.001	52.90% Frontal_Mid_2_R
LH_Cont_Par_1	9	3	0.33	0.076	0.196	0.178	6	2	212	66	70.67	0.258	0.270	0.024	2.00	0.186	0.225	0.124	71.29% Parietal_Inf_L
RH_Cont_Par_2	63	9	0.14	0.311	0.397	0.002	32	8	2015	503	287.86	0.263	0.476	0.001	4.57	0.459	0.650	<0.001	59.87% Angular_R
RH_Limbic_OFC_1	4	1	0.25	0.376	0.404	0.056	4	1	146	18	36.50	0.263	0.248	0.080	1.00	0.341	0.241	0.104	28.24% Rectus_R
RH_Default_Temp_3	10	1	0.10	0.713	0.761	<0.001	9	1	734	180	73.40	0.278	0.456	0.028	0.90	0.657	0.660	0.004	48.97% Temporal_Mid_R
RH_Default_Temp_2	4	1	0.25	0.378	0.504	<0.001	4	1	131	88	32.75	0.297	0.430	<0.001	1.00	0.343	0.470	<0.001	43.90% Temporal_Pole_Sup_R
LH_Default_PFC_6	9	2	0.22	0.300	0.287	0.063	8	2	308	66	68.44	0.301	0.304	0.003	1.78	0.283	0.232	0.066	73.85% Frontal_Mid_2_L
RH_Default_PFCv_2	23	5	0.22	0.117	0.038	0.590	14	3	631	79	137.17	0.307	0.135	0.107	3.04	0.241	0.103	0.188	49.04% Frontal_Inf_Tri_R
LH_Cont_PFCl_1	63	8	0.13	0.444	0.401	0.021	45	7	2075	226	263.49	0.337	0.384	0.007	5.71	0.232	0.325	0.030	54.13% Frontal_Inf_Tri_L
LH_SalVentAttn_ParOper_1	18	5	0.28	0.053	0.183	0.108	12	4	399	148	110.83	0.341	0.609	0.001	3.33	0.107	0.385	0.008	54.68% SupraMarginal_L
RH_Default_Par_1	48	5	0.10	0.688	0.718	<0.001	33	4	2063	120	214.90	0.384	0.481	0.005	3.44	0.602	0.702	<0.001	39.79% Angular_R
RH_DorsAttn_PrCv_1	22	5	0.23	0.096	0.400	<0.001	16	5	513	186	116.59	0.389	0.499	<0.001	3.64	0.135	0.417	<0.001	44.81% Frontal_Inf_Oper_R
LH_DorsAttn_Post_2	18	3	0.17	0.339	0.369	0.013	14	3	531	102	88.50	0.427	0.517	<0.001	2.33	0.329	0.379	0.007	29.06% Parietal_Inf_L
LH_SalVentAttn_PFCl_1	76	10	0.13	0.384	0.551	<0.001	43	10	2042	436	268.68	0.440	0.674	<0.001	5.66	0.338	0.607	<0.001	58.16% Frontal_Mid_2_L
LH_Default_Par_1	16	2	0.13	0.579	0.296	0.042	15	2	647	197	80.88	0.455	0.288	0.017	1.88	0.401	0.262	0.046	69.08% Temporal_Mid_L
LH_Vis_7	6	1	0.17	0.503	0.666	<0.001	6	1	163	48	27.17	0.478	0.661	<0.001	1.00	0.419	0.661	<0.001	42.60% Temporal_Mid_L
RH_Vis_7	31	4	0.13	0.496	0.587	0.004	20	3	1040	119	134.19	0.493	0.537	0.013	2.58	0.514	0.646	0.001	74.44% Occipital_Mid_R
RH_SomMot_4	23	3	0.13	0.494	0.754	<0.001	17	3	741	65	96.65	0.514	0.702	<0.001	2.22	0.477	0.714	<0.001	62.76% Postcentral_R
LH_DorsAttn_Post_3	8	1	0.13	0.641	0.549	0.007	4	1	138	18	17.25	0.641	0.608	<0.001	0.50	0.641	0.602	<0.001	48.76% Parietal_Sup_L
LH_SomMot_5	19	4	0.21	0.165	0.223	0.055	6	4	246	166	51.79	0.722	0.705	<0.001	1.26	0.69	0.654	<0.001	55.07% Postcentral_L
RH_Default_PFCdPFCm_3	22	2	0.09	0.736	0.813	<0.001	13	1	584	32	53.09	0.759	0.743	<0.001	1.18	0.736	0.780	<0.001	61.82% Frontal_Sup_2_R
RH_SomMot_1	31	2	0.06	0.895	0.926	<0.001	25	2	1333	105	86.00	0.766	0.807	<0.001	1.61	0.793	0.882	<0.001	61.86% Temporal_Sup_R
RH_DorsAttn_Post_3	19	1	0.05	0.915	0.824	<0.001	17	1	826	32	43.47	0.777	0.744	<0.001	0.89	0.774	0.808	<0.001	42.84% Parietal_Inf_R
LH_SomMot_4	25	2	0.08	0.812	0.930	<0.001	18	2	657	44	52.56	0.832	0.928	<0.001	1.44	0.802	0.927	<0.001	73.10% Postcentral_L
RH_Cont_Par_1	49	3	0.06	0.940	0.887	<0.001	30	3	1845	550	112.96	0.855	0.808	<0.001	1.84	0.936	0.875	<0.001	59.43% SupraMarginal_R

RH_DorsAttn_Post_5	25	2	0.08	0.831	0.806	<0.001	15	2	606	49	48.48	0.859	0.804	<0.001	1.20	0.831	0.803	<0.001	46.68% Precuneus_R
RH_DorsAttn_Post_2	17	1	0.06	0.894	0.887	<0.001	12	1	534	44	31.41	0.860	0.827	<0.001	0.71	0.891	0.853	0.001	85.28% Postcentral_R
RH_SalVentAttn_TempOccPar_2	50	4	0.08	0.835	0.780	<0.001	29	3	1295	112	103.60	0.884	0.822	<0.001	2.32	0.838	0.799	<0.001	68.61% SupraMarginal_R
LH_Default_Par_2	47	10	0.21	0.037	0.020	0.741	13	6	447	132	95.11	0.890	0.878	<0.001	2.77	0.743	0.685	<0.001	36.97% Angular_L
RH_DorsAttn_Post_1	47	3	0.06	0.918	0.553	0.005	26	2	1365	152	87.13	0.905	0.432	0.018	1.66	0.916	0.675	<0.001	64.75% Temporal_Mid_R
RH_DorsAttn_Post_4	40	3	0.08	0.871	0.945	<0.001	20	3	978	191	73.35	0.915	0.957	<0.001	1.50	0.907	0.956	<0.001	56.13% Parietal_Sup_R
RH_Cont_PFCl_1	169	19	0.11	0.617	0.491	<0.001	43	10	2052	398	230.70	0.959	0.813	<0.001	4.83	0.913	0.768	<0.001	44.35% Frontal_Sup_2_R
LH_SomMot_1	28	1	0.04	0.968	0.931	<0.001	17	1	747	18	26.68	0.967	0.919	<0.001	0.61	0.968	0.929	<0.001	77.45% Temporal_Sup_L
RH_SomMot_6	50	3	0.06	0.940	0.955	<0.001	21	2	1022	50	61.32	0.977	0.951	<0.001	1.26	0.987	0.955	<0.001	54.07% Precentral_R
LH_Default_PFC_5	159	9	0.06	0.999	0.993	<0.001	47	7	2226	350	126.00	0.999	0.997	<0.001	2.66	0.999	0.996	<0.001	51.49% Frontal_Sup_Medial_L

fNIRS experiments restricted to specific INS > rest, control, or randomization

Parcel	**N (ch)**				**N (exp)**		**N (sub)**		**Ratio * N (sub-all)**		**Ratio * N (exp-all)**		**AAL region**
	all	***sync***	***ratio***	***p***	***all***	***sync***	***all***	***sync***	***value***	***p***	***value***	***p***	
LH_Default_PFC_4	100	19	0.19	0.008	33	6	1514	280	275.27	0.008	7.03	0.051	55.26% Frontal_Sup_2_L
RH_Cont_PFCl_3	76	11	0.14	0.205	4	3	154	118	92.40	0.021	5.93	0.130	65.37% Frontal_Mid_2_R
RH_Default_PFCdPFCm_1	33	6	0.18	0.147	37	11	1704	484	323.76	0.027	6.00	0.015	29.90% Frontal_Med_Orb_R
RH_Default_PFCdPFCm_2	95	12	0.13	0.357	37	5	1613	216	245.46	0.052	5.05	0.384	41.38% Frontal_Sup_Medial_R
LH_Default_PFC_2	46	7	0.15	0.246	41	10	1946	396	281.66	0.063	5.63	0.048	37.52% Frontal_Inf_Tri_L
LH_SalVentAttn_PFCl_1	60	8	0.13	0.315	15	3	637	76	127.40	0.088	4.40	0.306	58.16% Frontal_Mid_2_L
RH_Cont_PFCl_2	50	6	0.12	0.465	5	2	182	66	78.00	0.090	4.44	0.210	52.90% Frontal_Mid_2_R
LH_Cont_PFCl_1	46	6	0.13	0.386	23	3	1059	154	162.92	0.112	4.57	0.176	54.13% Frontal_Inf_Tri_L
RH_Cont_PFCl_1	154	17	0.11	0.544	35	5	1569	174	204.65	0.144	4.19	0.843	44.35% Frontal_Sup_2_R
RH_SalVentAttn_TempOccPar_1	26	4	0.15	0.313	37	5	1727	206	207.24	0.153	3.54	0.143	53.36% Temporal_Sup_R
RH_Cont_Par_2	51	7	0.14	0.343	4	1	176	48	44.00	0.156	3.57	0.475	59.87% Angular_R
RH_Vis_3	15	3	0.20	0.225	2	1	62	18	31.00	0.161	3.00	0.081	52.97% Temporal_Inf_R
RH_Default_Par_1	35	3	0.09	0.783	40	10	1972	428	249.09	0.207	2.23	0.634	39.79% Angular_R
RH_Default_PFCv_2	16	5	0.31	0.039	33	8	1566	382	208.80	0.217	3.13	0.100	49.04% Frontal_Inf_Tri_R
LH_DorsAttn_Post_6	5	3	0.60	0.007	4	1	146	18	36.50	0.224	2.40	0.006	57.52% Parietal_Sup_L
RH_Vis_7	27	3	0.11	0.579	10	3	311	79	97.19	0.238	1.78	0.587	74.44% Occipital_Mid_R
RH_DorsAttn_Post_1	36	3	0.08	0.769	11	3	365	134	73.00	0.369	1.75	0.768	64.75% Temporal_Mid_R
LH_Default_PFC_5	135	6	0.04	0.997	9	2	311	90	51.83	0.389	1.69	0.999	51.49% Frontal_Sup_Medial_L
LH_Default_Par_2	35	9	0.26	0.013	6	1	163	48	27.17	0.456	2.57	0.502	36.97% Angular_L
LH_Cont_Par_1	7	3	0.43	0.035	26	6	1131	361	155.24	0.461	2.14	0.035	71.29% Parietal_Inf_L
RH_DorsAttn_PrCv_1	15	3	0.20	0.231	12	2	415	43	51.88	0.541	2.20	0.227	44.81% Frontal_Inf_Oper_R
RH_SomMot_6	46	3	0.07	0.901	16	2	760	55	84.44	0.548	1.24	0.939	54.07% Precentral_R
RH_SomMot_4	16	2	0.13	0.544	4	1	138	18	17.25	0.591	1.50	0.530	62.76% Postcentral_R
LH_SalVentAttn_ParOper_1	12	2	0.17	0.376	26	3	1157	98	99.17	0.601	1.50	0.371	54.68% SupraMarginal_L

LH_SomMot_5	19	4	0.21	0.133	13	2	417	44	46.33	0.614	1.26	0.636	55.07% Postcentral_L
RH_DorsAttn_Post_5	25	2	0.08	0.800	6	4	246	166	51.79	0.632	1.20	0.800	46.68% Precuneus_R
LH_SomMot_4	18	2	0.11	0.594	17	1	826	32	43.47	0.669	1.44	0.588	73.10% Postcentral_L
LH_Default_Temp_2	4	1	0.25	0.366	10	5	307	110	78.94	0.725	1.00	0.333	88.43% Temporal_Mid_L
RH_DorsAttn_Post_4	36	2	0.06	0.909	21	2	997	152	83.08	0.733	1.00	0.909	56.13% Parietal_Sup_R
RH_DorsAttn_Post_3	19	1	0.05	0.891	11	1	327	17	27.25	0.740	0.89	0.714	42.84% Parietal_Inf_R
RH_Limbic_OFC_1	4	1	0.25	0.376	10	1	355	44	27.31	0.744	1.00	0.346	28.24% Rectus_R
RH_SomMot_1	21	1	0.05	0.913	18	1	763	17	36.33	0.789	0.86	0.785	61.86% Temporal_Sup_R
RH_DorsAttn_Post_2	17	1	0.06	0.861	15	2	606	49	48.48	0.794	0.71	0.856	85.28% Postcentral_R
LH_SalVentAttn_FrOperIns_2	2	1	0.50	0.219	12	1	534	44	31.41	0.801	1.00	0.216	64.87% Insula_L
RH_Cont_Par_1	40	1	0.03	0.991	38	9	1722	376	190.09	0.804	0.63	0.984	59.43% SupraMarginal_R
LH_DorsAttn_Post_2	13	1	0.08	0.774	18	2	792	59	44.00	0.908	0.77	0.760	29.06% Parietal_Inf_L
LH_Default_Par_1	12	1	0.08	0.758	12	1	391	18	18.62	0.928	0.92	0.627	69.08% Temporal_Mid_L
LH_Vis_7	6	1	0.17	0.497	19	2	836	50	54.52	0.936	1.00	0.391	42.60% Temporal_Mid_L
RH_SalVentAttn_TempOccPar_2	39	1	0.03	0.988	25	1	1113	34	27.83	0.977	0.59	0.988	68.61% SupraMarginal_R
LH_SomMot_1	21	1	0.05	0.928	23	1	905	26	23.21	0.987	0.57	0.928	77.45% Temporal_Sup_L
LH_DorsAttn_Post_3	8	1	0.13	0.591	38	5	1778	242	79.02	0.997	0.50	0.591	48.76% Parietal_Sup_L

Table S6: Region-wise fNIRS meta-analyses

Results from region-wise meta-analysis of fNIRS INS experiments, for the complete and for a restricted set of experiments. *Parcel*: brain region label drawn from a functionally defined 100-parcel cortical parcellation (*21*). *N (ch/exp/sub)*: number of channels, experiments, and subjects associated to the respective region. *Ratio*: (number of INS channels / number of all channels). *Ratio * N (sub-all)*: (Ratio * number of subjects contributing to a parcel). *Ratio * N (exp-all)*: (Ratio * number of experiments contributing to a parcel). *p (M)*: Median *p* value resulting from iterative (1,000 iterations) recalculation of fNIRS meta-analysis after fNIRS coordinate randomization within a 1 cm cortical radius. *p (%)*: Percentage of sub-threshold (< 0.05) *p* values after coordinate randomization. Randomization analysis was only performed for the main fNIRS coordinate dataset. *P* values are estimated from null distributions generated by permuting (5,000 iterations) the fNIRS channel coordinate-atlas parcel assignment and recalculating the respective index. *AAL region*: Anatomical region with the largest coverage from the automated anatomic labelling atlas (*117*). The order is based on *p* values associated to "*Ratio * N (sub-all)"* and only those parcels in which at least one INS channel was observed are shown.
Abbreviations: fNIRS = functional near-infrared spectroscopy, INS = interpersonal neural synchronization.

Topic	rTPJ						Whole-brain		
	Reverse inference			Forward inference			Spearman correlation		
	q	z	prob.	q	z	lik.	p	q	Z(rho)
145_mind_mental_social	<0.001	6.81	0.02	<0.001	5.40	1.91	0.379	0.679	0.06
143_action_actions_observation	<0.001	5.32	0.02	<0.001	3.71	1.56	<0.001	0.005	0.64
82_motion_mt_moving	<0.001	5.25	0.01	<0.001	4.29	1.84	0.001	0.007	0.54
193_mirror_video_imitation	0.007	2.68	0.01	0.211	1.25	1.26	0.001	0.009	0.51
115_face_faces_fusiform	0.011	2.55	0.02	0.048	1.98	1.34	0.224	0.498	0.18
154_social_interactions_interaction	0.012	2.50	0.02	0.012	2.51	1.43	0.777	1.000	-0.19
138_real_virtual_reality	0.021	2.31	0.01	0.027	-2.21	1.54	0.012	0.075	0.44
30_events_future_personal	0.072	1.80	0.01	0.090	-1.70	1.45	0.838	1.000	-0.23
99_detection_novelty_oddball	0.072	1.80	0.01	0.025	-2.24	1.71	0.187	0.458	0.17
175_dopamine_dopaminergic_striatum	0.145	-1.46	0.00	0.997	0.00	0.58	1.000	1.000	-0.66
149_olfactory_taste_odor	0.204	-1.27	0.00	0.997	0.00	0.34	0.992	1.000	-0.46
100_gestures_abstract_race	0.243	1.17	0.01	0.210	-1.25	1.43	0.042	0.146	0.38
142_scene_scenes_perspective	0.243	1.17	0.01	0.217	-1.23	1.30	0.242	0.512	0.17
26_time_delay_temporal	0.243	1.17	0.02	0.217	1.23	1.17	0.381	0.679	0.07
64_attention_attentional_visual	0.244	1.16	0.03	0.217	1.23	1.14	<0.001	0.005	0.82
139_faces_emotional_facial	0.246	1.16	0.02	0.142	1.47	1.28	0.881	1.000	-0.22
157_somatosensory_stimulation_cortex	0.248	-1.15	0.01	0.997	0.00	0.65	0.394	0.689	0.07
191_eye_gaze_saccade	0.248	1.15	0.01	0.437	-0.78	1.17	0.059	0.180	0.35
97_adaptation_selective_stimulus	0.248	1.15	0.03	0.210	1.25	1.16	<0.001	0.005	0.64
8_cues_cue_target	0.252	1.14	0.01	0.335	0.96	1.17	0.041	0.146	0.35
181_creative_creativity_generation	0.261	1.12	0.00	0.185	-1.32	1.56	0.435	0.719	0.04
130_risk_high_taking	0.292	-1.05	0.00	0.997	0.00	0.72	0.998	1.000	-0.50
74_feedback_negative_performance	0.292	1.05	0.01	0.368	-0.90	1.22	0.470	0.750	0.03
11_cognitive_function_performance	0.292	-1.05	0.05	0.906	0.12	0.98	0.523	0.821	-0.02
108_visual_auditory_sensory	0.387	0.87	0.02	0.449	0.76	1.10	<0.001	0.005	0.61
111_memory_encoding_hippocampal	0.387	-0.87	0.01	0.997	0.00	0.84	0.835	1.000	-0.21
118_goal_goals_planning	0.387	-0.87	0.00	0.997	0.00	0.65	0.744	1.000	-0.15
125_expertise_experts_ic	0.387	-0.87	0.00	0.997	0.00	0.67	0.026	0.125	0.36
152_perceptual_perception_visual	0.387	-0.87	0.01	0.997	0.00	0.87	0.001	0.008	0.56
159_inhibition_response_inhibitory	0.387	0.87	0.01	0.217	1.23	1.23	0.461	0.749	0.03
161_women_men_sex	0.387	-0.87	0.01	0.997	0.00	0.81	0.999	1.000	-0.49
166_pictures_picture_images	0.387	-0.87	0.01	0.997	0.00	0.83	0.928	1.000	-0.20
184_spatial_location_space	0.387	0.87	0.02	0.476	0.71	1.09	0.010	0.073	0.48
198_repetition_priming_suppression	0.387	-0.87	0.01	0.997	0.00	0.84	0.057	0.180	0.36
3_task_switching_set	0.387	0.87	0.01	0.515	-0.65	1.11	0.100	0.281	0.27
39_light_shed_alertness	0.387	0.87	0.01	0.335	-0.96	1.27	0.688	1.000	-0.13
55_music_musical_pitch	0.387	-0.87	0.00	0.997	0.00	0.62	0.425	0.717	0.05
6_implicit_explicit_cd	0.387	0.87	0.01	0.216	-1.24	1.43	0.364	0.676	0.06
196_personality_trait_scores	0.433	-0.78	0.01	0.872	-0.16	0.96	0.998	1.000	-0.48
79_training_practice_trained	0.433	-0.78	0.01	0.997	0.00	0.85	0.338	0.641	0.11
187_speech_auditory_temporal	0.437	0.78	0.02	0.599	0.53	1.06	0.212	0.494	0.18
31_hearing_deaf_sign	0.442	0.77	0.00	0.416	-0.81	1.33	0.025	0.125	0.40
28_memory_retrieval_episodic	0.448	0.76	0.01	0.745	0.33	1.03	0.836	1.000	-0.23
197_reward_striatum_anticipation	0.466	-0.73	0.01	0.906	0.12	0.96	1.000	1.000	-0.58
117_object_objects_visual	0.484	0.70	0.01	0.449	0.76	1.12	0.030	0.125	0.42
58_autonomic_arousal_rate	0.484	-0.70	0.00	0.997	0.00	0.76	0.988	1.000	-0.44
20_wm_load_memory	0.491	-0.69	0.01	0.997	0.00	0.79	0.191	0.458	0.19
93_language_sentences_comprehension	0.491	0.69	0.01	0.449	0.76	1.12	0.102	0.281	0.28
128_prediction_error_outcome	0.500	0.67	0.01	0.281	1.08	1.21	0.762	1.000	-0.12
137_regulation_emotion_reappraisal	0.503	0.67	0.01	0.449	-0.76	1.16	0.997	1.000	-0.36
182_experience_subjective_ratings	0.503	0.67	0.01	0.416	0.81	1.14	0.967	1.000	-0.28
5_body_bodies_eba	0.503	0.67	0.01	0.335	-0.96	1.29	0.049	0.165	0.37
127_task_performance_cognitive	0.513	-0.65	0.14	0.821	0.23	1.00	0.029	0.125	0.34
158_pet_glucose_metabolism	0.520	0.64	0.00	0.772	-0.29	1.01	1.000	1.000	-0.56
95_verbs_verb_nouns	0.567	0.57	0.00	0.745	-0.33	1.03	0.056	0.180	0.34
186_decision_making_choice	0.625	0.49	0.02	0.449	0.76	1.11	0.811	1.000	-0.19

23_reasoning_relational_relations	0.628	0.48	0.00	0.452	-0.75	1.21	0.289	0.585	0.14
173_touch_ct_tactile	0.630	-0.48	0.00	0.997	0.00	0.72	0.010	0.073	0.47
43_conflict_interference_incongruent	0.630	0.48	0.01	0.519	0.64	1.10	0.023	0.125	0.40
146_pain_painful_chronic	0.657	-0.44	0.01	0.997	0.00	0.78	0.903	1.000	-0.29
18_color_shape_shapes	0.718	0.36	0.01	0.449	-0.76	1.20	0.001	0.007	0.55
57_learning_learned_sequence	0.718	-0.36	0.01	0.997	0.00	0.85	0.791	1.000	-0.17
90_imagery_mental_rotation	0.718	-0.36	0.00	0.997	0.00	0.74	0.093	0.272	0.33
150_reading_phonological_readers	0.730	-0.35	0.01	0.997	0.00	0.82	0.001	0.007	0.57
153_phase_women_menstrual	0.853	-0.19	0.00	0.916	-0.11	0.87	0.947	1.000	-0.33
172_verbal_fluency_overt	0.853	-0.19	0.01	0.997	0.00	0.81	0.030	0.125	0.37
179_memory_working_task	0.853	-0.19	0.01	0.957	0.05	0.94	0.137	0.346	0.24
2_problem_problems_arithmetic	0.853	-0.19	0.00	0.957	-0.05	0.88	0.134	0.346	0.26
52_control_cognitive_task	0.853	-0.19	0.01	0.821	0.23	0.99	0.323	0.625	0.11
121_tool_tools_knowledge	0.857	0.18	0.00	0.636	-0.47	1.11	0.035	0.136	0.41
13_fear_conditioning_extinction	0.857	0.18	0.00	0.732	-0.34	1.05	0.999	1.000	-0.44
131_test_performance_intelligence	0.857	0.18	0.01	0.599	-0.53	1.10	0.855	1.000	-0.23
160_bias_biases_spd	0.857	-0.18	0.00	0.821	-0.23	0.97	0.825	1.000	-0.14
163_language_chinese_english	0.857	-0.18	0.01	0.957	-0.05	0.90	0.010	0.073	0.47
167_human_humans_animal	0.857	0.18	0.01	0.817	0.23	1.00	0.814	1.000	-0.20
177_mood_rumination_induction	0.857	0.18	0.00	0.519	-0.64	1.18	0.983	1.000	-0.38
180_amygdala_threat_fear	0.857	-0.18	0.01	0.821	-0.23	0.99	0.998	1.000	-0.45
65_recognition_correct_familiarity	0.857	0.18	0.01	0.719	-0.36	1.05	0.304	0.602	0.11
9_semantic_word_knowledge	0.857	-0.18	0.01	0.965	0.04	0.92	0.286	0.585	0.13
42_negative_positive_vmpfc	0.891	0.14	0.01	0.599	0.53	1.07	1.000	1.000	-0.58
116_task_matching_strategy	0.912	-0.11	0.01	0.906	-0.12	0.95	0.015	0.092	0.42
91_movement_motor_movements	0.926	-0.09	0.01	0.997	0.00	0.74	0.221	0.498	0.22
92_executive_control_functions	0.926	-0.09	0.01	0.957	-0.05	0.91	0.403	0.693	0.06
183_orientation_colour_separation	0.959	-0.05	0.00	0.821	-0.23	0.97	0.238	0.512	0.17
162_words_word_lexical	0.960	-0.05	0.01	0.997	0.00	0.87	0.029	0.125	0.39
169_acupuncture_stimulation_vstm	0.960	-0.05	0.00	0.946	-0.07	0.82	0.816	1.000	-0.18
112_context_empathy_contextual	0.962	0.05	0.01	0.722	-0.36	1.05	0.759	1.000	-0.17
147_target_search_targets	0.963	-0.05	0.01	0.821	0.23	0.99	0.036	0.136	0.34
189_category_categories_categorization	0.974	0.03	0.01	0.745	-0.33	1.03	0.117	0.314	0.28
19_illusion_physical_perceived	0.974	0.03	0.00	0.772	-0.29	1.02	<0.001	0.007	0.53
66_emotional_negative_amygdala	0.988	0.02	0.02	0.775	0.29	1.01	0.998	1.000	-0.45

Table S7: Functional-decoding results

Functional decoding of the rTPJ cluster using reverse and forward inference estimates, and the whole-brain INS distributions usting spatial Spearman correlations (Z-transformed), sorted by reverse inference *q* values. Topics are selected from 200 latent Dirichlet allocation topics distributed with the Neurosynth database (version 7). For whole-brain correlations, *p* values are derived from comparison to correlations with topic-wise null maps (10,000 permutations) and were false discovery rate-corrected across all topics (*q*). All associations significant after multiple comparison correction in any analysis are marked in bold.
Abbreviations: rTPJ = right temporo-parietal junction, prob. = probability, lik. = likelihood.

In-vivo & post-mortem neurotransmitter atlases

Atlas	Whole-brain			Cortex-only		Baseline-adjusted	
	Z (ρ)	***p***	***q***	***Z (ρ)***	***p***	***Z (ρ)***	***p***
GABAa	0.51	<0.001	0.005	0.43	0.002	0.51	<0.001
SV2a	0.40	0.002	0.022	0.29	0.047	0.41	0.001
mGluR5	0.37	0.003	0.026	0.26	0.089	0.36	0.005
5HT2a	0.43	0.011	0.065	0.19	0.160	0.49	0.005
M1	0.27	0.032	0.154	0.28	0.063	0.26	0.040
5HT6	0.19	0.084	0.320				
5HT1a	0.27	0.093	0.320				
5HT1b	0.18	0.115	0.346				
NET	0.17	0.180	0.480				
NMDA	-0.06	0.590	1.000				
D1	-0.07	0.623	1.000				
D2	-0.12	0.697	1.000				
CB1	-0.08	0.726	1.000				
5HT4	-0.13	0.737	1.000				
a4b2	-0.16	0.755	1.000				
FDOPA	-0.19	0.782	1.000				
DAT	-0.19	0.788	1.000				
OXT	-0.19	0.791	1.000				
H3	-0.20	0.908	1.000				
MU	-0.23	0.929	1.000				
5HTT	-0.35	0.942	1.000				
VAChT	-0.29	0.956	1.000				
OXTR	-0.39	0.984	1.000				
CD38	-0.57	1.000	1.000				

GABA-related gene co-expression clusters

Atlas	Whole-brain		
	Z (ρ)	***p***	***q***
Cluster 3	0.45	0.005	0.014
Cluster 2	0.43	0.007	0.014
Cluster 4	-0.19	0.932	0.952
Cluster 1	-0.23	0.952	0.952

Table S8: Results of neurotransmitter association analyses

Spatial correlations between interpersonal neural synchronization Z-maps and neurotransmitter receptor distributions derived from invivo nuclear imaging atlases (*144*, *145*) or post-mortem mRNA expression data (*19*, *20*). Correlation coefficients are r-to-Z transformed partial Spearman's ρ, *p* values are uncorrected and derived from null-correlations, *q* values are false discovery-corrected *p* values according to the Benjamini-Hochberg procedure. The two right main columns show sensitivity analyses of the significant positive associations (i) calculated only on cortical parcels and (ii) calculated after additional inclusion of functional baseline activation rate (BL) in partial correlations of INS and nuclear imaging maps. Rows are sorted by main *p* values.

Neuronal cell types

Category	N (genes)	Average Z (ρ)	p (norm)	q (norm)	p (perm)	q (perm)
Adult-Ex3	9	0.36	< 0.001	0.001	< 0.001	< 0.001
Adult-In5	7	0.12	0.001	0.013	0.001	0.012
Adult-In6	5	0.19	0.005	0.039	0.004	0.032
Adult-Ex4	15	0.12	0.030	0.147	0.025	0.125
Adult-OtherNeuron	38	0.07	0.031	0.147	0.026	0.125
Adult-Ex5	21	0.11	0.051	0.206	0.049	0.197
Adult-Ex2	9	0.06	0.095	0.325	0.095	0.326
Adult-Ex1	17	-0.01	0.566	1.000	0.563	1.000
Adult-Ex6	34	-0.11	0.993	1.000	0.994	1.000
Adult-Ex7	6	-0.07	0.908	1.000	0.906	1.000
Adult-Ex8	54	-0.07	0.931	1.000	0.928	1.000
Adult-In1	2	-0.30	0.994	1.000	0.993	1.000
Adult-In2	7	-0.10	0.991	1.000	0.993	1.000
Adult-In3	17	-0.02	0.751	1.000	0.751	1.000
Adult-In4	11	-0.04	0.788	1.000	0.791	1.000
Adult-In7	10	-0.03	0.759	1.000	0.762	1.000
Adult-In8	3	0.02	0.368	1.000	0.369	1.000
Adult-Astro	37	-0.23	1.000	1.000	1.000	1.000
Adult-Endo	76	-0.16	0.992	1.000	0.992	1.000
Dev-quiescent	15	-0.04	0.785	1.000	0.780	1.000
Dev-replicating	25	-0.05	0.971	1.000	0.973	1.000
Adult-Micro	20	-0.25	0.998	1.000	0.999	1.000
Adult-OPC	39	-0.19	0.999	1.000	0.999	1.000
Adult-Oligo	35	-0.03	0.649	1.000	0.651	1.000

Developmental regional enrichment

Category	N (genes)	Average Z (ρ)	p (norm)	q (norm)	p (perm)	q (perm)
child_CBC	165	0.16	< 0.001	0.001	< 0.001	< 0.001
adolescent_CBC	155	0.15	< 0.001	0.001	< 0.001	< 0.001
adult_A1C	31	0.32	< 0.001	0.001	< 0.001	< 0.001
adult_V1C	67	0.32	< 0.001	0.001	< 0.001	< 0.001
adult_CBC	193	0.14	< 0.001	0.001	< 0.001	< 0.001
adolescent_STC	5	0.50	< 0.001	< 0.001	< 0.001	0.001
adult_STC	67	0.28	< 0.001	0.001	< 0.001	0.001
adult_S1C	45	0.31	< 0.001	0.001	< 0.001	0.001
adult_IPC	55	0.27	< 0.001	0.001	< 0.001	0.001
infant_CBC	121	0.10	< 0.001	0.001	< 0.001	0.001
adult_M1C	30	0.27	< 0.001	0.002	< 0.001	0.001
adolescent_DFC	27	0.19	< 0.001	0.001	< 0.001	0.002
adolescent_VFC	8	0.24	< 0.001	0.001	< 0.001	0.002
adult_VFC	43	0.26	< 0.001	0.001	< 0.001	0.002
infant_V1C	47	0.21	< 0.001	0.001	0.001	0.003
adolescent_OFC	14	0.26	< 0.001	0.001	0.001	0.003
adolescent_IPC	17	0.31	< 0.001	0.001	0.001	0.004
adult_OFC	41	0.25	< 0.001	0.001	0.001	0.004
infant_ITC	8	0.19	0.001	0.005	0.001	0.005
adult_DFC	57	0.21	0.001	0.005	0.002	0.007
adolescent_V1C	11	0.18	0.002	0.008	0.002	0.007
infant_IPC	16	0.21	0.002	0.008	0.003	0.010
infant_MFC	8	0.18	0.004	0.013	0.004	0.014
adult_ITC	37	0.17	0.004	0.014	0.006	0.019
child_V1C	31	0.12	0.006	0.019	0.006	0.019
infant_S1C	35	0.15	0.008	0.024	0.007	0.022
prenatal_V1C	171	0.07	0.009	0.025	0.008	0.024
adolescent_S1C	9	0.15	0.010	0.028	0.009	0.025
adolescent_ITC	15	0.13	0.010	0.028	0.010	0.026

DisGeNET psychiatric disease markers

Category	N (genes)	Average Z (ρ)	p (norm)	q (norm)	p (perm)	q (perm)
Seasonal Affective Disorder	14	0.200	< 0.001	0.001	< 0.001	< 0.001

Psychosis, Brief Reactive	11	0.238	< 0.001	0.001	< 0.001	< 0.001
Schizophreniform Disorders	11	0.238	< 0.001	0.001	< 0.001	< 0.001
Language Development Disorders	11	0.305	< 0.001	0.001	< 0.001	0.006
Speech Delay	11	0.305	< 0.001	0.001	< 0.001	0.006
Semantic-Pragmatic Disorder	11	0.305	< 0.001	0.001	< 0.001	0.006
Neurodevelopmental Disorders	89	0.151	< 0.001	0.001	< 0.001	0.006
Schizoaffective Disorder	25	0.136	< 0.001	0.003	< 0.001	0.006
Abnormal behavior	15	0.173	< 0.001	0.003	< 0.001	0.006
Global developmental delay	125	0.081	< 0.001	0.006	< 0.001	0.006
Major Affective Disorder 2	13	0.156	< 0.001	0.003	0.001	0.011
Opioid-Related Disorders	5	0.128	0.001	0.012	0.003	0.022
Opioid abuse	5	0.128	0.001	0.012	0.003	0.022
Narcotic Abuse	5	0.128	0.001	0.012	0.003	0.022
Opiate Addiction	5	0.128	0.001	0.012	0.003	0.022
Narcotic Dependence	5	0.128	0.001	0.012	0.003	0.022
Opiate Abuse	5	0.128	0.001	0.012	0.003	0.022
Manic Disorder	65	0.061	0.003	0.025	0.003	0.022
Phencyclidine Abuse	7	0.146	0.004	0.025	0.003	0.023
Phencyclidine-Related Disorders	7	0.146	0.004	0.025	0.003	0.023
Depression, Postpartum	6	0.189	0.004	0.025	0.004	0.027
Intellectual Disability	416	0.047	0.004	0.026	0.004	0.027
Developmental Coordination Disorder	7	0.117	0.005	0.034	0.005	0.031
Motor Skills Disorders	7	0.117	0.005	0.034	0.005	0.031
Profound Mental Retardation	126	0.041	0.008	0.043	0.006	0.036
Mental Retardation, Psychosocial	126	0.041	0.008	0.043	0.006	0.036
Mental deficiency	126	0.041	0.008	0.043	0.006	0.036
Manic	71	0.048	0.010	0.054	0.008	0.045

Gene ontology biological processes

Category	N (genes)	Average Z (ρ)	p (norm)	q (norm)	p (perm)	q (perm)
neg. reg. of voltage-gated calcium channel activity	5	0.23	< 0.001	0.008	< 0.001	< 0.001
pos. reg. of skeletal muscle cell differentiation	5	0.42	< 0.001	0.008	< 0.001	< 0.001
reg. of water loss via skin	9	0.21	< 0.001	0.011	< 0.001	< 0.001
pos. reg. of nonmotile primary cilium assembly	6	0.24	< 0.001	0.011	< 0.001	< 0.001
deadenylation-dependent decapping of nuclear-transcribed mRNA	8	0.28	< 0.001	0.011	< 0.001	< 0.001
protein K6-linked ubiquitination	7	0.26	< 0.001	0.011	< 0.001	< 0.001
reg. of macromitophagy	5	0.28	< 0.001	0.011	< 0.001	< 0.001
cerebellar Purkinje cell differentiation	10	0.23	< 0.001	0.011	< 0.001	< 0.001
reg. of Golgi to plasma membrane protein transport	7	0.37	< 0.001	0.011	< 0.001	< 0.001
reg. of mRNA splicing, via spliceosome	65	0.14	< 0.001	0.011	< 0.001	< 0.001
phosphorelay signal transduction system	7	0.26	< 0.001	0.011	< 0.001	< 0.001
cardiac muscle adaptation	17	0.16	< 0.001	0.011	< 0.001	< 0.001
muscle hypertrophy in response to stress	16	0.19	< 0.001	0.011	< 0.001	< 0.001
cardiac muscle hypertrophy in response to stress	16	0.19	< 0.001	0.011	< 0.001	< 0.001
response to parathyroid hormone	7	0.24	< 0.001	0.011	< 0.001	< 0.001
reg. of protein sumoylation	21	0.14	< 0.001	0.011	< 0.001	< 0.001
cell differentiation in hindbrain	16	0.17	< 0.001	0.013	< 0.001	< 0.001
reg. of Rac protein signal transduction	12	0.21	< 0.001	0.013	0.001	0.020
histone H2A monoubiquitination	12	0.21	< 0.001	0.013	< 0.001	< 0.001
N-terminal protein lipidation	6	0.30	< 0.001	0.013	< 0.001	< 0.001
nephric duct development	8	0.19	< 0.001	0.013	< 0.001	0.010
neg. reg. of glucocorticoid receptor signaling pathway	6	0.34	< 0.001	0.013	< 0.001	0.010
histone H4-K5 acetylation	16	0.17	< 0.001	0.013	< 0.001	< 0.001
histone H4-K8 acetylation	16	0.17	< 0.001	0.013	< 0.001	< 0.001
cerebellar Purkinje cell layer formation	11	0.19	< 0.001	0.013	< 0.001	< 0.001
reg. of skeletal muscle cell differentiation	14	0.15	< 0.001	0.013	< 0.001	< 0.001
neg. reg. of mitophagy	6	0.31	< 0.001	0.013	< 0.001	< 0.001
reg. of alternative mRNA splicing, via spliceosome	35	0.13	< 0.001	0.013	< 0.001	0.015
reg. of production of miRNAs involved in gene silencing by miRNA	9	0.15	< 0.001	0.013	< 0.001	< 0.001
serine phosphorylation of STAT3 protein	6	0.35	< 0.001	0.013	< 0.001	< 0.001

pyrimidine nucleotide catabolic process	11	0.15	< 0.001	0.013	< 0.001	0.010
Golgi ribbon formation	11	0.15	< 0.001	0.013	< 0.001	0.010
startle response	24	0.14	< 0.001	0.013	< 0.001	< 0.001
histone deubiquitination	22	0.16	< 0.001	0.013	< 0.001	0.010
neg. reg. of peptidyl-tyrosine phosphorylation	32	0.13	< 0.001	0.013	< 0.001	< 0.001
establishment of meiotic spindle localization	5	0.19	< 0.001	0.013	< 0.001	< 0.001
pos. reg. of circadian rhythm	13	0.14	< 0.001	0.013	< 0.001	< 0.001
serine phosphorylation of STAT protein	8	0.23	< 0.001	0.013	< 0.001	< 0.001
locomotion involved in locomotory behavior	7	0.15	< 0.001	0.013	< 0.001	< 0.001
histone H4-K12 acetylation	7	0.22	< 0.001	0.013	< 0.001	0.010
macromitophagy	17	0.26	< 0.001	0.013	< 0.001	0.010
neg. reg. of histone H3-K9 methylation	10	0.21	< 0.001	0.013	< 0.001	< 0.001
cerebellar Purkinje cell layer morphogenesis	14	0.18	< 0.001	0.013	< 0.001	< 0.001
establishment of skin barrier	7	0.18	< 0.001	0.014	< 0.001	0.010
mRNA 3'-splice site recognition	6	0.26	< 0.001	0.014	< 0.001	0.015
reg. of circadian rhythm	82	0.10	< 0.001	0.014	< 0.001	0.015
response to muscle inactivity involved in reg. of muscle adaptation	5	0.23	< 0.001	0.014	< 0.001	< 0.001
response to denervation involved in reg. of muscle adaptation	5	0.23	< 0.001	0.014	< 0.001	< 0.001
reg. of type B pancreatic cell development	7	0.39	< 0.001	0.014	0.001	0.020
protein desumoylation	8	0.20	< 0.001	0.014	< 0.001	< 0.001

Table S9: Results of gene category enrichment analyses

Gene category enrichment analyses were calculated using ABAnnotate (*32*) on different databases; neuronal cell type markers (*146–148*), region-wise developmental mRNA expression data (*149*), psychiatric disease markers (*150*) and Gene Ontology biological process annotations (*151*, *152*). The method was developed by Fulcher et al. (*153*). Spatial Spearman correlations were calculated between the interpersonal neural synchrony (INS) Z-map and the gene expression profiles drawn from the Allen Brain Atlas (*19*) of each gene annotated to a category. Correlation coefficients were averaged for each category. This process was repeated for 5,000 null maps derived from the INS map and significance was evaluated by comparison of the "real" category-wise average correlation with the 5,000 null correlations (*p(perm)*). To approximate p-values below 1/5000, a Gassian distribution of category-wise average correlations was fitted to the distribution of permutation-derived scores (*p(norm)*). Resulting *p* values were false discovery rate-corrected according to the Benjamini-Hochberg procedure (*q*). Rows are sorted according to the parametric uncorrected *p* values. Shown are all results for cell types, only significant for regional developmental enrichment, and the top 50 Gene Ontology categories. Full results are provided in the GitHub repository accompanying this publication.

Abbreviations: perm = permutation, norm = Gaussian normal distribution, CBC = cerebellar cortex, A1C = primary auditory cortex, V1C = primary visual cortex, STC = posterior (caudal) superior temporal cortex, S1C = primary somatosensory cortex, IPC = posteroventral (inferior) parietal cortex, M1C = primary motor cortex, DFC = dorsolateral prefrontal cortex, VFC = ventrolateral prefrontal cortex, OFC = orbital frontal cortex, ITC = inferolateral temporal cortex, MFC = anterior (rostral) cingulate (medial prefrontal) cortex, reg = regulation, pos = positive, neg = negative.

Cluster ID	N (terms)	*Representative GO term*			
		GO term ID	GO term description	p (norm)	Average Z (ρ)
1	16	GO:1901386	negative regulation of voltage-gated potassium channel activity	2.120E-06	0.23
2	49	GO:2001016	positive regulation of skeletal muscle cell differentiation	2.370E-06	0.42
3	36	GO:0033561	regulation of water loss via skin	8.690E-06	0.21
4	80	GO:0000290	deadenylation-dependent decapping of nuclear-transcribed mRNA	1.180E-05	0.28
5	13	GO:0085020	protein K6-linked ubiquitination	1.210E-05	0.26
6	18	GO:1901524	regulation of mitophagy	1.280E-05	0.28
7	26	GO:0021702	cerebellar Purkinje cell differentiation	1.330E-05	0.23
8	19	GO:0071107	response to parathyroid hormone	2.450E-05	0.24
9	30	GO:0033233	regulation of protein sumoylation	2.470E-05	0.14
10	21	GO:0006498	N-terminal protein lipidation	4.560E-05	0.30
11	9	GO:2000323	negative regulation of glucocorticoid receptor signaling pathway	4.700E-05	0.34
12	15	GO:0051295	establishment of meiotic spindle localization	7.030E-05	0.19
13	21	GO:0042501	serine phosphorylation of STAT protein	7.190E-05	0.23
14	5	GO:0031987	locomotion involved in locomotory behavior	7.250E-05	0.15
15	31	GO:0000389	mRNA 3'-splice site recognition	9.360E-05	0.26
16	13	GO:0014894	response to denervation involved in regulation of muscle adaptation	1.003E-04	0.23
17	16	GO:0030213	hyaluronan biosynthetic process	1.069E-04	0.19
18	6	GO:0032042	mitochondrial DNA metabolic process	1.802E-04	0.16
19	2	GO:0086027	AV node cell to bundle of His cell signaling	1.835E-04	0.30
20	6	GO:0000301	retrograde transport, vesicle recycling within Golgi	2.339E-04	0.13
21	19	GO:0015851	nucleobase transport	2.574E-04	0.34
22	2	GO:0042118	endothelial cell activation	3.987E-04	0.17
23	1	GO:0010659	cardiac muscle cell apoptotic process	6.881E-04	0.08
24	1	GO:0008228	opsonization	1.870E-03	0.21
25	2	GO:0039703	RNA replication	1.968E-03	0.08
26	1	GO:0039694	viral RNA genome replication	1.968E-03	0.08
27	2	GO:0086003	cardiac muscle cell contraction	3.916E-03	0.07

Table S10: Results of GeneOntology category clustering

The data were generated using GO-Figure! (*154*). GO categories significantly associated to the interpersonal neural synchrony Z-map (see Table S9) were clustered based on semantic similarity (similarity threshold ≥ .2) and for each cluster a representative term was selected in a data-driven fashion. *N (terms)* shows the number of GO categories annoatated to each cluster. The list is ordered according to the *p* values of the representative terms and shows only GO terms that could be clustered. See Table S9 for further descriptions.
Abbreviations: GO = GeneOntology.

5 Supplementary Figures

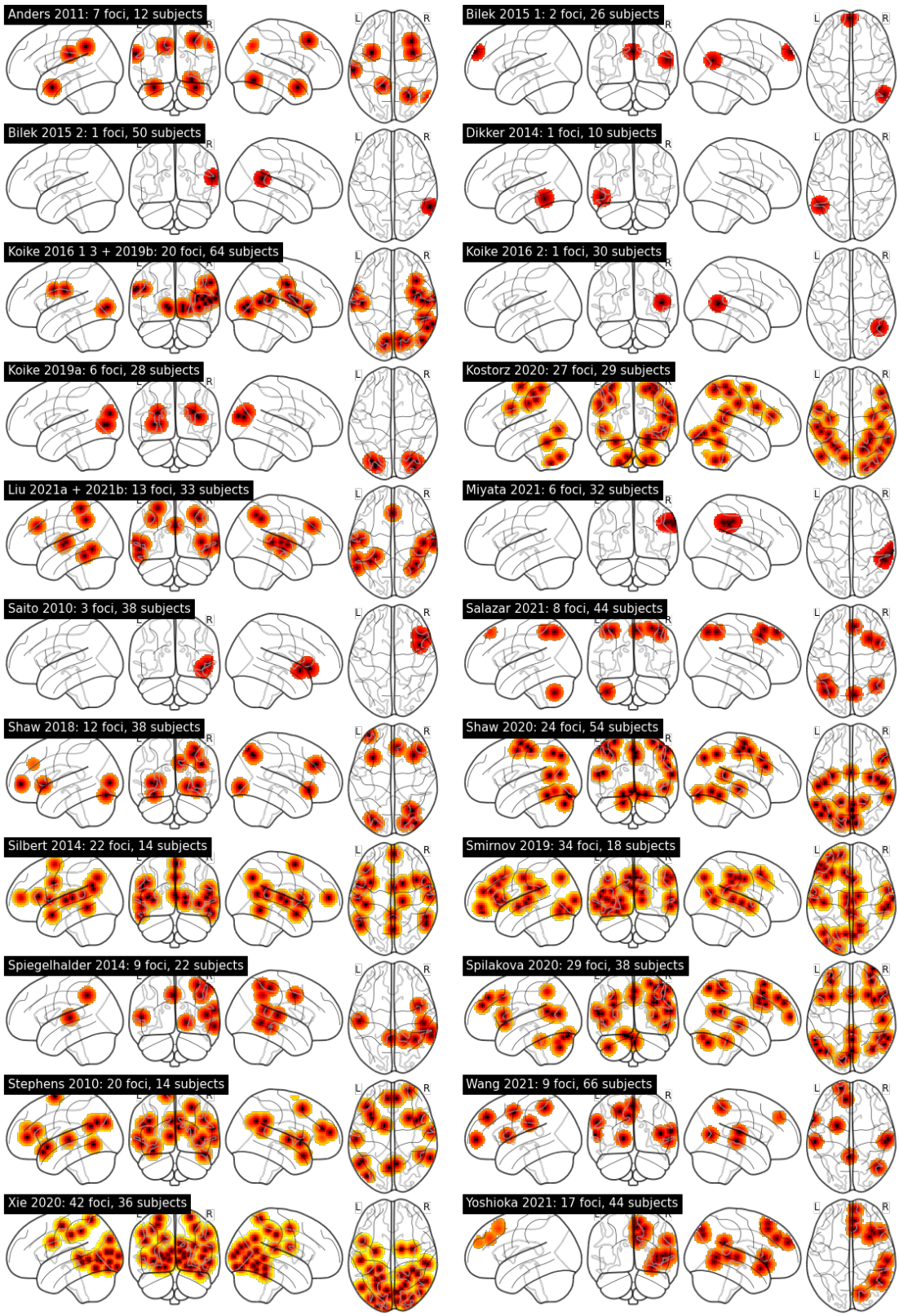

Figure S1: INS foci reported in each fMRI experiment

Foci are plotted individually for each experiment and smoothed using the activation likelihood estimation kernel depending on the reported sample size.

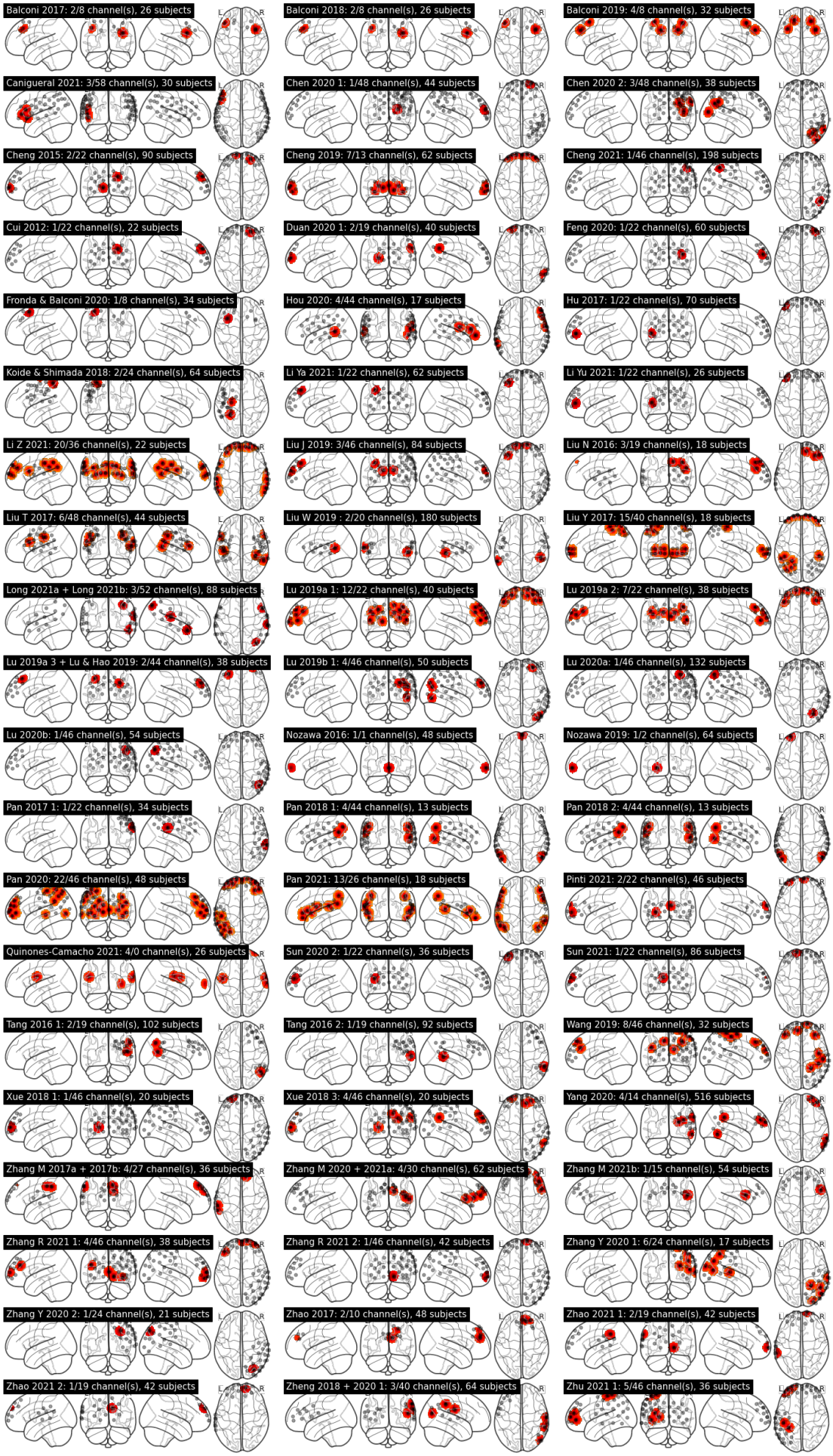
Balconi 2017: 2/8 channel(s), 26 subjects
Balconi 2018: 2/8 channel(s), 26 subjects
Balconi 2019: 4/8 channel(s), 32 subjects
Canigueral 2021: 3/58 channel(s), 30 subjects
Chen 2020 1: 1/48 channel(s), 44 subjects
Chen 2020 2: 3/48 channel(s), 38 subjects
Cheng 2015: 2/22 channel(s), 90 subjects
Cheng 2019: 7/13 channel(s), 62 subjects
Cheng 2021: 1/46 channel(s), 198 subjects
Cui 2012: 1/22 channel(s), 22 subjects
Duan 2020 1: 2/19 channel(s), 40 subjects
Feng 2020: 1/22 channel(s), 60 subjects
Fronda & Balconi 2020: 1/8 channel(s), 34 subjects
Hou 2020: 4/44 channel(s), 17 subjects
Hu 2017: 1/22 channel(s), 70 subjects
Koide & Shimada 2018: 2/24 channel(s), 64 subjects
Li Ya 2021: 1/22 channel(s), 62 subjects
Li Yu 2021: 1/22 channel(s), 26 subjects
Li Z 2021: 20/36 channel(s), 22 subjects
Liu J 2019: 3/46 channel(s), 84 subjects
Liu N 2016: 3/19 channel(s), 18 subjects
Liu T 2017: 6/48 channel(s), 44 subjects
Liu W 2019 : 2/20 channel(s), 180 subjects
Liu Y 2017: 15/40 channel(s), 18 subjects
Long 2021a + Long 2021b: 3/52 channel(s), 88 subjects
Lu 2019a 1: 12/22 channel(s), 40 subjects
Lu 2019a 2: 7/22 channel(s), 38 subjects
Lu 2019a 3 + Lu & Hao 2019: 2/44 channel(s), 38 subjects
Lu 2019b 1: 4/46 channel(s), 50 subjects
Lu 2020a: 1/46 channel(s), 132 subjects
Lu 2020b: 1/46 channel(s), 54 subjects
Nozawa 2016: 1/1 channel(s), 48 subjects
Nozawa 2019: 1/2 channel(s), 64 subjects
Pan 2017 1: 1/22 channel(s), 34 subjects
Pan 2018 1: 4/44 channel(s), 13 subjects
Pan 2018 2: 4/44 channel(s), 13 subjects
Pan 2020: 22/46 channel(s), 48 subjects
Pan 2021: 13/26 channel(s), 18 subjects
Pinti 2021: 2/22 channel(s), 46 subjects
Quinones-Camacho 2021: 4/0 channel(s), 26 subjects
Sun 2020 2: 1/22 channel(s), 36 subjects
Sun 2021: 1/22 channel(s), 86 subjects
Tang 2016 1: 2/19 channel(s), 102 subjects
Tang 2016 2: 1/19 channel(s), 92 subjects
Wang 2019: 8/46 channel(s), 32 subjects
Xue 2018 1: 1/46 channel(s), 20 subjects
Xue 2018 3: 4/46 channel(s), 20 subjects
Yang 2020: 4/14 channel(s), 516 subjects
Zhang M 2017a + 2017b: 4/27 channel(s), 36 subjects
Zhang M 2020 + 2021a: 4/30 channel(s), 62 subjects
Zhang M 2021b: 1/15 channel(s), 54 subjects
Zhang R 2021 1: 4/46 channel(s), 38 subjects
Zhang R 2021 2: 1/46 channel(s), 42 subjects
Zhang Y 2020 1: 6/24 channel(s), 17 subjects
Zhang Y 2020 2: 1/24 channel(s), 21 subjects
Zhao 2017: 2/10 channel(s), 48 subjects
Zhao 2021 1: 2/19 channel(s), 42 subjects
Zhao 2021 2: 1/19 channel(s), 42 subjects
Zheng 2018 + 2020 1: 3/40 channel(s), 64 subjects
Zhu 2021 1: 5/46 channel(s), 36 subjects

Figure S2: INS foci reported in each fNIRS experiment

Interpersonal neural synchrony (INS) channels are plotted individually for each experiment and, for vizualization purposes, smoothed using the activation likelihood estimation kernel set to a fixed "sample size" of n = 10. Gray markers show all channels reported by, or reconstructed for, each study. Only those experiments reporting at least one INS channel are shown.

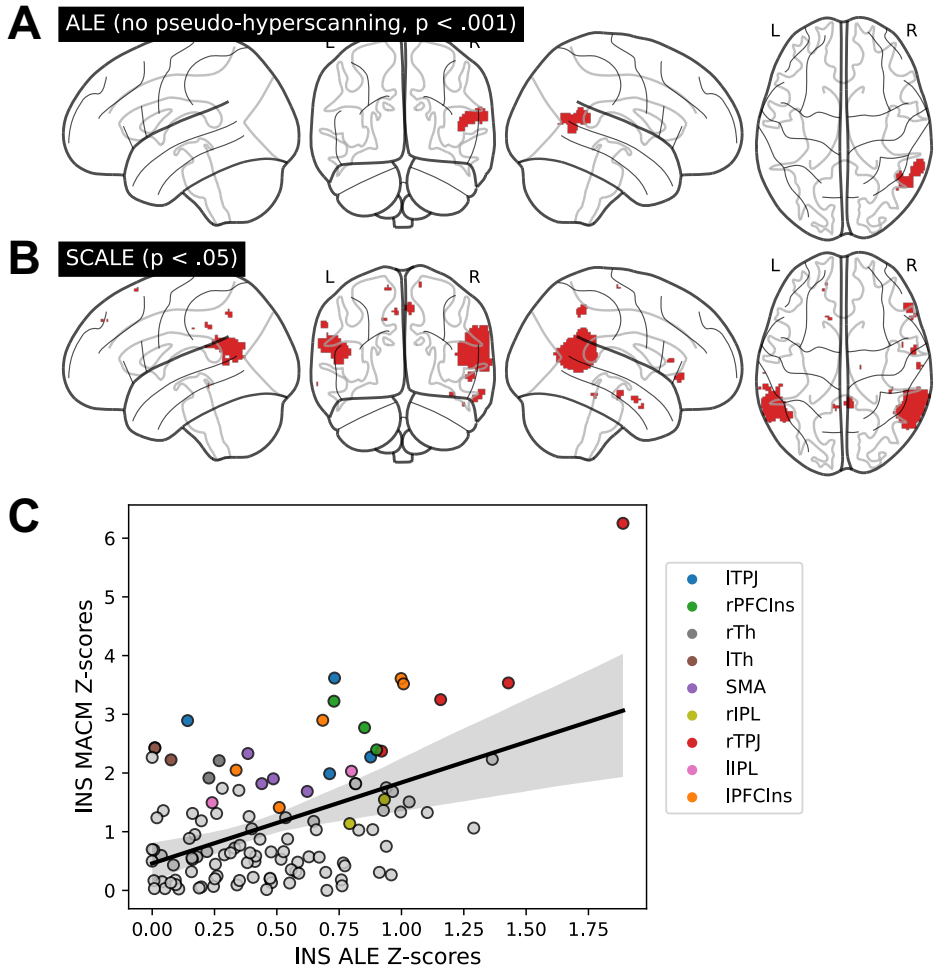

Figure S3: ALE and MACM sensitivity analyses

A: ALE without pseudo-hyperscanning studies. **B**: MACM corrected for baseline activation (SCALE). The method as implemented in NiMARE (*158*) does not support multiple comparison correction and was thresholded at voxel-level $p < .05$, uncorrected, for demonstration purposes. **C**: Spatial correlation between whole-brain distributions of INS and the rTPJ-associated MACM map to demonstrate comparable distributions patterns going beyond rTPJ activation.
Abbreviations: ALE = activation likelihood estimation, SCALE = specific coactivation likelihood estimation, INS = interpersonal neural synchronization, MACM = meta-analytic coactivation modeling, r/lTPJ = right/left temporoparietal junction, rSTG = right superior temporal gyrus, rIns = right insula, r/lPFCIns = right/left prefrontal cortex-insula, SMA = supplementary motor area, r/lTh = left thalamus, r/lIPL = left inferior parietal lobule, lPrec = left precuneus.

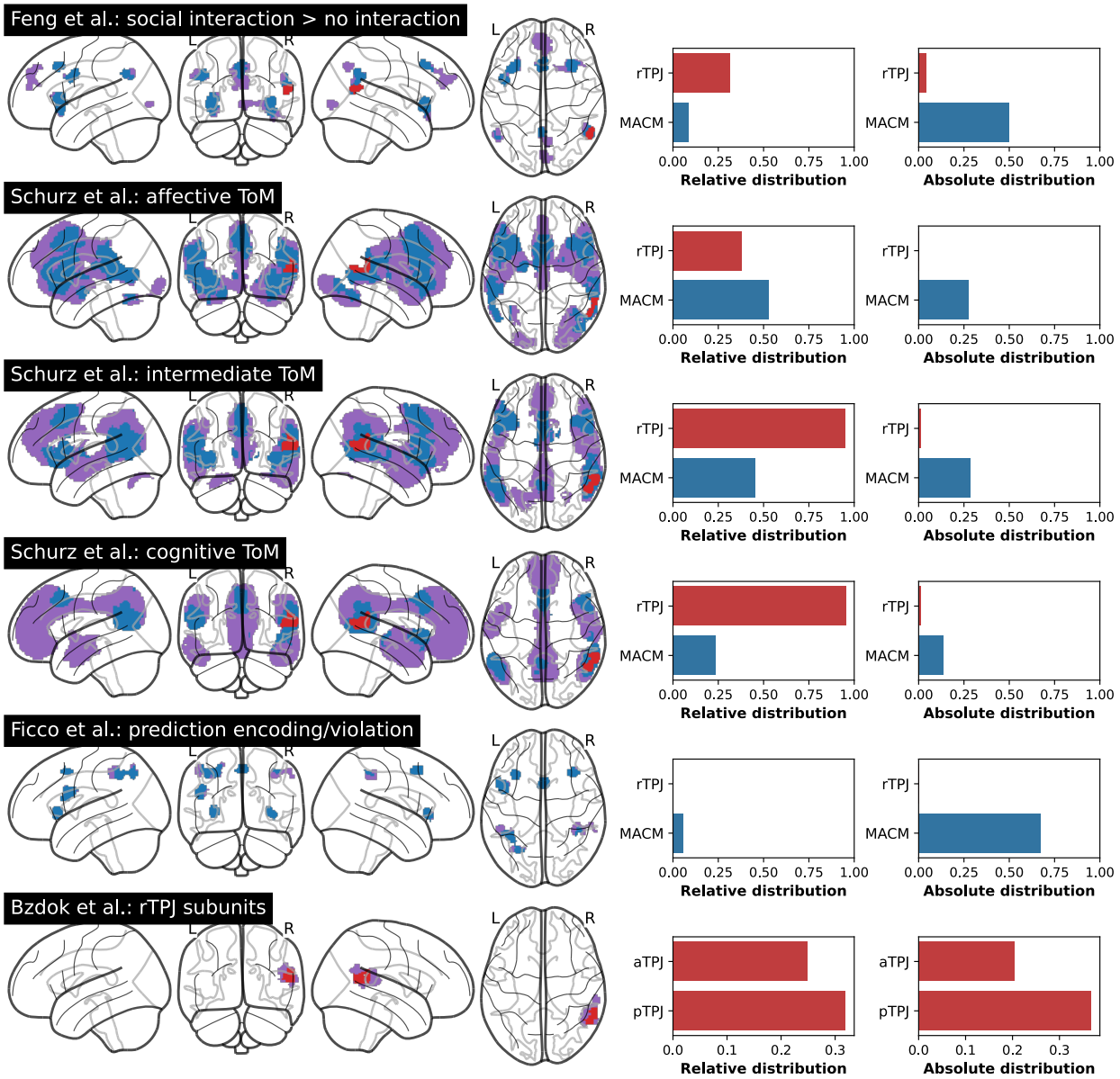

Figure S4: Spatial overlap with prior meta-analytically derived networks and rTPJ subunits

Sources: Feng et al., 2021 (*159*); Schurz et al., 2021 (*160*); Ficco et al., 2021 (*161*); Bzdok et al., 2013 (*162*). Original networks are plotted in purple, overlayed by conjunctions with the rTPJ-MACM network (blue) and the rTPJ cluster (red). For the upper five rows, the right side shows relative and absolute distributions of rTPJ cluster and MACM network within the corresponding meta-analytically derived network. The lowest row shows distributions of the INS-rTPJ cluster within two subunits of the rTPJ. Relatived distribution: proportion of "INS-voxels" within a given network vs. all "INS-voxels". Absolute distribution: proportion of "INS-voxels" within a given network vs. all voxels within the network.

Abbreviations: rTPJ = right temporoparietal junction, MACM = meta-analytic connectivity modeling, ToM = theory of mind, INS = interpersonal neural synchronization.

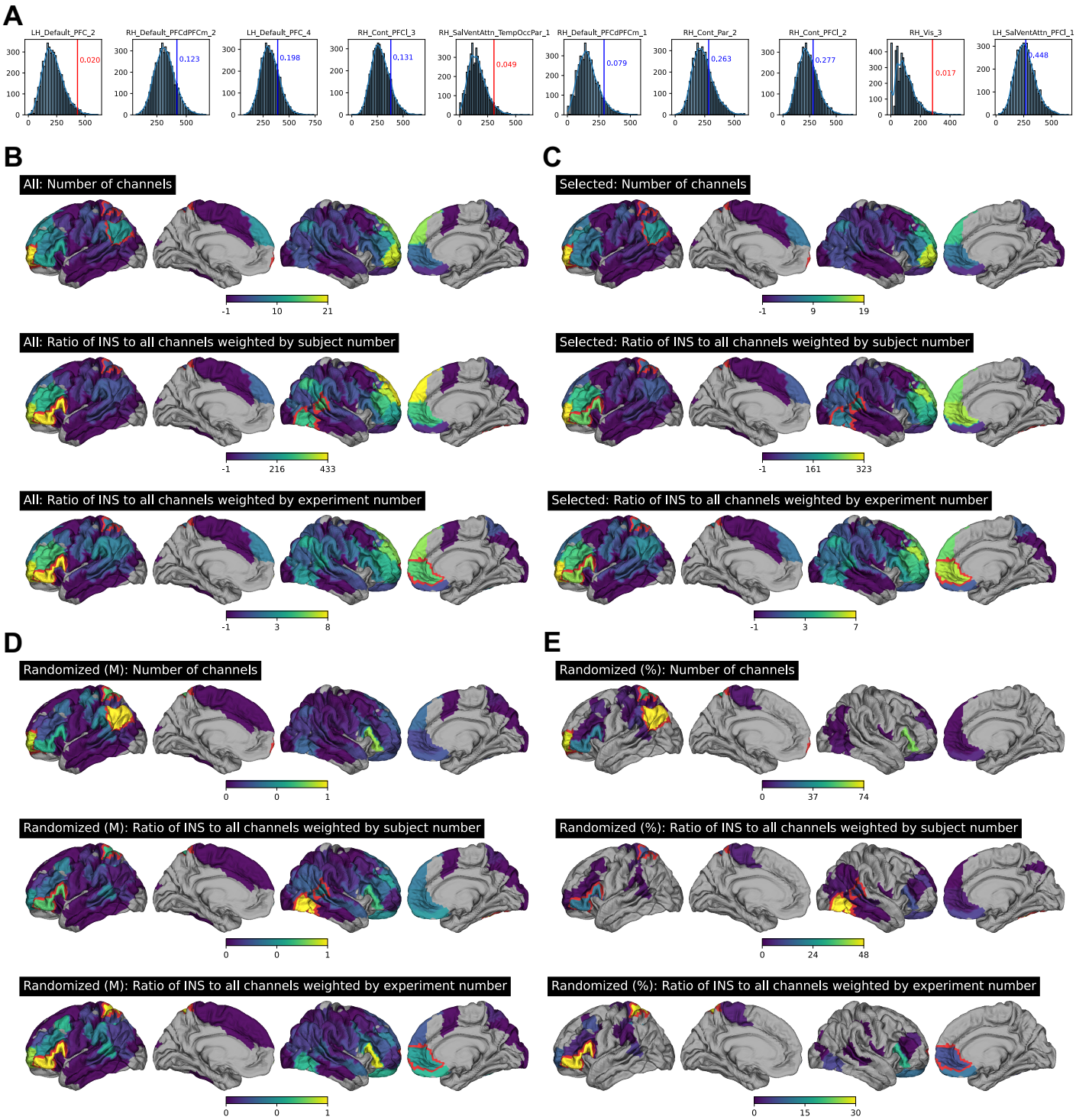

Figure S5: Complete meta-analytic results of INS fNIRS experiments

A: Histograms for the top ten regions resulting from the permutations regarding the meta-analytic fNIRS INS analysis that included all experiments and focused on the parcel-wise ratio of INS vs. all channels weighted by the number of subjects. Vertical lines and numbers show the "real" result and the uncorrected *p* value estimated from each null distribution. **B**: Full fNIRS meta-analysis results for all included experiments. The middle row is shown in main Figure 2B. **C**: Full fNIRS meta-analysis results restricted to experiments explicitly assessing INS compared to rest, control, or randomization. **D**: Median (M) $\log_{10}$-transformed *p* values resulting from fNIRS meta-analysis after repeated randomization of fNIRS coordinates (radius = 1 cm, 1,000 iterations). **E**: Percentage of sub-threshold *p* values after coordinate randomization.

Abbreviations: INS = interpersonal neural synchrony, fNIRS = functional near-infrared spectroscopy.

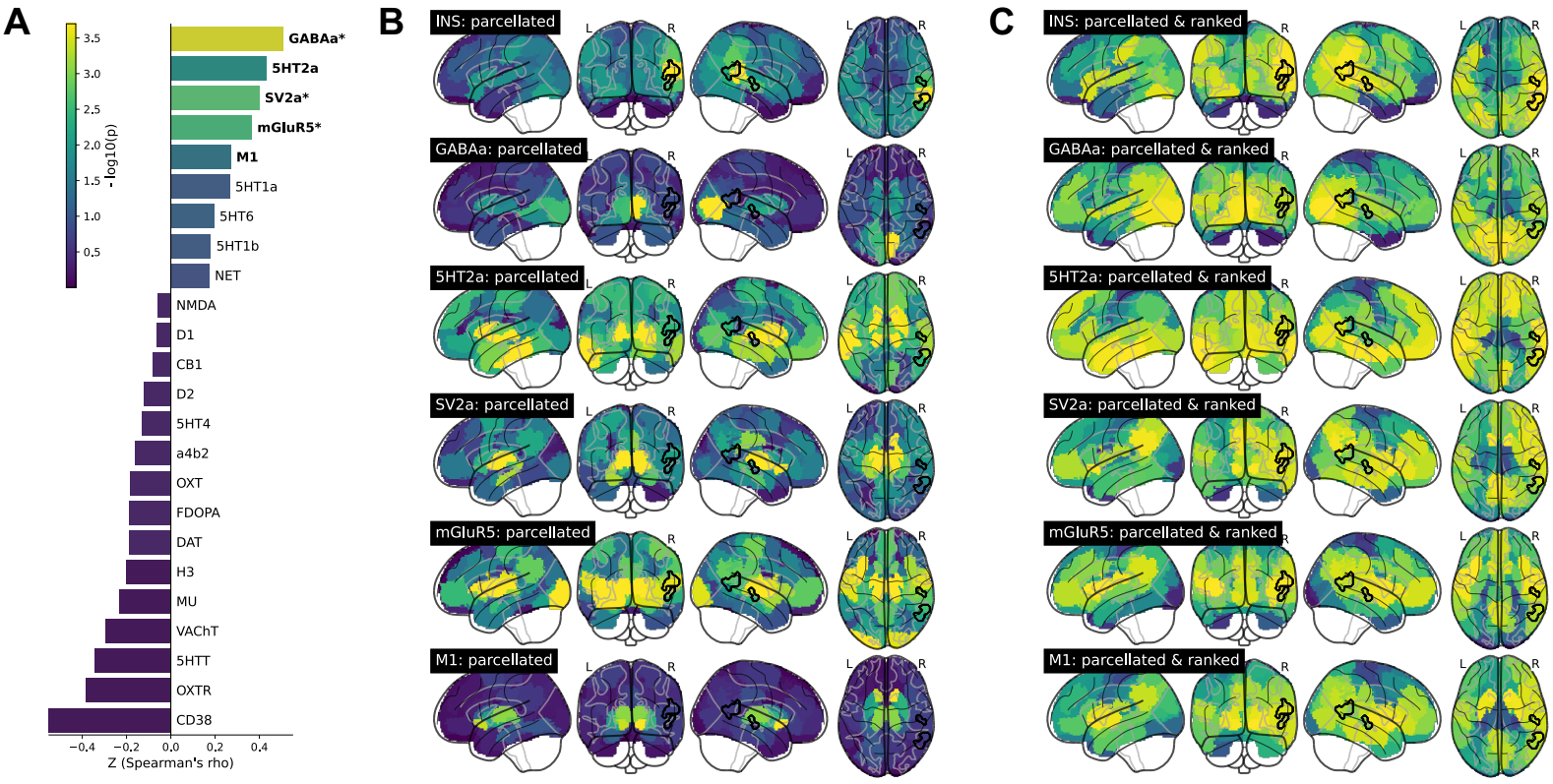

Figure S6: Spatial associations of INS to neurotransmitter distributions

A: Spatial correlations between whole-brain INS distribution and invivo neurotransmitter receptor/ postmortem gene expression distributions. Color-coded *p* values are uncorrected, correlations significant at uncorrected $p < .05$ derived from nonparametric permutation are printed in bold, *p* values surviving false discovery rate correction ($q < .05$) are marked by asterisks. Nuclear imaging-derived maps were correlated with the INS map using partial Spearman correlations controlling for local gray matter volume to account for partial volume effects. Correlation coefficients were compared to those calculated from 5,000 spatial autocorrelation-preserving null maps derived from each indicidual transmitter map using JuSpyce. **B**: Parcellated and Z-transformed PET maps significantly associated to INS. **C**: To better demonstrate the spatial alignment between INS and PET maps, parcellated values were ranked and the ranks were reassigned to the brain volumes (yellow = highest rank). Black outline shows significant clusters resulting from the main activation likelihood estimation analysis.
See Table S3 for full neurotransmitter receptor names, nuclear imaging tracers, and template sources, and Table S8 for full JuSpyce results.
Abbreviations: INS = interpersonal neural synchrony, PET = positron emission tomography.

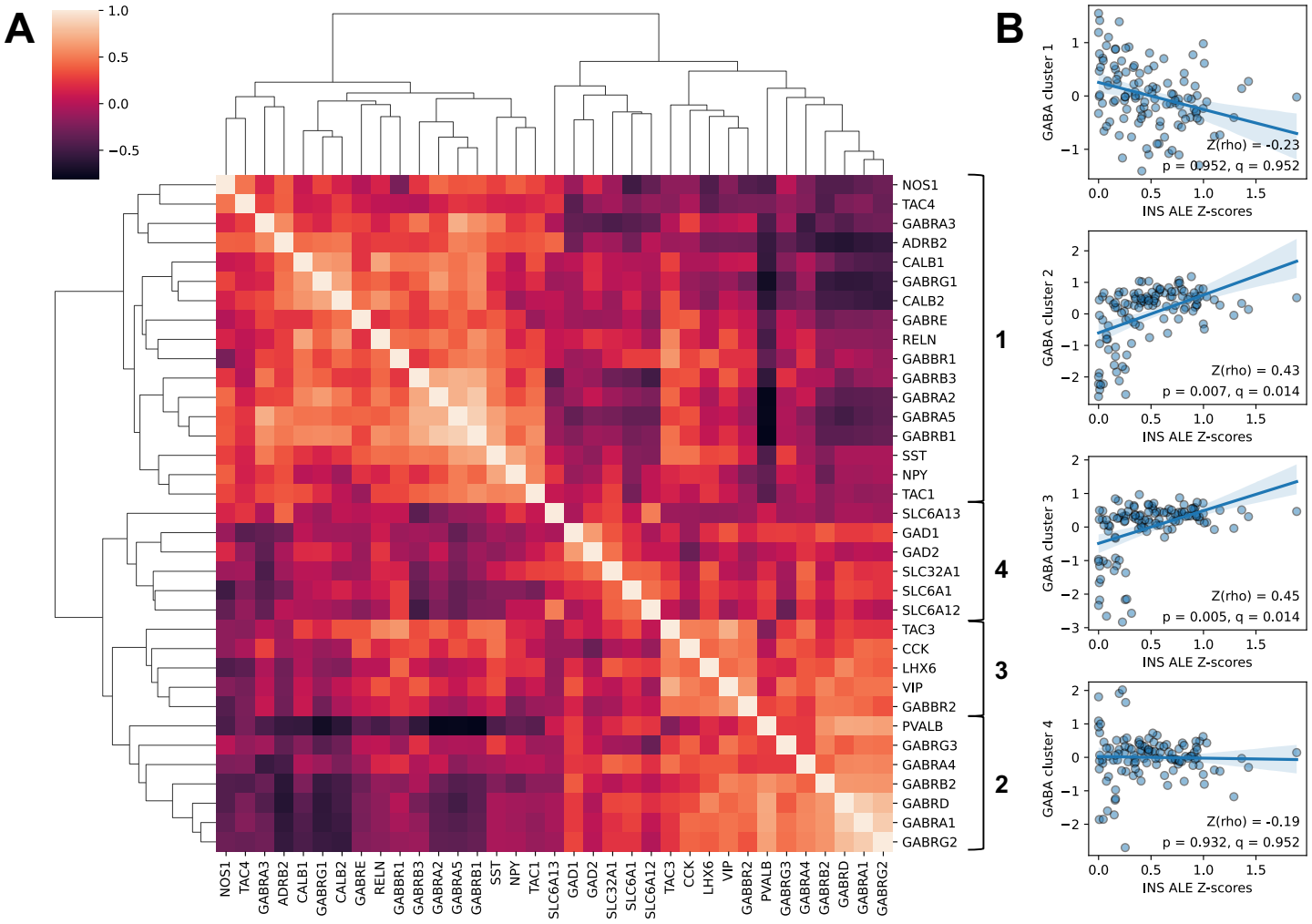

Figure S7: Validation of INS-GABA$_A$ associations using mRNA expression data

A: Clustered correlation heatmap of expression profiles of GABA-related genes. Colors represent Spearman correlations. Coexpression clusters were estimated using a hierarchical clustering algorithm based on Euclidean pairwise distances. **B**: Correlation between the INS distribution and gene cluster-wise averaged expression values; the correlations with clusters 2 and 3 are significant ($q < .05$).
Abbreviations: INS = interpersonal neural synchronization, ALE = activation likelihood estimation.

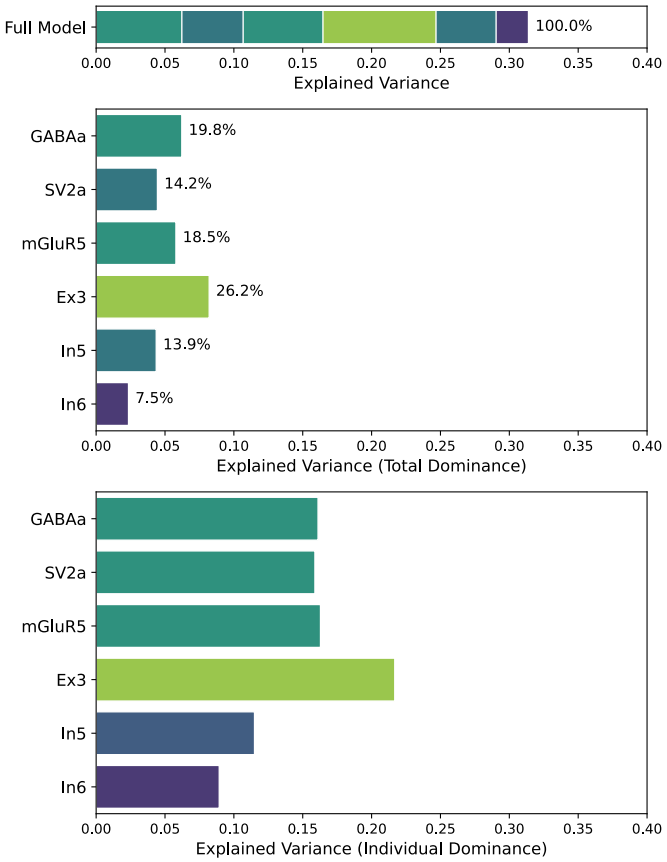

Figure S8: Variance of the INS distribution explained by significantly associated nuclear imaging and neuronal cell type data

Results from a dominance analysis using significantly positively associated nuclear imaging and neuronal cell type atlases as predictors and the INS Z-map as target. As in the main univariate correlation analyses, local gray matter volume was regressed out of both predictors and target before performing the dominance analysis. Upper: R^2 of the complete multilinear regression model ($R^2 = .31$). Middle: "Total dominance" which can be interpreted as the relative contribution of a predictor to the explained variance of the complete model in interaction with the remaining predictors and therefore can also be expressed in percent of total R^2. Lower: "Individual dominance" which can be interpreted as each individual predictor's explained variance independent of all other predictors.
Abbreviations: INS = interpersonal neural synchronization.

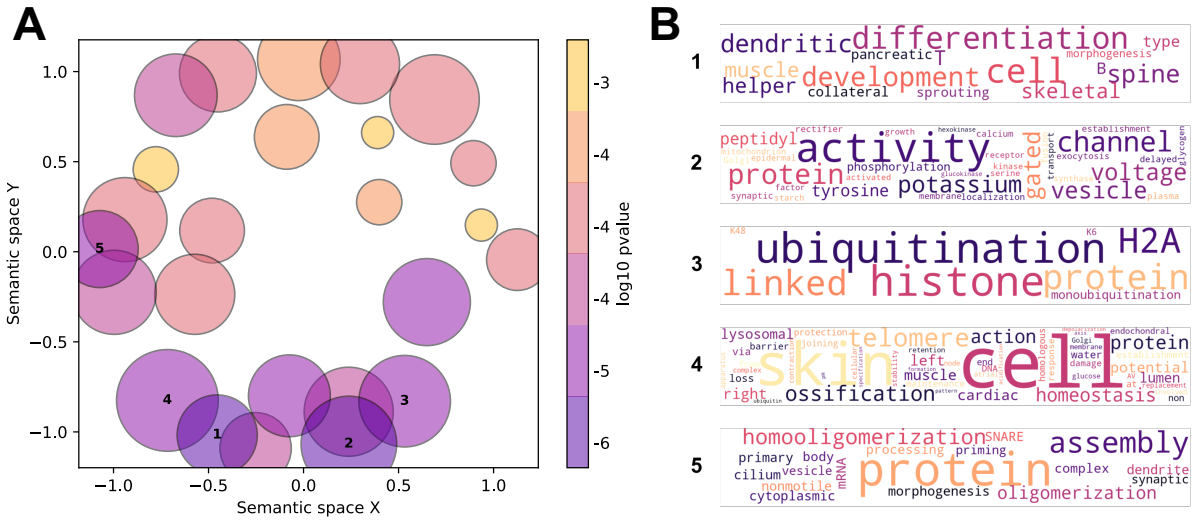

Figure S9: Clustering of GeneOntology biological process categories spatially associated with INS

A: Two-dimensional reduction of the pairwise semantic similarity matrix of 474 Gene Ontology (GO) categories spatially associated to INS. Each point represents one cluster of n biologial process categories formed by a similarity threshold of .2 with the point size depicting n. Point color represents $log(p)$ associated with a representive GO term identified for each cluster. **B**: Word clouds built from combined category descriptions of the five semantic clusters most strongly associated to INS (marked by numbers 1-5 in both panels). Word size is based on word frequency within each semantic cluster.